MODELING AND ANALYSIS OF VECTOR-BORNE DISEASES ON COMPLEX NETWORKS

by

LING XUE

B.S. Harbin University of Science and Technology, China, 2002
M.S. Harbin University of Science and Technology, China, 2005

AN ABSTRACT OF A DISSERTATION

submitted in partial fulfillment of the
requirements for the degree

DOCTOR OF PHILOSOPHY

Department of Electrical and Computer Engineering
College of Engineering

KANSAS STATE UNIVERSITY
Manhattan, Kansas
2013

Abstract

Vector-borne diseases not only cause devastating economic losses, they also significantly impact human health in terms of morbidity and mortality. From an economical and humane point of view, mitigation and control of vector-borne diseases are essential. Studying dynamics of vector-borne disease transmission is a challenging task because vector-borne diseases show complex dynamics impacted by a wide range of ecological factors. Understanding these factors is important for the development of mitigation and control strategies.

Mathematical models have been commonly used to translate assumptions concerning biological (medical, demographical, behavioral, immunological) aspects into mathematics, linking biological processes of transmission and dynamics of infection at population level. Mathematical analysis translates results back into biology. Classical deterministic epidemic models do not consider spatial variation, assuming space is homogeneous. Spatial spread of vector-borne diseases observed many times highlights the necessity of incorporating spatial dynamics into mathematical models. Heterogeneous demography, geography, and ecology in various regions may result in different epidemiological characteristics. Network approach is commonly used to study spatial evolution of communicable diseases transmitted among connected populations.

In this dissertation, the spread of vector-borne diseases in time and space, is studied to understand factors that contribute to disease evolution. Network-based models have been developed to capture different features of disease transmission in various environments. Network nodes represent geographical locations, and the weights represent the level of contact between regional pairings. Two competent vector populations, *Aedes* mosquitoes and *Culex* mosquitoes, and two host populations, cattle and humans were considered. The deterministic model was applied to the 2010 Rift Valley fever outbreak in three provinces of South

Africa. Trends and timing of the outbreak in animals and humans were reproduced. The deterministic model with stochastic parameters was applied to hypothetical Rift Valley fever outbreak on a large network in Texas, the United States. The role of starting location and size of initial infection in Rift Valley fever virus spread were studied under various scenarios on a large-scale network.

The reproduction number, defined as the number of secondary infections produced by one infected individual in a completely susceptible population, is typically considered an epidemic threshold of determining whether a disease can persist in a population. Extinction thresholds for corresponding continuous-time Markov chain model is used to predict whether a disease can perish in a stochastic setting.

The network level reproduction number for diseases vertically and horizontally transmitted among multiple species on heterogeneous networks was derived to predict whether a disease can invade the whole system in a deterministic setting. The complexity of computing the reproduction number is reduced because the expression of the reproduction number is the spectral radius of a matrix whose size is smaller than the original next generation matrix. The expression of the reproduction number may have a wide range of applications to many vector-borne diseases. Reproduction numbers can vary from below one to above one or from above one to below one by changing movement rates in different scenarios. The observations provide guidelines on executing movement bans in case of an epidemic.

To compute the extinction threshold, corresponding Markov chain process is approximated near disease free equilibrium. The extinction threshold for continuous-time Markov chain model was analytically connected to the reproduction number under some assumptions. Numerical simulation results agree with analytical results without assumptions, proposing a mathematical problem of proving the existence of the relationships in general. The distance of the extinction threshold were shown to be closer to one than the reproduction number. Consistent trends of probability of extinction varying with disease parameters observed through numerical simulations provide novel insights into disease mit-

igation, control, and elimination.

MODELING AND ANALYSIS OF VECTOR-BORNE DISEASES ON COMPLEX NETWORKS

by

LING XUE

B.S. Harbin University of Science and Technology, China, 2002
M.S. Harbin University of Science and Technology, China, 2005

A DISSERTATION

submitted in partial fulfillment of the
requirements for the degree

DOCTOR OF PHILOSOPHY

Department of Electrical and Computer Engineering
College of Engineering

KANSAS STATE UNIVERSITY
Manhattan, Kansas
2013

Approved by:

Major Professor
Caterina Scoglio

Copyright

Abstract

Vector-borne diseases not only cause devastating economic losses, they also significantly impact human health in terms of morbidity and mortality. From an economical and humane point of view, mitigation and control of vector-borne diseases are essential. Studying dynamics of vector-borne disease transmission is a challenging task because vector-borne diseases show complex dynamics impacted by a wide range of ecological factors. Understanding these factors is important for the development of mitigation and control strategies.

Mathematical models have been commonly used to translate assumptions concerning biological (medical, demographical, behavioral, immunological) aspects into mathematics, linking biological processes of transmission and dynamics of infection at population level. Mathematical analysis translates results back into biology. Classical deterministic epidemic models do not consider spatial variation, assuming space is homogeneous. Spatial spread of vector-borne diseases observed many times highlights the necessity of incorporating spatial dynamics into mathematical models. Heterogeneous demography, geography, and ecology in various regions may result in different epidemiological characteristics. Network approach is commonly used to study spatial evolution of communicable diseases transmitted among connected populations.

In this dissertation, the spread of vector-borne diseases in time and space, is studied to understand factors that contribute to disease evolution. Network-based models have been developed to capture different features of disease transmission in various environments. Network nodes represent geographical locations, and the weights represent the level of contact between regional pairings. Two competent vector populations, *Aedes* mosquitoes and *Culex* mosquitoes, and two host populations, cattle and humans were considered. The deterministic model was applied to the 2010 Rift Valley fever outbreak in three provinces of South

Africa. Trends and timing of the outbreak in animals and humans were reproduced. The deterministic model with stochastic parameters was applied to hypothetical Rift Valley fever outbreak on a large network in Texas, the United States. The role of starting location and size of initial infection in Rift Valley fever virus spread were studied under various scenarios on a large-scale network.

The reproduction number, defined as the number of secondary infections produced by one infected individual in a completely susceptible population, is typically considered an epidemic threshold of determining whether a disease can persist in a population. Extinction thresholds for corresponding continuous-time Markov chain model is used to predict whether a disease can perish in a stochastic setting.

The network level reproduction number for diseases vertically and horizontally transmitted among multiple species on heterogeneous networks was derived to predict whether a disease can invade the whole system in a deterministic setting. The complexity of computing the reproduction number is reduced because the expression of the reproduction number is the spectral radius of a matrix whose size is smaller than the original next generation matrix. The expression of the reproduction number may have a wide range of applications to many vector-borne diseases. Reproduction numbers can vary from below one to above one or from above one to below one by changing movement rates in different scenarios. The observations provide guidelines on executing movement bans in case of an epidemic.

To compute the extinction threshold, corresponding Markov chain process is approximated near disease free equilibrium. The extinction threshold for continuous-time Markov chain model was analytically connected to the reproduction number under some assumptions. Numerical simulation results agree with analytical results without assumptions, proposing a mathematical problem of proving the existence of the relationships in general. The distance of the extinction threshold were shown to be closer to one than the reproduction number. Consistent trends of probability of extinction varying with disease parameters observed through numerical simulations provide novel insights into disease mit-

igation, control, and elimination.

Table of Contents

List of Figures

List of Tables

Acknowledgments

Many people from various corners of the world have contributed to the production of this dissertation, although my name appears on its cover. I owe my gratitude to all those who have made this dissertation possible and because of whom my graduation experience is cherishable.

First and foremost, I would like to express my sincere gratitude to my advisor, Dr. Caterina Scoglio, for her guidance, patience, enthusiasm, understanding, and most importantly, her friendship during my graduate studies at Kansas State University. She encouraged me to become an independent thinker and researcher, which is invaluable not only for my research but also for my career.

My sincere thanks also go to the members of my dissertation committee, Dr. H. Morgan Scott, Dr. Lee Cohnstaedt, and Dr. Don Gruenbacher, for their helpful suggestions, contributions, good-natured support, and the generous gift of their time and expertise to better my work. My gratitude is extended to Dr. Kenneth J. Linthicum and Dr. Seth C. Britch for their comments on mosquito models.

I thank my fellows in the Sunflower networking group, K-State epicenter: Sakshi Pahwa, Mina Youssef, Faryad Darabi Sahneh, Yunzhao Li, Phillip Schumm, Ali Sydney, and Ala Fard for the stimulating discussions and all memorable time we spent together.

I'm grateful to the librarians at Hale library and Fielder library in Kansas State University for introducing, assisting, and advising me the techniques of searching for literature and useful resources owned by the library, as well as promptly sending me resources borrowed from other libraries. I especially thank Alice Trussell and Asha Muthukrishnan from Fielder Library, and Regina Beard, Livia Olsen, and Marty Courtois for their support on literature search over the years.

My thanks must go to Dr. Bo Norby from Texas A & M University, Dr. Doyle R. Fuchs from Texas Department of Agriculture, Dr. Kelebogile Olifant from Statistics South

Africa, and Dr. Jacqueline Weyer from National Institute for Communicable Diseases for their assistance on research data.

I give special thanks to my family. Words cannot express how grateful I am to them. I would like to thank my parents-in-law for their endless spiritual support. I am grateful to my parents, Wenbin Xue and Yuqing Wang, for giving birth to me in the first place, supporting me spiritually, always having faith in me, and encouraging me to pursue this advanced degree. I must express my appreciation to the person who supports me more than anyone else: my husband, Zhaobing Fan. Thank you for your unwavering love, patience, tolerance, unyielding devotion, and especially I cannot thank you enough for supporting and encouraging me through this experience. I extend my thanks to my beloved daughter, Ruhanna Fan, for being such a nice girl, always cheering me up.

Last but not at least, I appreciate the financial support from the United States (U.S.) Department of Homeland Security under Grant Award Number 2010-ST061-AG0001, a grant through the Kansas Biosciences Authority, the financial support from National Agricultural Biosecurity Center, and the funding provided by U.S. Department of Agriculture - the Agricultural Research Service with Specific Cooperative Agreement 58-5430-1-0356.

Dedication

I dedicate my dissertation work to my wonderful family, particularly to my patient and tolerant husband, and my daughter, Ruhanna Fan, who is the joy of our lives. I also dedicate this work to my parents and terrific parents-in-law who are always supporting me spiritually.

Preface

This dissertation is submitted for the degree of Doctor of Philosophy at Kansas State University. The research described herein was conducted under the supervision of Professor Caterina Scoglio in Electrical & Computer Engineering Department, Kansas State University.

This work is to the best of my knowledge, original, except where acknowledgments and references are made to previous work. Part of this work has been presented in the following publications:

Ling Xue, Caterina Scoglio. The Network-level reproduction number and extinction threshold for vector-borne diseases. Submitted. http://arxiv.org/abs/1308.0718v2

Ling Xue, Lee W. Cohnstaedt, H. M. Scott, Caterina Scoglio. A hierarchical network approach for modeling Rift Valley fever epidemics with applications in North America. PLOS ONE, 8(5): e62049, 2013.

Ling Xue, Caterina Scoglio. The network level reproduction number for infectious diseases with both vertical and horizontal transmission. Mathematical Biosciences, 243(1): 67-80, 2013.

Ling Xue, H. M. Scott, Lee W. Cohnstaedt, Caterina Scoglio. A network-based meta-population approach for mathematical modeling Rift Valley fever epidemics. Journal of Theoretical Biology, 306(5): 129-144, 2012.

This dissertation should be of interest to a large scientific community, including mathematicians, epidemiologists, entomologists, public health scientists, scholars of decision anal-

ysis, practitioners of policy analysis, as well as high-level policy makers.

This research is based upon work supported by the U.S. Department of Homeland Security, Kansas Biosciences Authority, National Agricultural Biosecurity Center, and U.S. Department of Agriculture - the Agricultural Research Service with Specific Cooperative Agreement 58-5430-1-0356. The views and conclusions contained in this publication are those of the authors and should not be interpreted as necessarily representing the official policies, either explicit or implicit, of the U.S. Department of Homeland Security, Kansas Biosciences Authority, National Agricultural Biosecurity Center, and U.S. Department of Agriculture.

Chapter 1

Introduction

Vector-borne diseases greatly impact health of humans and animals and are among the leading causes of worldwide death every year [54]; approximately half of the world's population is infected with at least one type of vector-borne disease and millions of people die of vector-borne diseases each year [29]. These diseases also cause significant economic losses in regard to animal trade, agriculture, health care, tourism, as well as the destruction of ecosystems throughout the world. Therefore, control and prevention of vector-borne diseases are both economical and humane.

1.1 Background

Rift Valley fever (RVF) is one of the vector-borne diseases with enormous health and economic impacts on domestic animals and humans [70], especially in countries where the disease is endemic and in others where sporadic epidemics and epizootics have occurred. The disease has been shown to be endemic in semi-arid zones such as northern Senegal [24, 81, 132], and RVF epidemics often appear at 5-15-year cycles [81].

Aedes and *Culex* genera of mosquitoes are thought to be primary RVF disease vectors with respect to vector competence [25]. The virus is maintained between epidemics through vertical transmission within *Aedes* mosquitoes [72] and is considered to be propagated and amplified during epidemics by *Aedes* and *Culex* mosquitoes. High RVF transmission is typically related to persistent, above average rainfall and El Niño/Southern Oscillation

(ENSO) events in Eastern Africa, which create favorable mosquito habitats [71]. *Aedes* mosquitoes lay eggs in dry mud [132] and the eggs can survive for many years [43]. After flooding, RVF virus-infected eggs can develop into infected adult mosquitoes [43]. Infected adult *Aedes* mosquitoes then feed on animals which become infected, and spread the infection to other *Aedes* and *Culex* genera adult mosquitoes feeding on infected animals. The species of vectors capable of transmitting RVF virus have wide global distribution [55], and therefore, a possibility exists for the virus to spread out of its current expanding geographic range [31].

Rift Valley fever virus was first isolated from the blood of a newborn lamb in 1931 and later from the blood of adult sheep and cattle [8, 127]. Rift Valley fever virus is generally distributed through regions of Eastern and Southern Africa where sheep and cattle are present [125]. Primary economic losses of RVF outbreak in livestock arise due to abortion and mortality, which tend to be higher in young animals [31, 125], and bans on livestock exports during an epidemic [8, 31]. Animal movements, typically motivated by livestock trading and marketing, may accelerate the transmission of zoonotic diseases among animal holdings covering a vast area [13]. In 1977, the trade of sheep from East Africa during Ramadan was considered a likely pathway for the introduction of RVF virus to Egypt [2, 33, 105]. A boy from Anjouan, an island of Comoros archipelago, was diagnosed with RVF virus on the French island of Mayotte in 2007 [25]. Rift Valley fever virus was likely introduced by live ruminants imported from Kenya or Tanzania in the livestock trade during the 2006-2007 RVF outbreak [25].

Humans can acquire RVF virus from the bites of infected mosquitoes or directly from contact with bodily fluids of infected animals [1]. Individuals working with animals, such as farmers and veterinarians, are the most vulnerable to infection during animal outbreaks [87] due to increased exposure to mosquitoes in an outdoor environment and direct contact with animals. Rift Valley fever virus infection causes morbidity (ranging from nondescript fever to meningo-encephalitis and hemorrhagic disease) and mortality (with case fatality rates of 0.2-5%) in humans [70]. In Egypt in 1977, 18,000 human cases with 698 deaths resulted from

the disease [34, 105]. During 1997-1998, Kenya experienced the largest recorded outbreak with 89,000 human cases and 478 deaths [44]. More than 200 persons died of RVF in Mauritania in 1987 [60]. Tanzania and Somalia reported 1,000 human cases and 300 deaths from an outbreak associated with above-normal rainfall in the region during 2006-2007 [44]. The first recorded outbreak outside of Africa occurred in the Arabian Peninsula during 2000-2001 and caused 683 human cases and 95 deaths [44].

1.2 Motivation

Communicable diseases are readily transmitted from one region to another [104, 120]. Population travel continues to influence the temporal and spatial spread of infectious diseases [10, 104]. The introduction of infectious agents resulting in spatial spread of effective infections in various locations at different times [10], revealed great economic losses, many animal and human cases, and deaths. Noteworthy examples include the fourteenth century plague in Europe [104, 109] and the sixteenth century smallpox epidemic in the New World [104]. More recent epidemics, including HIV/AIDS and West Nile virus in North America [94] and SARS in Asia [128], show infections spreading over vast regions and even crossing continents [11].

Globalization of trade and travel is one key factor driving the emergence of vector-borne diseases; heterogeneous structure also plays an important role in infectious disease dynamics [61]. A pathways analysis [62] has shown RVF virus may be introduced into the United States in various ways [62, 65] and identified several regions of the United States that are most susceptible to RVF virus introduction. Therefore, effective models must be developed to better understand potential dynamics of RVF in heretofore unaffected regions in case this virus appears in the Western hemisphere [46]. Such preparedness can assist in the avoidance of rapid spread of the virus throughout North America, as occurred with West Nile virus since 1999 [24, 46].

Spatially structured models, such as metapopulation models or multiple-patch models

are commonly used in epidemiological modeling to capture the roles of heterogeneity in space [100]. Metapopulation models describe systems containing spatially discrete subpopulations connected by the movement of individuals between a set of patches or nodes [53, 111]. Modeling the dynamics of large metapopulations is complex, presenting challenges during analysis [12]. One approach considers the mobility of individuals between discrete regions [12], creating a directed network where each node represents a subpopulation in a location. Links are placed between two locations if possibility of transmission exists, such as movement or proximity [16]. Network models are commonly used in epidemiology to understand the spread of infectious diseases through connected populations [85, 119]. The importance of tracking mobility rates and movement patterns is highlighted in the foot-and-mouth outbreak of 2001 in the United Kingdom [11]. In that case, infected cattle were widely distributed before the movement ban was announced [64], prompting necessary development of a transportation network capturing the spatial spread of foot-and-mouth disease [11].

Epidemiological modeling plays an important role in planning, implementing, and evaluating detection, control, and prevention programs [77]. Mathematical modeling is based on economic, clear and precise mathematical formulations, such as applications of differential, integral, or functional differential equations [77]. Mathematical models of infection transmission include interpretation of transmission processes and are often useful in answering questions that cannot be answered with only empirical data analysis [82], as well as assisting in the exploration of biological and critical ecological characteristics of disease transmission [76, 102]. A dynamic model of vector-borne diseases may be used to learn many characteristics of an outbreak such as the probability, size, and duration time of an epidemic, or the probability for the epidemic to die out [18] to improve understanding of disease transmission and persistence. Efficient mitigation strategies deduced from model results may stop an outbreak at early stages by reducing spreading parameters [18].

Many communicable diseases are propagated by two distinct mechanisms: vertical and

horizontal transmission [19]. Vertical transmission occurs when infection is passed from mother to a portion of offspring [19, 41], often transmitted by insect eggs and/or plant seeds [68]. A variety of diseases are transmitted vertically and horizontally, including the human diseases: rubella, hepatitis B, Chagas disease, and AIDS [21, 68]. Vertical transmission is a proven factor in the size and persistence of RVF epidemic [27]. The prevalence of vertical transmission establishes it as a crucial biological mechanism [21], potentially affecting infectious spreading in elaborate ways [6]. Therefore, vertical transmission maintains the spread of infection [6, 20]. The logical complement of vertical transmission is horizontal transmission. For animal and human diseases [68], horizontal transmission often occurs through direct or indirect contact with infectious hosts or infectious vectors, such as biting insects [68].

Numerical tools are commonly used to obtain quantitative results and analytic tools are used to understand model behaviors [10]. The reproduction number, defined as the average number of new infected individuals produced by one infectious individual, in a population with only susceptibles [38], is arguably the most important quantity in communicable disease modeling [38]. Theoretically, R_0 plays an important role in analyzing dynamics of an epidemic [38] and is commonly used to estimate the dynamics of emerging infectious diseases at the beginning of an outbreak, thus aiding in the design of control strategies for established infections [38]. If $R_0 > 1$, one infectious individual generally produces more than one infection, leading to the spread of an epidemic; whereas, on average, if $R_0 < 1$, one infectious individual generates less than one infection [30], and the epidemic may die out [37]. The same trajectory can always be observed with deterministic models given the same initial conditions [63]. The next generation matrix approach developed by [37], [36, Chapter 5] and popularized by [118] is one of many methods applied to compute R_0 for compartmental models. This method manages matrix size by including only infected and asymptomatically infected states [67]. The next generation matrix relates the number of new cases in various generations and provides the basis of defining and computing R_0 [38].

According to current knowledge, an insightful explicit expression of R_0 for complex transmission among multiple species in heterogeneous environments has not yet been presented.

If it is possible for an epidemic to reoccur, a real world epidemic does not allow observation of the same infection happening to the same person at the same time [63]. Moreover, deterministic models have the disadvantage that the number of infected individuals may go to less than one [74], as compared with stochastic models. Markov chain models are more realistic because they take only integer values instead of continuously varying quantities [74] and take into account chances by approximating or mimicking random or probabilistic factors. The last infectious individual may recover before the infection is transmitted to other susceptible individuals, resulting in disease extinction [74]. Consequently, an infection introduced to a completely susceptible population may not invade the system even if $R_0 > 1$ [74]. The extinction threshold, E_0, and probability of disease extinction are of interest. Bienaymé-Galton-Watson branching processes are commonly used to study disease extinction involving multi-type infections.

Deriving relationships between R_0 and E_0 is a complex task for vector-borne diseases transmitted on heterogeneous networks due to many parameters and large matrices. According to current knowledge, very little research has been conducted in this field.

1.3 State of Art

An RVF risk mapping model [7] developed by Anyamba et al. successfully predicted areas where outbreaks of RVF in humans and animals were expected using climate data for the Horn of Africa from December 2006 to May 2007 according to sea surface temperature (SST) patterns, cloud cover, rainfall, and ecological indicators (primarily vegetation). Current mathematical RVF virus transmission models are useful in representing infection transmission process [82] but are limited in determining and testing relevant risk factors. For the Ferlo area of Senegal, a pond-level metapopulation model, which only considered vectors, was developed assuming *Aedes* mosquitoes were the only vector and rainfall was the

only driving force [43]. RVF virus was predicted to persist only if livestock moved between ponds and rainfall did not occur in all ponds simultaneously [43]. Very few mathematical dynamic transmission models have explored mechanisms of RVF virus circulation [82] on a larger geographical scale. A theoretical model in a closed system including *Aedes* and *Culex* mosquitoes and livestock population was proposed [46]. The key result was RVF virus can persist in a closed system for ten years if the contact rate between hosts and vectors is high [46, 82]. Another theoretical RVF virus transmission mathematical model [84] modified the model in [46] by adding human hosts, merging all mosquitoes into one class, and removing mosquito egg compartment and vertical transmission of mosquitoes. Results showed that the disease prevalence in mosquitoes is sensitive to mosquito death rate, while disease prevalence in livestock and humans is sensitive to livestock and human recruitment rates [84]. An ordinary differential equation (ODE) metapopulation involving livestock and human mobility [89] analyzed the likelihood of pathogen establishment and provided hypothesized examples to illustrate the methodology [89]. A three-patch model studied the spread of RVF during the process in which animals enter Egypt from Sudan, are moved up the Nile, and are then consumed at population centers [47].

The limited work on R_0 for metapopulations with vertical transmission discovered during this research included the modeling of horizontal and vertical transmission dynamics of a parasite with one ODE for infection due to vertical transmission and one ODE for infection due to horizontal transmission [73]. In this special case, R_0 is the sum of the reproduction numbers for both types of transmission, and does not hold for a more complicated situation, such as the model [131] in which the next generation matrices for the two types of transmission are not both scalars.

Lloyd [74] reviewed theory of branching processes and computed extinction probability using branching processes for Ross malaria model [101] taking into account stochasticity and heterogeneity. Pénisson [92] presented several statistical tools to study extinction of populations consisted of different types of individuals. Allen and Lahodny Jr [4] computed

reproduction numbers for deterministic models, and extinction thresholds for corresponding continuous-time Markov chain (CTMC) models using continuous-time branching processes, and derived relationships between the two thresholds. A CTMC model is a stochastic counterpart of a deterministic ODE model [4]. Lahodny Jr and Allen [66] estimated probability of disease extinction for a Susceptible-Infected-Susceptible (SIS) multipatch model and illustrated differences between thresholds for deterministic models and stochastic models numerically. Allen and van den Driessche [5] established connections between extinction thresholds for continuous-time models and discrete-time models and illustrated the relations through numerical simulations. Although probability of disease extinction is defined as the probability for the number of infections to become zero when time goes to infinity, various numerical approximations for many types of models within finite time showed agreement with predicted extinction probability using branching processes [4, 5, 66].

1.4 Contribution and Organization

In this dissertation, spatial and temporal evolution of vector-borne diseases was studied using metapopulation models and important epidemic thresholds, R_0 and E_0, were derived. A metapopulation is considered as a network with nodes representing subpopulations in different nodes, links placed between a pair of nodes if possibility of transmission exists, and weights identifying differences between various pair of links.

1.4.1 Contribution

This dissertation includes theoretical and numerical analysis of vector-borne diseases. The contribution is as follows:

1. Vertical transmission, a crucial biological mechanism, which is ignored by most modelers, was incorporated into the models, although complexity of solving or analyzing the models was increased.

2. The spatial and temporal propagation of RVF were modeled accurately by considering heterogeneous environments in various locations.

3. The timing and trends of epidemic in three provinces of South Africa were reproduced, which is beyond the scope of a model for homogeneous populations.

4. Outcomes (human and cattle cases and timing of the epidemic characteristics) of the discrete-time model with stochastic parameters indicated which biotic factors will play an important role if RVF virus is introduced to the United States.

5. An explicit, easily applicable expression of the reproduction number considering vertical and horizontal transmission in a general multi-species, metapopulation model reduced the complexity of computing R_0 for diseases with complex transmission.

6. The bounds derived for an RVF metapopulation model facilitated predicting whether an RVF outbreak will invade a heterogeneous network.

7. Numerical simulation results for trends of R_0 varying with livestock movement rates provided guidelines on properly executing movement bans to control an RVF outbreak.

8. Novel relationships between extinction thresholds and reproduction numbers are analytically and numerically derived for vector-borne diseases transmitted on heterogeneous networks.

9. Consistent trends of extinction probability varying with disease parameters observed through extensive numerical simulations may improve understanding of thresholds for disease persistence and provide insights into mitigation strategies to increase disease extinction probability.

10. Key parameters in predicting uncertainty of the extinction threshold were identified using Latin Hypercube Sampling/Partial Rank Correlation Coefficient (LHS/PRCC) and their significances were ranked.

1.4.2 Organization

The metapopulation ODE model [131] presented in Chapter 2 included main vectors, *Aedes* and *Culex* mosquitoes, and main hosts, livestock and humans and movement of the populations. The simulation results reproduced spatial and temporal evolution of 2010 RVF outbreak in three provinces of South Africa.

A discrete-time RVF model [129] with parameters following PERT distributions was presented in Chapter 3. To investigate the role of starting location, and the size of initial infection in RVF virus spread, the proposed model was applied to a hypothetical RVF outbreak in the ranching areas of Texas on a 3621-node large network.

The reproduction number for diseases vertically and horizontally transmitted by multiple species on heterogeneous networks [130] was presented in Chapter 4. The explicit expression of the reproduction number was applied to an RVF metapopulation model on heterogeneous networks to study relationships between R_0 and parameters.

Relationships between R_0 and E_0 of corresponding CTMC models were analytically and numerically derived for vector-borne diseases in Chapter 5. The significance of parameters for determining uncertainty of the extinction threshold was ranked by Latin Hypercube Sampling/Partial Rank Correlation Coefficient. The relationships between the probability of extinction and parameters were numerically explored.

Chapter 2

Modeling Rift Valley Fever Virus Transmission on Small Networks

Rift Valley fever virus has been expanding geographical distribution with resulting crucial implications for health of humans and animals. Emergence of RVF in the Middle East and its continuing presence in many areas of Africa, has negatively impacted medical and veterinary infrastructures and human morbidity, mortality, and economic endpoints. Furthermore, worldwide attention should be directed towards broader infection dynamics of RVF virus because suitable hosts, vectors, and environmental conditions for additional epidemics likely exist on other continents, including Asia, Europe, and America.

In this chapter, we present a model incorporating *Aedes* and *Culex* mosquito vector, and livestock and human host populations based on weighted contact networks in which nodes represent geographical regions and weights represent contact level between regional pairs for each vector or host species. Environmental factors such as rainfall, temperature, wind, and evaporation are incorporated into the model. For each subpopulation, a system of ODEs describes dynamics of the population in a specific geographical location and transitions among different compartments, after contacting RVF virus. The model is tested using the 2010 RVF outbreak in three South African provinces: Free State, Northern Cape, and Eastern Cape as a case study. An extensive set of simulation results shows potential of the proposed approach to accurately describe the spatial-temporal evolution of RVF epidemics.

This chapter is organized as follows: Section 2.1 describes the compartmental mathematical model, Section 2.2 introduces the case study using outbreak data from South Africa, 2010, and Section 2.3 concludes this research.

2.1 Model Formulation

Compartmental models for RVF virus transmission among homogeneous populations and heterogeneous networks are presented in this chapter. See Table 2.1 for parameters and values used in numerical simulations.

2.1.1 Homogeneous Population Model

Rift Valley fever virus transmission between different species is depicted in Figure 2.1. Primary vectors, *Aedes* and *Culex* mosquitoes and primary hosts, livestock and humans are considered in the model. *Aedes* and *Culex* mosquitoes discussed here only include competent vectors of RVF. Transmission dynamics of vector are described by Susceptible-Exposed-Infected (SEI) model and transmission dynamics of hosts are described by Susceptible-Exposed-Infected-Removed (SEIR) model. Infectious *Aedes* mosquitoes not only transmit RVF virus to susceptible livestock and humans, but also to their own eggs [46, 72]. *Culex* mosquitoes acquire RVF virus during blood meals on an infected animal and then amplify the transmission while feeding on livestock and humans [127]. Direct ruminant-to-human contact is the primary way for humans to acquire the infection [7, 33]. Accidental RVF virus infections have been recorded in laboratory staff handling blood and tissue from infected animals [7]. Typically humans are considered dead-end hosts that do not contribute significantly to propagation of the epidemic [24]. No direct human-to-human transmission of RVF virus in field conditions has been recorded thus far [62]. Mosquitoes will not spontaneously recover once they become infectious [46]. Livestock and humans either perish from the infection or recover [46]. All four species have a specified incubation period [127]. *Aedes* and *Culex* mosquitoes are distributed among susceptible S_a, exposed E_a, and infected I_a

compartments. The subscripts $a = 1$ and $a = 3$ represent *Aedes* and *Culex* mosquitoes, respectively. The size of each adult mosquito population is $N_1 = S_1 + E_1 + I_1$ for adult *Aedes* mosquitoes and $N_3 = S_3 + E_3 + I_3$ for adult *Culex* mosquitoes. Livestock and human hosts contain susceptible S_b, exposed E_b, infected I_b, and recovered R_b individuals. The subscripts $b = 2$ and $b = 4$ represent livestock and humans, respectively. The size of host populations is $N_b = S_b + E_b + I_b + R_b$. The four populations are modeled with carrying capacity K_1, K_2, K_3, K_4, respectively.

Parameter	Description	Value	Dimension	Source
β_{12}	contact rate: *Aedes* to livestock	0.002	1/day	[46]
β_{21}	contact rate: livestock to *Aedes*	0.0021	1/day	[46]
β_{23}	contact rate: livestock to *Culex*	0.000003	1/day	[46]
β_{32}	contact rate: *Culex* to livestock	0.00001	1/day	[46]
β_{14}	contact rate: *Aedes* to humans	0.000046	1/day	Assume
β_{24}	contact rate: livestock to humans	0.00017	1/day	[84]
β_{34}	contact rate: *Culex* to humans	0.0000001	1/day	Assume
γ_2	recovery rate in livestock	0.14	1/day	[46]
γ_4	recovery rate in humans	0.14	1/day	[106–108]
d_1	death rate of *Aedes* mosquitoes	0.025	1/day	[46]
d_2	death rate of livestock	1/3650	1/day	[46]
d_3	death rate of *Culex* mosquitoes	0.025	1/day	[46]
d_4	death rate of humans	1/18615	1/day	[106–108]
b_1	number of *Aedes* eggs laid per day	0.05	1/day	[46]
b_2	birth rate of livestock	0.0028	1/day	[46]
b_3	number of *Culex* eggs laid per day	weather dependent	1/day	[52]
b_4	daily birth rate of humans	1/14600	1/day	[106–108]

Continued on next page

Table 2.1 – continued from previous page

Parameter	Description	Value	Dimension	Source
$1/\epsilon_1$	incubation period in *Aedes* mosquitoes	6	days	[46]
$1/\epsilon_2$	incubation period in livestock	4	days	[46]
$1/\epsilon_3$	incubation period in *Culex* mosquitoes	6	days	[46]
$1/\epsilon_4$	incubation period in humans	4	days	[127]
μ_2	mortality rate in livestock	0.0312	1/day	[46]
μ_4	mortality rate in humans	0.0001	1/day	[106–108]
q_1	transovarial transmission rate in *Aedes*	0.05	-	[46]
$1/\theta_1$	development time of *Aedes*	15	days	[46]
θ_3	development rate of *Culex*	weather dependent	1/day	[52]
K_1	carrying capacity of *Aedes* mosquitoes	1000000000	-	[88]
K_2	carrying capacity of livestock	10000000	-	Assume
K_3	carrying capacity of *Culex* mosquitoes	1000000000	-	[88]
K_4	carrying capacity of humans	10000000	-	Assume
f	fraction of people working with animals	0.82	-	[87]
τ	return rate	3	times/day	[14]
p	reduction in ω_{2ij} due to infection	$\frac{1}{2}$	-	Assume

Table 2.1: Parameters of the compartmental Rift Valley fever models.

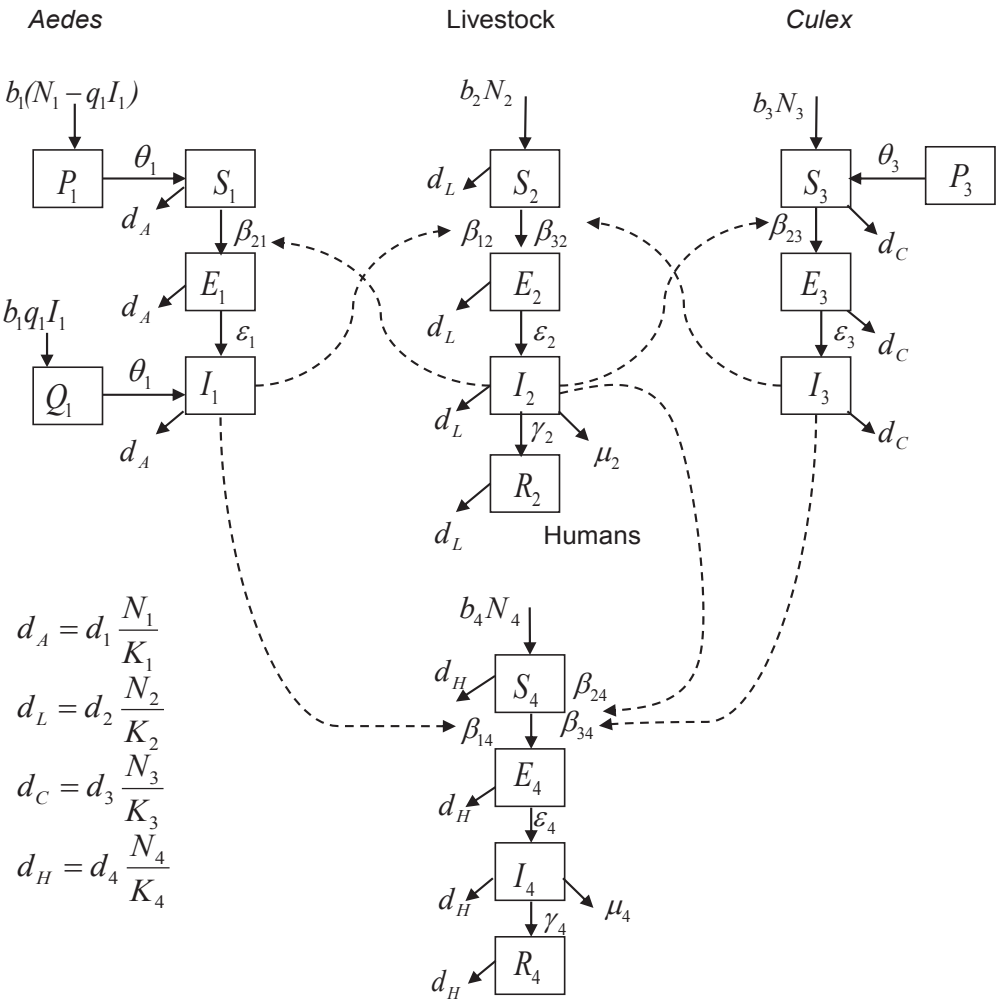

Figure 2.1: *Flow diagram of Rift Valley fever virus transmission with each species, namely, Aedes* mosquitoes, *Culex* mosquitoes, livestock, and humans homogeneously mixed (solid lines represent transition between compartments and dashed lines represent transmission between different species).

Aedes Mosquito Population Model

$$\begin{aligned}
\frac{dP_1}{dt} &= b_1 (N_1 - q_1 I_1) - \theta_1 P_1 \\
\frac{dQ_1}{dt} &= b_1 q_1 I_1 - \theta_1 Q_1 \\
\frac{dS_1}{dt} &= \theta_1 P_1 - \beta_{21} S_1 I_2 / N_2 - d_1 S_1 N_1 / K_1 \\
\frac{dE_1}{dt} &= \beta_{21} S_1 I_2 / N_2 - \varepsilon_1 E_1 - d_1 E_1 N_1 / K_1
\end{aligned} \tag{2.1}$$

$$\frac{dI_1}{dt} = \theta_1 Q_1 + \varepsilon_1 E_1 - d_1 I_1 N_1 / K_1$$
$$\frac{dN_1}{dt} = \theta_1 (P_1 + Q_1) - d_1 N_1 N_1 / K_1$$

where:

P_1 = the number of uninfected *Aedes* mosquito eggs,

Q_1 = the number of infected *Aedes* mosquito eggs,

S_1 = the number of susceptible *Aedes* mosquitoes,

E_1 = the number of exposed *Aedes* mosquitoes,

I_1 = the number of infected *Aedes* mosquitoes,

N_1 = the total number of *Aedes* mosquitoes.

The above model is a modified SEI model, including compartments P and Q, which represent uninfected eggs and infected eggs, respectively. Infected eggs are produced at a rate $b_1 q_1 I_1$ and uninfected eggs are produced at a rate $b_1 N_1 - b_1 q_1 I_1$. *Aedes* eggs develop into susceptible adult mosquitoes at a rate $\theta_1 P_1$ and develop into infected adult mosquitoes at a rate $\theta_1 Q_1$. Natural death rate for compartment X is $d_1 X_1 N_1 / K_1$, where X represents P, Q, S, E, and I. The rate at which *Aedes* mosquitoes are infected by livestock is $\beta_{21} S_1 I_2 / N_2$. Exposed *Aedes* mosquitoes transfer to infected compartment at a rate $\varepsilon_1 E_1$.

Culex Mosquito Population Model

$$\begin{aligned}
\frac{dP_3}{dt} &= b_3 N_3 - \theta_3 P_3 \\
\frac{dS_3}{dt} &= \theta_3 P_3 - \beta_{23} S_3 I_2 / N_2 - d_3 S_3 N_3 / K_3 \\
\frac{dE_3}{dt} &= \beta_{23} S_3 I_2 / N_2 - \varepsilon_3 E_3 - d_3 E_3 N_3 / K_3 \\
\frac{dI_3}{dt} &= \varepsilon_3 E_3 - d_3 I_3 N_3 / K_3 \\
\frac{dN_3}{dt} &= \theta_3 P_3 - d_3 N_3 N_3 / K_3
\end{aligned} \tag{2.2}$$

where:

P_3 = the number of uninfected *Culex* mosquito eggs,

S_3 = the number of susceptible *Culex* mosquitoes,

E_3 = the number of exposed *Culex* mosquitoes,

I_3 = the number of infected *Culex* mosquitoes,

N_3 = the total number of *Culex* mosquitoes.

Besides compartments S, E, and I, compartment P is added to represent uninfected eggs. Only uninfected eggs are included because female *Culex* mosquitoes do not transmit RVF virus vertically. Egg laying rate of *Culex* mosquitoes is b_3N_3. Natural death rate of *Culex* mosquitoes in compartment X is $d_3X_3N_3/K_3$, where X can be P, S, E, and I. *Culex* eggs develop into susceptible adult *Culex* mosquitoes at a rate θ_3P_3. Infection rate by livestock is $\beta_{23}S_3I_2/N_2$. Exposed *Culex* mosquitoes transfer into infected compartment at a rate ε_3E_3.

Livestock Population Model

$$\begin{aligned}
\frac{dS_2}{dt} &= b_2N_2 - d_2S_2N_2/K_2 - \beta_{12}S_2I_1/N_1 - \beta_{32}S_2I_3/N_3 \\
\frac{dE_2}{dt} &= \beta_{12}S_2I_1/N_1 + \beta_{32}S_2I_3/N_3 - \varepsilon_2E_2 - d_2E_2N_2/K_2 \\
\frac{dI_2}{dt} &= \varepsilon_2E_2 - \gamma_2I_2 - \mu_2I_2 - d_2I_2N_2/K_2 \\
\frac{dR_2}{dt} &= \gamma_2I_2 - d_2R_2N_2/K_2 \\
\frac{dN_2}{dt} &= b_2N_2 - d_2N_2N_2/K_2 - \mu_2I_2
\end{aligned} \tag{2.3}$$

where:

S_2 = the number of susceptible livestock,

E_2 = the number of exposed livestock,

I_2 = the number of infected livestock,

N_2 = the total number of livestock.

The birth rate and natural death rate of livestock are b_2N_2 and $d_2X_2N_2/K_2$, respectively.

Compartment X can be S, E, I, and R. The mortality rate due to RVF virus infection is $\mu_2 I_2$. The rates at which livestock are infected by *Aedes* mosquitoes and *Culex* mosquitoes are $\beta_{12} S_2 I_1/N_1$ and $\beta_{32} S_2 I_3/N_3$, respectively. The incubation rate and recovery rate are $\varepsilon_2 E_2$ and $\gamma_2 I_2$, respectively.

Human Population Model

$$\begin{aligned}
\frac{dS_4}{dt} &= b_4 N_4 - \beta_{14} S_4 I_1/N_1 - f\beta_{24} S_4 I_2/N_2 - \beta_{34} S_4 I_3/N_3 - d_4 S_4 N_4/K_4 \\
\frac{dE_4}{dt} &= \beta_{14} S_4 I_1/N_1 + f\beta_{24} S_4 I_2/N_2 + \beta_{34} S_4 I_3/N_3 - d_4 E_4 N_4/K_4 - \varepsilon_4 E_4 \\
\frac{dI_4}{dt} &= \varepsilon_4 E_4 - \gamma_4 I_4 - \mu_4 I_4 - d_4 I_4 N_4/K_4 \\
\frac{dR_4}{dt} &= \gamma_4 I_4 - d_4 R_4 N_4/K_4 \\
\frac{dN_4}{dt} &= b_4 N_4 - d_4 N_4 N_4/K_4 - \mu_4 I_4
\end{aligned} \tag{2.4}$$

where:

S_4 = the number of susceptible humans,

E_4 = the number of exposed humans,

I_4 = the number of infected humans,

N_4 = the total number of humans.

The birth rate and natural death rate for humans are $b_4 N_4$ and $d_4 X_4 N_4/K_4$, respectively. Compartment X can be S, E, I, and R. The mortality rate is $\mu_4 I_4$. The rates at which humans acquire RVF virus infection from *Aedes* mosquitoes, *Culex* mosquitoes, and livestock are $\beta_{14} S_4 I_1/N_1$, $\beta_{34} S_4 I_3/N_3$, and $f\beta_{24} S_4 I_2/N_2$, respectively. The assumption is made that only those who work with animals can be infected by animals. The coefficient f $(0 < f < 1)$ represents the fraction of humans working with animals. The incubation rate and mortality rate are $\varepsilon_4 E_4$ and $\gamma_4 I_4$, respectively.

Environmental Parameters for *Culex*

Equation (2.5) is used to model the development rate of *Culex* mosquitoes [52]. The daily egg laying rate in Equation (2.6) is a function of moisture [52]. Moisture in Equation (2.7) is obtained by summing the difference of precipitation [86] and evaporation (mm) [69] over the proceeding seven days [52]. In Equations (2.5) to (2.8), η, HA, HH, K, TH, E_{max}, E_{var}, E_{mean}, b_0 are parameters [52] described in Table 2.2. This model is specific for West Nile virus model in 2010 in the northern U.S. More appropriate parameters can be applied as they become available.

$$\theta_3(temp,t) = \eta * \frac{(temp(t)+K)}{298.15} * \frac{exp[\frac{HA}{1.987} * (\frac{1}{298.15} - \frac{1}{temp(t)+K})]}{1+exp[\frac{HH}{1.987} * (\frac{1}{TH} - \frac{1}{temp(t)+K})]}, \tag{2.5}$$

$$b_3(temp,prcp,T_d,t) = b_0 + \frac{Emax}{1+exp[-\frac{mois(t)-Emean}{Evar}]}, \tag{2.6}$$

$$mois(t) = \sum_{D=t-6}^{t} prcp(D) - evap(D), \tag{2.7}$$

$$evap(t) = \frac{700(temp(t)+0.006h)/(100-lat)}{80-temp(t)} + \frac{15(temp(t)-T_d(t))}{80-temp(t)}. \tag{2.8}$$

Here:

$temp(t)$ = air temperature in units of ^oC [69],

lat = the latitude (degrees) [69],

$T_d(t)$ = the mean dew-point in units of ^oC [69],

h = the elevation (meters) [69],

$prcp$ = daily precipitation [69],

K = Kelvin parameter [69].

2.1.2 Metapopulation Model

A metapopulation model is a model with several subpopulations. The assumption is made that homogeneity within each subpopulation and heterogeneity among different subpopu-

Parameter	Description	Value	Source
η	parameter of the development rate	0.25	[52]
HA	parameter of the development rate	28094	[52]
HH	parameter of the development rate	35692	[52]
TH	parameter of the development rate	298.6	[52]
b_0	minimum constant fecundity rate	3	[52]
E_{max}	maximum daily egg laying rate	3	[52]
E_{mean}	value at which moisture index=$0.5E_{max}$	0	[52]
E_{var}	the variance of the daily egg laying rate	12	[52]

Table 2.2: *Parameters in Equations* (2.5) *and* (2.6).

lations exist. The *Aedes* and *Culex* mosquitoes in location i ($i = 1, \cdots, n$), are distributed among susceptible S_{ai}, exposed E_{ai}, and infected I_{ai} compartments. The subscripts $a = 1$ and $a = 3$ represent *Aedes* and *Culex*, respectively. The size of each adult mosquito population in location i is $N_{1i} = S_{1i} + E_{1i} + I_{1i}$ for adult *Aedes* mosquitoes and $N_{3i} = S_{3i} + E_{3i} + I_{3i}$ for adult *Culex* mosquitoes. The livestock and human hosts contain susceptible S_{bi}, exposed E_{bi}, infected I_{bi}, and recovered R_{bi} individuals. The subscripts $b = 2$ and $b = 4$ represent livestock and humans, respectively. The size of host populations in location i is $N_{2i} = S_{2i} + E_{2i} + I_{2i} + R_{2i}$ for livestock hosts and $N_{4i} = S_{4i} + E_{4i} + I_{4i} + R_{4i}$ for human hosts. The four populations are modeled with a specified carrying capacity K_1, K_2, K_3, K_4, respectively.

Movement between Nodes

Weighted networks for each population are depicted in Figure 2.2. The subscripts ω_{kij} on the left-hand side of Equations (2.9), (2.10), and (2.11) represent the movement from node i to node j for species k, where $k = 1, 2, 3, 4$ represent *Aedes*, livestock, *Culex*, and humans, respectively. The difference in line thickness represents difference in weight. Thicker lines represent larger weight. The weight for each population is between 0 and 1. Rift Valley fever virus has been documented to be spread by wind [105] and wind dispersal of mosquitoes has changed geographic distribution and accelerated the spread of RVF virus to new geographic areas [62]. Some locations can become secondary epidemic sites after the virus has been

introduced (especially in irrigated areas, e.g., Gazeera in Sudan or rice valleys in the center of Madagascar) [81]. Livestock trade and transport can also affect geographic distribution of RVF [24]. One critical objective in developing effective models is to determine major factors involved in the disease propagation process. Therefore, the weights are parameterized due to mosquito movement with wind [28, 62], livestock movement due to transportation to feedlots or trade centers [110], and human mobility due to commuting [14], as shown in Equations (2.9), (2.10), and (2.11). The movement rate of infected livestock is reduced due to infection [127]. The wind data for the capital of each province are used as wind data [121] for the province. The distance vector is calculated with longitude and latitude in the center of each location. The weight for livestock movement network is a function of the number of animals sold [106] and the number of livestock in feedlots [90]. Distance, human population, commuting rate, and return rate [108] are taken into account for the weight of human movement network. The weight for mosquito movement network is a function of distance and the projection of wind in the direction of distance vector [28].

$$\omega_{1ij} = \omega_{3ij} = c_1 \frac{\vec{W}_i \cdot \vec{d_{ij}}}{|\vec{d_{ij}}|} \frac{1}{|\vec{d_{ij}}|}, \tag{2.9}$$

$$\omega_{2ij} = c_2 \frac{FM_j}{FM_i} \frac{1}{|\vec{d_{ij}}|}, \tag{2.10}$$

$$\omega_{4ij} = \frac{\sigma_{ij}}{N_{4i}}, \tag{2.11}$$

$$\sigma_{ij} = c_3 \frac{N_{4i}^{\alpha} N_{4j}^{\gamma}}{e^{\beta |\vec{d_{ij}}|}}, \tag{2.12}$$

$$\omega_i = \sum_{j=1, j \neq i}^{n} \omega_{4ij}. \tag{2.13}$$

Here:

$\vec{W}_i$ = the wind vector in location i [28],

$\vec{d_{ij}}$ = the distance vector from location i to location j,

$\omega_{1ij}(t)$ = the weight for mosquitoes moving from location i to location j,

$\omega_{2ij}(t)$ = the weight for livestock moving from location i to location j,

$\sigma_{ij}(t)$ = the number of commuters between location i and location j,

FM_i = the number of animals in markets and feedlots in location i.

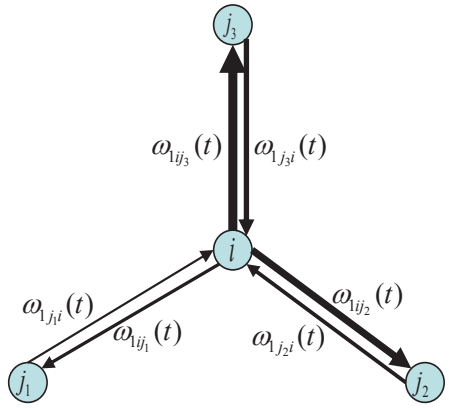

(a) *Aedes* movement due to wind

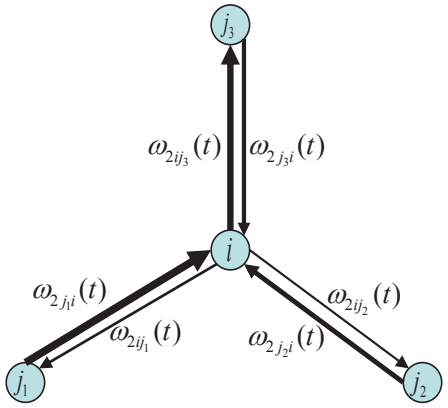

(b) Livestock movement network

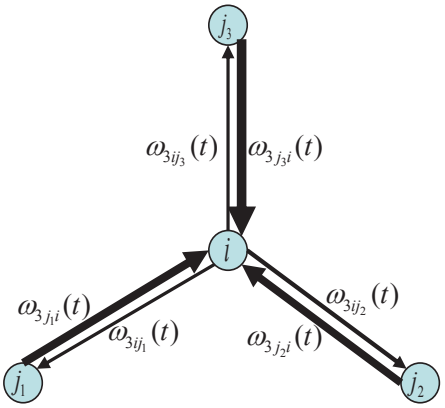

(c) *Culex* movement due to wind

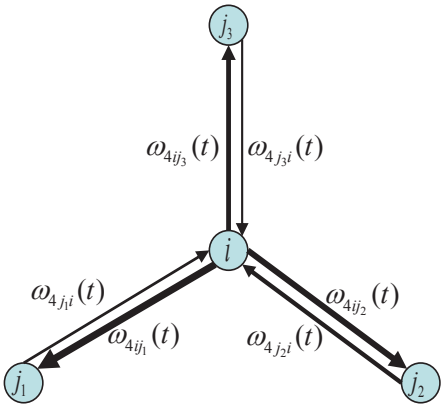

(d) Human movement due to commuting

Figure 2.2: *Network graphs for node i with three neighbors as an example. The assumption was made that mosquitoes and livestock stay in their destinations at each time step, but humans may return to source location.*

Aedes Movement between Nodes

$$\begin{aligned}
\frac{dP_{1i}}{dt} &= b_1\left(N_{1i} - q_1 I_{1i}\right) - \theta_1 P_{1i} \\
\frac{dQ_{1i}}{dt} &= b_1 q_1 I_{1i} - \theta_1 Q_{1i} \\
\frac{dS_{1i}}{dt} &= \theta_1 P_{1i} - \beta_{21} S_{1i} I_{2i}/N_{2i} - d_1 S_{1i} N_{1i}/K_1 + \sum_{j=1, j\neq i}^{n} \omega_{1ji} S_{1j} - \sum_{j=1, j\neq i}^{n} \omega_{1ij} S_{1i} \\
\frac{dE_{1i}}{dt} &= \beta_{21} S_{1i} I_{2i}/N_{2i} - \varepsilon_1 E_{1i} - d_1 E_{1i} N_{1i}/K_1 + \sum_{j=1, j\neq i}^{n} \omega_{1ji} E_{1j} - \sum_{j=1, j\neq i}^{n} \omega_{1ij} E_{1i} \\
\frac{dI_{1i}}{dt} &= \theta_1 Q_{1i} + \varepsilon_1 E_{1i} - d_1 I_{1i} N_{1i}/K_1 + \sum_{j=1, j\neq i}^{n} \omega_{1ji} I_{1j} - \sum_{j=1, j\neq i}^{n} \omega_{1ij} I_{1i} \\
\frac{dN_{1i}}{dt} &= \theta_1 (P_{1i} + Q_{1i}) - d_1 N_{1i} N_{1i}/K_1 + \sum_{j=1, j\neq i}^{n} \omega_{1ji} N_{1j} - \sum_{j=1, j\neq i}^{n} \omega_{1ij} N_{1i}
\end{aligned} \tag{2.14}$$

The change in the number of *Aedes* mosquitoes due to mobility in compartment X is given as $\sum_{j=1, j\neq i}^{n} \omega_{1ji} X_{1j} - \sum_{j=1, j\neq i}^{n} \omega_{1ij} X_{1i}$ [63].

Culex Movement between Nodes

$$\begin{aligned}
\frac{dP_{3i}}{dt} &= b_3 N_{3i} - \theta_3 P_{3i} \\
\frac{dS_{3i}}{dt} &= \theta_3 P_{3i} - \beta_{23} S_{3i} I_{2i}/N_{2i} - d_3 S_{3i} N_{3i}/K_3 + \sum_{j=1, j\neq i}^{n} \omega_{3ji} S_{3j} - \sum_{j=1, j\neq i}^{n} \omega_{3ij} S_{3i} \\
\frac{dE_{3i}}{dt} &= \beta_{23} S_{3i} I_{2i}/N_{2i} - \varepsilon_3 E_{3i} - d_3 E_{3i} N_{3i}/K_3 + \sum_{j=1, j\neq i}^{n} \omega_{3ji} E_{3j} - \sum_{j=1, j\neq i}^{n} \omega_{3ij} E_{3i} \\
\frac{dI_{3i}}{dt} &= \varepsilon_3 E_{3i} - d_3 I_{3i} N_{3i}/K_3 + \sum_{j=1, j\neq i}^{n} \omega_{3ji} I_{3j} - \sum_{j=1, j\neq i}^{n} \omega_{3ij} I_{3i} \\
\frac{dN_{3i}}{dt} &= \theta_3 P_{3i} - d_3 N_{3i} N_{3i}/K_3 + \sum_{j=1, j\neq i}^{n} \omega_{3ji} N_{3j} - \sum_{j=1, j\neq i}^{n} \omega_{3ij} N_{3i}
\end{aligned} \tag{2.15}$$

The change in the number of *Culex* mosquitoes in compartment X due to movement is given as $\sum_{j=1, j\neq i}^{n} \omega_{3ji} X_{3j} - \sum_{j=1, j\neq i}^{n} \omega_{3ij} X_{3i}$ [63].

Livestock Movement between Nodes

$$\frac{dS_{2i}}{dt} = b_2 N_{2i} - \beta_{12} S_{2i} I_{1i}/N_{1i} - \beta_{32} S_{2i} I_{3i}/N_{3i} - d_2 S_{2i} N_{2i}/K_2 + \sum_{j=1,j\neq i}^{n} \omega_{2ji} S_{2j} - \sum_{j=1,j\neq i}^{n} \omega_{2ij} S_{2i}$$

$$\frac{dE_{2i}}{dt} = \beta_{12} S_{2i} I_{1i}/N_{1i} + \beta_{32} S_{2i} I_{3i}/N_{3i} - \varepsilon_2 E_{2i} - d_2 E_{2i} N_{2i}/K_2 + \sum_{j=1,j\neq i}^{n} \omega_{2ji} E_{2j} - \sum_{j=1,j\neq i}^{n} \omega_{2ij} E_{2i}$$

$$\frac{dI_{2i}}{dt} = \varepsilon_2 E_{2i} - d_2 I_{2i} N_{2i}/K_2 - \gamma_2 I_{2i} - \mu_2 I_{2i} + p \sum_{j=1,j\neq i}^{n} \omega_{2ji} I_{2j} - p \sum_{j=1,j\neq i}^{n} \omega_{2ij} I_{2i}$$

$$\frac{dR_{2i}}{dt} = \gamma_2 I_{2i} - d_2 R_{2i} N_{2i}/K_2 + \sum_{j=1,j\neq i}^{n} \omega_{2ji} R_{2j} - \sum_{j=1,j\neq i}^{n} \omega_{2ij} R_{2i}$$

$$\frac{dN_{2i}}{dt} = b_2 N_{2i} - d_2 N_{2i} N_{2i}/K_2 - \mu_2 I_{2i} + \sum_{j=1,j\neq i}^{n} \omega_{2ji} N_{2j} - \sum_{j=1,j\neq i}^{n} \omega_{2ij} N_{2i}$$

The change in the number of livestock due to movement is $\sum_{j=1,j\neq i}^{n} \omega_{2ji} X_{2j}$-$\sum_{j=1,j\neq i}^{n} \omega_{2ij} X_{2i}$ [63]. The assumption is made that the movement rate of the infected livestock is p ($0 < p < 1$) of livestock in other compartments. This value of the movement rate was selected in the absence of further information.

Human Movement between Nodes

$$\begin{aligned}\frac{dS_{4i}}{dt} &= b_4 N_{4i} - d_4 S_{4i} N_{4i}/K_4 - \frac{\beta_{14} S_{4i} I_{1i}/N_{1i}}{1+\sigma_i/\tau} - \frac{\beta_{24} f S_{4i} I_{2i}/N_{2i}}{1+\sigma_i/\tau} - \sum_{j=1,j\neq i}^{n} \frac{\beta_{14} S_{4i} I_{1j}/N_{1j}\sigma_{ij}/\tau}{1+\sigma_i/\tau} \\ &\quad - \frac{\beta_{34} S_{4i} I_{3i}/N_{3i}}{1+\sigma_i/\tau} - \sum_{j=1,j\neq i}^{n} \frac{\beta_{24} f S_{4i} I_{2j}/N_{2j}\sigma_{ij}/\tau}{1+\sigma_i/\tau} - \sum_{j=1,j\neq i}^{n} \frac{\beta_{34} S_{4i} I_{3j}/N_{3j}\sigma_{ij}/\tau}{1+\sigma_i/\tau} \\ \frac{dE_{4i}}{dt} &= \frac{\beta_{14} S_{4i} I_{1i}/N_{1i}}{1+\sigma_i/\tau} + \frac{\beta_{24} f S_{4i} I_{2j}/N_{2i}}{1+\sigma_i/\tau} + \frac{\beta_{34} S_{4i} I_{3i}/N_{3i}}{1+\sigma_i/\tau} + \sum_{j=1,j\neq i}^{n} \frac{\beta_{14} S_{4i} I_{1j}/N_{1j}\sigma_{ij}/\tau}{1+\sigma_i/\tau} - \varepsilon_4 E_{4i} \\ &\quad + \sum_{j=1,j\neq i}^{n} \frac{\beta_{24} f S_{4i} I_{2j}/N_{2j}\sigma_{ij}/\tau}{1+\sigma_{ij}/\tau} + \sum_{j=1,j\neq i}^{n} \frac{\beta_{34} S_{4i} I_{3j}/N_{3j}\sigma_{ij}/\tau}{1+\sigma_i/\tau} - d_4 E_{4i} N_{4i}/K_4 \\ \frac{dI_{4i}}{dt} &= \varepsilon_4 E_{4i} - \gamma_4 I_{4i} - \mu_4 I_{4i} - d_4 I_{4i} N_{4i}/K_4 \\ \frac{dR_{4i}}{dt} &= \gamma_4 I_{4i} - d_4 R_{4i} N_{4i}/K_4 \\ \frac{dN_{4i}}{dt} &= b_4 N_{4i} - d_4 N_{4i} N_{4i}/K_4 - \mu_4 I_{4i}\end{aligned}$$

Humans from location i can stay in location i or move to location j at time t [14]. Humans are infected by *Aedes* mosquitoes, *Culex* mosquitoes, and livestock at rates $\beta_{14}(S_{4ii}\frac{I_{1i}}{N_{1i}} +$

$\sum_{j=1,j\neq i}^{n} S_{4ij}\frac{I_{1j}}{N_{1j}}$) [14], $\beta_{34}(S_{4ii}\frac{I_{3i}}{N_{3i}}+\sum_{j=1,j\neq i}^{n}\beta_{34}S_{4ij}\frac{I_{3j}}{N_{3j}})$ [14], and $f\beta_{24}(S_{4ii}\frac{I_{2i}}{N_{2i}}+\sum_{j=1,j\neq i}^{n}S_{4ij}\frac{I_{2j}}{N_{2j}})$ [14], respectively.

Here:

S_{4ii} = the number of humans that are from location i and stay in location i at time t,

S_{4ij} = the number of humans that are from location i and stay in location j at time t ,

ω_{4ij} = commuting rate between subpopulation i and each of its neighbor j,

ω_i = daily total rate of commuting for population i.

Change in the number of susceptible humans that are from location i and stay in location i [14] is:

$$\frac{\partial S_{4ii}}{\partial t} = \sum_{j=1,j\neq i}^{n} \tau S_{4ij} - \sum_{j=1,j\neq i}^{n} \omega_{4ij} S_{4ii}.$$

Change in the number of susceptible humans that are from location i and stay in location j [14] is:

$$\frac{\partial S_{4ij}}{\partial t} = \omega_{4ij} S_{4ii} - \tau S_{4ij}.$$

Subpopulations S_{4ii} and S_{4ij} are relaxed to equilibrium values [14]:

$$S_{4ii} = \frac{S_{4i}}{1+\omega_i/\tau},$$
$$S_{4ij} = \frac{S_{4i}}{1+\omega_i/\tau}\omega_{4ij}/\tau.$$

2.2 Case Study: South Africa 2010 outbreaks

Incidence data for the South African RVF outbreak in 2010 was applied in this case study.

2.2.1 Incidence Data Analysis

Incidence data for animals are obtained from [39, 126], and incidence data for human subpopulations are collected from [35, 87]. In regard to animal data, sheep population is considered. Because granularity of human incidence data is provided at province level, each node in the network represents a province. Three provinces were selected: Free State (location 1), Northern Cape (location 2), and Eastern Cape (location 3) because they had the highest

levels of RVF incidence for humans. Curves of the incidence data are shown in Figure 2.3 using green histograms, while red curves represent simulations obtained with this model. The epidemic first began in Free State Province and later in Northern Cape Province, as shown in Figure 2.3. Sustained heavy rainfall likely triggered the outbreak, causing infected eggs to hatch in the Free State Province. Additionally, the numbers of animal and human cases in Eastern Cape Province are less than the corresponding numbers in the other two provinces.

2.2.2 Sensitivity Analysis

Three parameters c_1, c_2, and c_3, are estimated using the least square approach based on minimization of errors between incidence data of humans and percentage of humans calculated by the mathematical model. The solutions are $c_1 = 0.009$, $c_2 = 0.05$, and $c_3 = 0.005$. The objective function is:

$$F = \sum_{t=t_0}^{t_f} \sum_{i=1}^{n} [(I_{4i}(t) - PR_{4i}(t))^2], \tag{2.16}$$

where

n = the number of nodes,

t_0 = starting time,

t_f = end time,

$I_{4i}(t)$ = human prevalence calculated by the model,

$PR_{4i}(t)$ = human prevalence reported.

To conduct a sensitivity analysis for parameters c_1, c_2, and c_3 in Equations (2.9), (2.10), and (2.12), each parameter was varied within $\pm 10\%$ of the values $c_1 = 0.009$, $c_2 = 0.05$, and $c_3 = 0.005$, while keeping other parameters constant. This analysis allows an evaluation on impacts of parameters on model outputs. The proportion of infected humans obtained from simulation at time t with $c_1 = 0.009$, $c_2 = 0.05$, and $c_3 = 0.005$ is denoted by $I_{Oi}(t)$. The proportion of infected humans obtained from simulation with parameters varying within

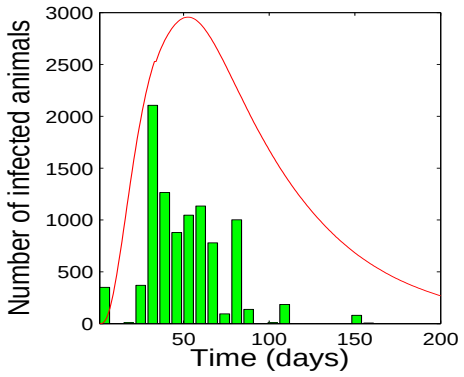

(a) Simulation results and incidence data for sheep in Free State Province

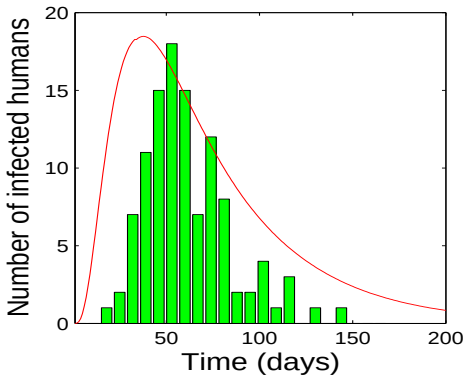

(b) Simulation results and incidence data for humans in Free State Province

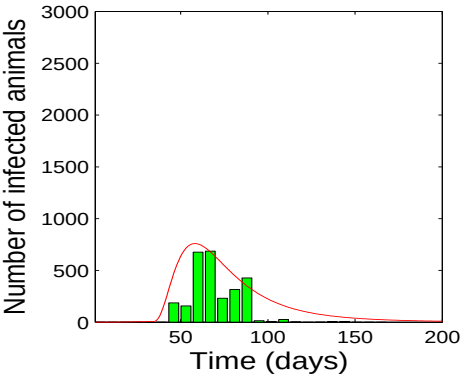

(c) Simulation results and incidence data for sheep in Northern Cape Province

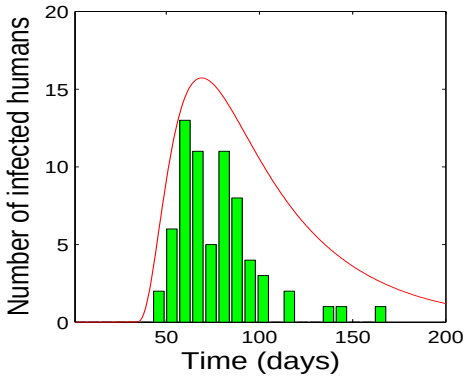

(d) Simulation results and incidence data for humans in Northern Cape Province

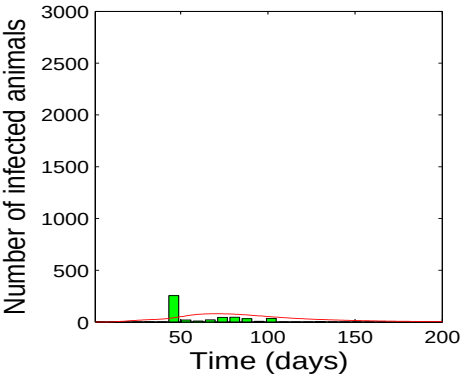

(e) Simulation results and incidence data for sheep in Eastern Cape Province

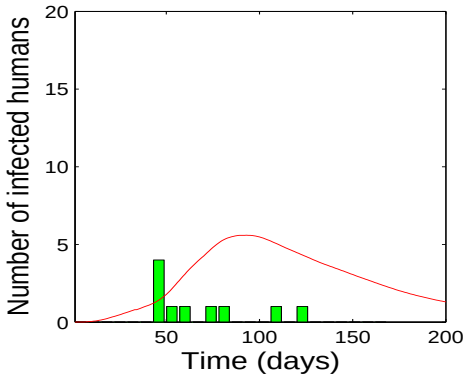

(f) Simulation results and incidence data for humans in Eastern Cape Province

Figure 2.3: *Simulation results and incidence data from January,* 2010 *in South Africa (bars represent data and lines represent simulation results).*

$\pm 10\%$ of bound is represented by $I_{4i}(t)$. Relative errors between the proportion of infected humans are calculated for each set of parameters in each location at time t as $|\frac{I_{4i}(t)-I_{Oi}(t)}{I_{4i}(t)}|$. Relative errors, lower bound, and upper bound of the parameters are shown in Figure 2.4.

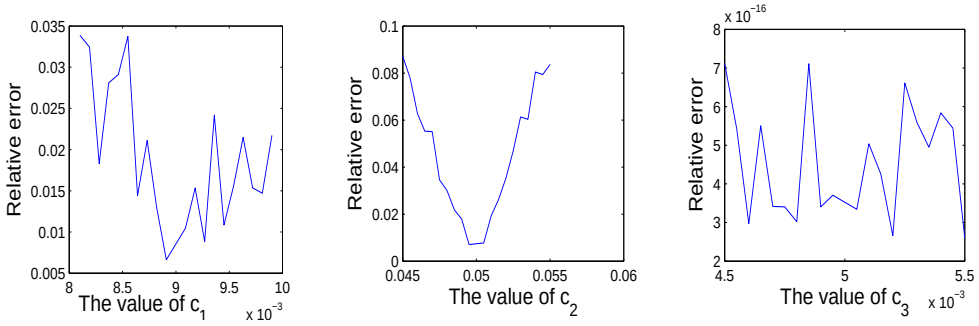

(a) Relative error of the number of infected humans with different value of c_1

(b) Relative error of the number of infected humans with different value of c_2

(c) Relative error of the number of infected humans with different value of c_3

Figure 2.4: *Relative errors of the fraction of infected humans with varying one of the parameters c_1, c_2, and c_3.*

All values of relative errors shown in Figure 2.4 are smaller than 10%, proving the model is robust with limited uncertainties in the parameter estimation. The rest of the parameters, such as contact rates β_{12}, β_{21}, β_{23}, β_{32}, death rates d_1, d_3, and recovery rate γ_2 are key parameters of determining uncertainty of the model output tested by Latin Hypercube Sampling/Partial Rank Correlation Coefficient [46]. Similarly, β_{14}, β_{24}, β_{34}, and γ_4 are also key parameters for determining uncertainty of the model output.

2.2.3 Analysis of Simulation Results

The role of movement in the spread of RVF spread was numerically analyzed while changing movement rates. If initial numbers of infected eggs are: $Q_{11} = 10$, $Q_{12} = 0$, and $Q_{13} = 0$ and c_1, c_2, and c_3 are not all equal to zero, then infected animals and humans appear in each province, as shown in Figure 2.5.

If initial number of infected eggs in each node remained the same and the assumption was made that movement is not allowed, i.e., $c_1 = 0$, $c_2 = 0$, and $c_3 = 0$, then the numbers

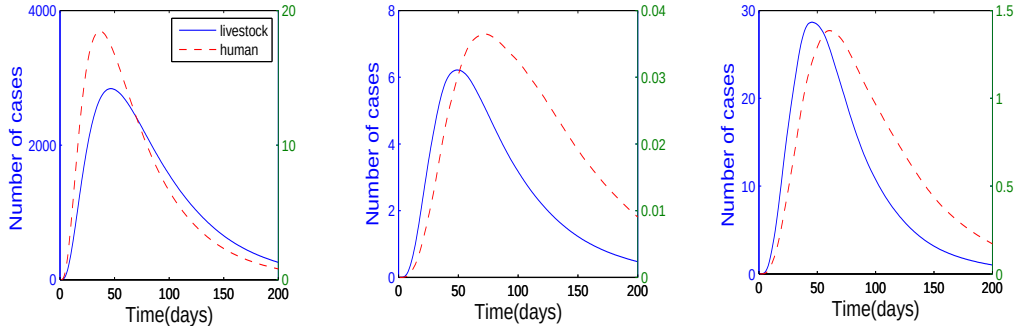

(a) Free State Province (b) Northern Cape Province (c) Eastern Cape Province

Figure 2.5: *Simulation results with nonzero movement weights (solid lines represent livestock with y-axis on the left and dashed lines represent humans with y-axis on the right).*

of infected animals and humans remain zero in the other two nodes, as shown in Figure 2.6. Mitigation strategy, such as a movement ban, can be tested and simulations reproduced RVF outbreak in three South African provinces by this model, as shown in Figure 2.3. The model can identify the maximum number of infected individuals among the three provinces and it reproduces the timing of the outbreak, which is beyond the scope of a model for homogeneous populations.

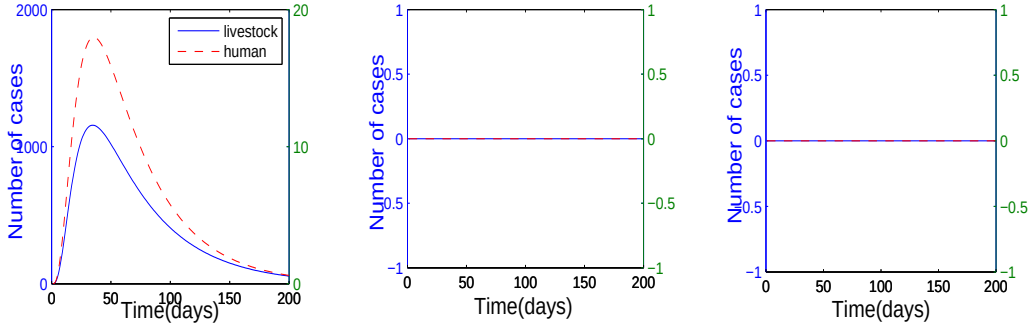

(a) Free State Province (b) Northern Cape Province (c) Eastern Cape Province

Figure 2.6: *Simulation results with $c_1 = c_2 = c_3 = 0$ (solid lines represent livestock with y-axis on the left and the dashed lines represent humans with y-axis on the right).*

Animal incidence curves produced by the model were an overestimation of the data since underreporting is very common during outbreaks. The incidence data for Eastern

Cape Province may be better approximated by a stochastic model according to the law of large numbers. The model has shown the ability of fitting the incidence data, reproducing timing and trend of RVF outbreak.

2.3 Discussions

A compartmental ODE model was presented to describe spread of RVF virus in time and space, with the latter driven as a function of contact networks. Main vectors and hosts of RVF were included in the model. The model was based on weighted contact networks in which nodes represent geographical regions and weights represent level of contact between regional pairings for each set of species. Parameters representing mosquito propagation and development are not constant but are functions of climate factors. The model was tested, calibrated, and evaluated using data from the recent 2010 RVF outbreak in South Africa, mapping the epidemic spread within and among three South African provinces. Not only was the starting time reproduced, but trends of RVF virus transmission with time in various locations were also reproduced. The model showed to be very promising notwithstanding data limitation. An extensive set of simulation results showed the potential of proposed model for accurately describing the RVF spreading process in additional regions of the world.

Chapter 3

Modeling Rift Valley Fever Virus Transmission on Large Networks

In the event RVF virus is introduced to the U.S. or other non-endemic areas, understanding potential patterns of spread and risk areas based on disease vectors and hosts will be vital for developing mitigation strategies.

Due to a lack of empirical data on disease vector species and their vector competence, a discrete-time epidemic model with stochastic parameters following several PERT distributions is developed to model dynamic interactions between hosts and likely North American mosquito vectors in dispersed geographic areas. Spatial effects and climate factors are also addressed in the model. Simulations of the model are easily implemented, even for networks with thousands of nodes, and outputs of the model can easily be compared with incidence data, if available. The model is applied to a large directed asymmetric network of $3,621$ nodes to examine a hypothetical introduction to various counties of Texas, an important ranching area in the U.S. Network nodes represent livestock farms, livestock markets, and feedlots, and links represent cattle movements and mosquito diffusion between different nodes. Cattle and mosquito (*Aedes* and *Culex*) populations are treated with different contact networks to assess virus propagation. Heterogeneous aspects of the spreading are considered in the model through realistic modeling of the cattle movement among different types of nodes on the network.

The role of starting locations has been shown to be important in the final size of rinderpest epidemic [79]. To study the role of initial conditions, spread of RVF virus is assessed under various initial infection conditions (infected mosquito eggs, adults, or cattle).

This chapter is organized as follows. Section 3.1 presents the discrete-time model with stochastic parameters. In Section 3.2, the model is applied to study hypothetical outbreak in Texas, U.S. on a large network. Section 3.3 summarizes and discusses the findings.

3.1 Model Formulation

Aedes mosquitoes, *Culex* mosquitoes, livestock, and human populations are considered in the model. Movement of each population is represented by networks in which nodes represent locations and links represent movement flow between locations. For mosquito diffusion network, nodes represent farms and links represent mosquito diffusion from one farm to neighboring farms, with weights ω_{1ij}, and ω_{3ij} representing diffusion rates for *Aedes* and *Culex*, respectively. For livestock movement network, nodes represent farms, livestock markets, and feedlots and weights represent movement rates from node i to node j, denoted by ω_{2ij}. Mosquito and livestock networks are depicted in Figures 3.1(a) and 3.1(b), respectively.

The model is based on the RVF virus transmission flow diagram illustrated in [131]. Only mosquito species known to be competent vectors of RVF virus transmission are considered and are broadly grouped by *Aedes* and *Culex* genera mosquitoes. Adult *Aedes* and *Culex* populations are distributed among susceptible S_{ai}, exposed E_{ai}, and infected I_{ai} compartments, where subscripts $a = 1$ and $a = 3$ represent *Aedes* and *Culex* mosquitoes, respectively. Uninfected and infected mosquitoes eggs are represented by P_{ai} and Q_{ai}, respectively. Only uninfected *Culex* eggs are incorporated in the model, considering *Culex* mosquitoes do not display vertical transmission. Livestock and human hosts are likewise classified into compartments S_{bi}, E_{bi}, I_{bi}, and R_{bi}, where subscripts $b = 2$ and $b = 4$ represent livestock and humans, respectively. Ranges of parameters in the models are listed in Table 3.1. The description of each parameter is the same as the description for corresponding parameter in

Table 2.1 and omitted in this chapter and following chapters. Transitions to be discussed below are for location i at day t.

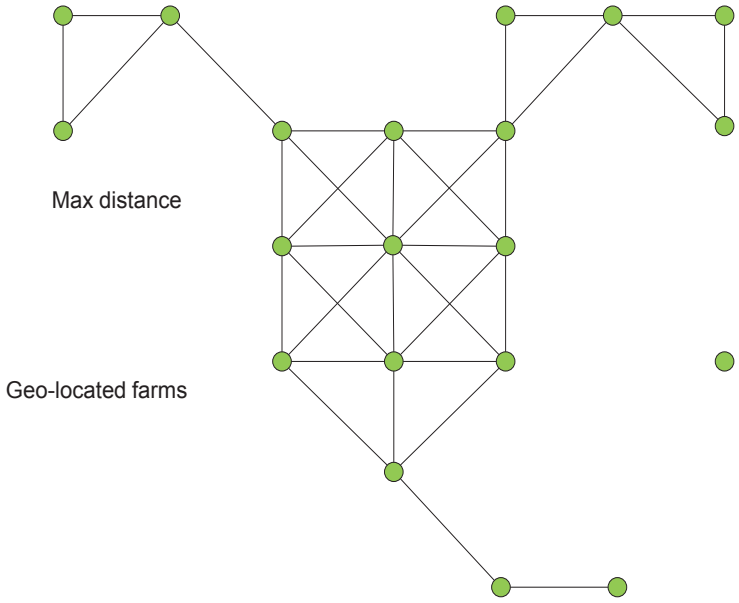

(a) An example of mosquito diffusion network

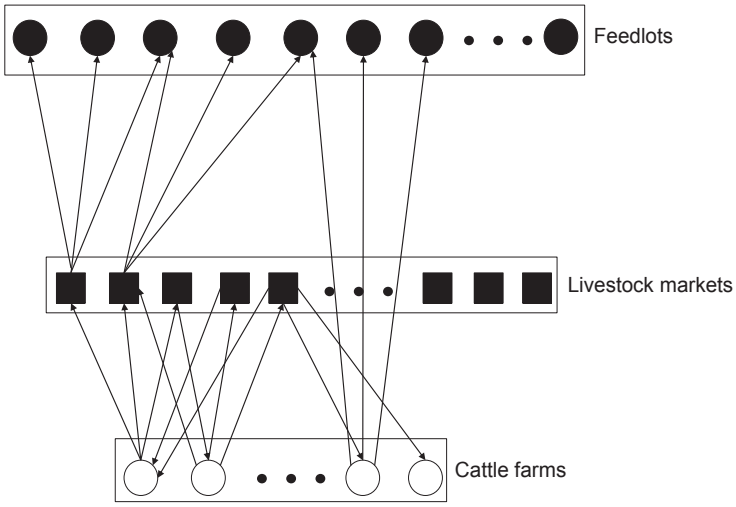

(b) An example of livestock movement network

Figure 3.1: *Mosquito diffusion and livestock movement networks.*

3.1.1 *Aedes* Population Model

$$
\begin{aligned}
P_{1i}(t+1) - P_{1i}(t) &= b_1(N_{1i}(t) - q_1 I_{1i}(t)) - \theta_1 P_{1i}(t)) \\
Q_{1i}(t+1) - Q_{1i}(t) &= b_1 q_1 I_{1i}(t) - \theta_1 Q_{1i}(t) \\
S_{1i}(t+1) - S_{1i}(t) &= \theta_1 P_{1i}(t) + \sum_{j=1, j\neq i}^{n} \omega_{1ji} S_{1j}(t) - \sum_{j=1, j\neq i}^{n} \omega_{1ij} S_{1i}(t) - d_1 S_{1i}(t) N_{1i}(t)/K_1 \\
&\quad - \beta_{21} S_{1i}(t) I_{2i}(t)/N_{2i}(t) \\
E_{1i}(t+1) - E_{1i}(t) &= \sum_{j=1, j\neq i}^{n} \omega_{1ji} E_{1j}(t) - \sum_{j=1, j\neq i}^{n} \omega_{1ij} E_{1i}(t) - d_1 E_{1i}(t) N_{1i}(t)/K_1 \\
&\quad + \beta_{21} S_{1i}(t) I_{2i}(t)/N_{2i}(t) - \varepsilon_1 E_{1i}(t) \\
I_{1i}(t+1) - I_{1i}(t) &= \sum_{j=1, j\neq i}^{n} \omega_{1ji} I_{1j}(t) - \sum_{j=1, j\neq i}^{n} \omega_{1ij} I_{1i}(t) + \theta_1 Q_{1i}(t) - d_1 I_{1i}(t) N_{1i}(t)/K_1 \\
&\quad + \varepsilon_1 E_{1i}(t) \\
N_{1i}(t+1) &= S_{1i}(t+1) + E_{1i}(t+1) + I_{1i}(t+1)
\end{aligned}
$$

The daily number of *Aedes* eggs laid is $b_1 N_{1i}(t)$, including $b_1 q_1 I_{1i}(t)$ infected eggs, and $b_1 N_{1i}(t) - b_1 q_1 I_{1i}(t)$ uninfected eggs. After the development period, $\theta_1 P_{1i}(t)$ uninfected eggs develop into susceptible adult *Aedes* mosquitoes and $\theta_1 Q_{1i}(t)$ infected eggs develop into infected adult *Aedes* mosquitoes. The number of *Aedes* mosquitoes infected by livestock is $\beta_{21} S_{1i}(t) I_{2i}(t)/N_{2i}(t)$. Following the incubation period, $\varepsilon_1 E_{1i}(t)$ *Aedes* mosquitoes transfer from exposed compartment to infected compartment. The number of *Aedes* mosquitoes dying naturally in compartment X is $d_1 X_{1i}(t)$. Change in the number of *Aedes* mosquitoes due to mobility in compartment X is $\sum_{j=1, j\neq i}^{n} \omega_{1ji} X_{1j}(t) - \sum_{j=1, j\neq i}^{n} \omega_{1ij} X_{1i}(t)$ [63].

3.1.2 *Culex* Population Model

$$
\begin{aligned}
P_{3i}(t+1) - P_{3i}(t) &= b_3(t)N_{3i}(t) - \theta_3(t)P_{3i}(t) \\
S_{3i}(t+1) - S_{3i}(t) &= \theta_3(t)P_{3i}(t) + \sum_{j=1,j\neq i}^{n} \omega_{3ji}S_{3j}(t) - \sum_{j=1,j\neq i}^{n} \omega_{3ij}S_{3i}(t) - d_3S_{3i}(t)N_{3i}(t)/K_3 \\
&\quad - \beta_{23}S_{3i}(t)I_{2i}(t)/N_{2i}(t) \\
E_{3i}(t+1) - E_{3i}(t) &= \sum_{j=1,j\neq i}^{n} \omega_{3ji}E_{3j}(t) - \sum_{j=1,j\neq i}^{n} \omega_{3ij}E_{3i}(t) - \varepsilon_3E_{3i}(t) - d_3E_{3i}(t)N_{3i}(t)/K_3 \\
&\quad + \beta_{23}S_{3i}(t)I_{2i}(t)/N_{2i}(t) \\
I_{3i}(t+1) - I_{3i}(t) &= \sum_{j=1,j\neq i}^{n} \omega_{3ji}I_{3j}(t) - \sum_{j=1,j\neq i}^{n} \omega_{3ij}I_{3i}(t) + \varepsilon_3E_{3i}(t) - d_3I_{3i}(t)N_{3i}(t)/K_3 \\
N_{3i}(t+1) &= S_{3i}(t+1) + E_{3i}(t+1) + I_{3i}(t+1)
\end{aligned}
$$

The daily number of *Culex* eggs laid is $b_3N_{3i}(t)$. After the development period, $\theta_3P_{3i}(t)$ eggs develop into susceptible adult *Culex* mosquitoes. After the incubation period, $\varepsilon_3E_{3i}(t)$ *Culex* mosquitoes transfer to infected compartment I. The number of *Culex* mosquitoes acquiring infection from livestock is denoted by $\beta_{23}S_{3i}(t)I_{2i}(t)/N_{2i}(t)$ and the number of *Culex* mosquitoes removed from compartment X due to natural death is $d_3X_{3i}(t)$. The percentage of *Culex* mosquitoes moving from location i to location j is ω_{3ij}. Change in the number of *Culex* mosquitoes due to movement in compartment X is $\sum_{j=1,j\neq i}^{n} \omega_{3ji}X_{3j}(t) - \sum_{j=1,j\neq i}^{n} \omega_{3ij}X_{3i}(t)$ [63].

3.1.3 Livestock Population Model

$$
\begin{aligned}
S_{2i}(t+1) - S_{2i}(t) &= b_2(t)\delta_b(i)N_{2i}(t) + \sum_{j=1,j\neq i}^{n} \omega_{2ji}S_{2j}(t) - \sum_{j=1,j\neq i}^{n} \omega_{2ij}S_{2i}(t) \\
&\quad - d_2\delta_d(i)S_{2i}(t)N_{2i}(t)/K_2 - \beta_{12}S_{2i}(t)I_{1i}(t)/N_{1i}(t) - \beta_{32}S_{2i}(t)I_{3i}(t)/N_{3i}(t) \\
E_{2i}(t+1) - E_{2i}(t) &= \sum_{j=1,j\neq i}^{n} \omega_{2ji}E_{2j}(t) - \sum_{j=1,j\neq i}^{n} \omega_{2ij}E_{2i}(t) - d_2\delta_d(i)E_{2i}(t)N_{2i}(t)/K_2 \\
&\quad - \varepsilon_2E_{2i}(t) + \beta_{12}S_{2i}(t)I_{1i}(t)/N_{1i}(t) + \beta_{32}S_{2i}(t)I_{3i}(t)/N_{3i}(t) \\
I_{2i}(t+1) - I_{2i}(t) &= p\sum_{j=1,j\neq i}^{n} \omega_{2ji}I_{2j}(t) - p\sum_{j=1,j\neq i}^{n} \omega_{2ij}I_{2i}(t) - d_2\delta_d(i)I_{2i}(t)N_{2i}(t)/K_2 \\
&\quad + \varepsilon_2E_{2i}(t) - \gamma_2I_{2i}(t) - \mu_2I_{2i}(t)
\end{aligned}
$$

$$R_{2i}(t+1) - R_{2i}(t) = \sum_{j=1,j\neq i}^{n} \omega_{2ji} R_{2j}(t) - \sum_{j=1,j\neq i}^{n} \omega_{2ij} R_{2i}(t) + \gamma_2 I_{2i}(t) - d_2 \delta_d(i) R_{2i}(t) N_{2i}(t)/K_2$$
$$N_{2i}(t+1) = S_{2i}(t+1) + E_{2i}(t+1) + I_{2i}(t+1) + R_{2i}(t+1)$$

The daily number of newborn livestock in location i is $b_2(t)N_{2i}(t)$. The variables $\delta_b(i)$ and $\delta_d(i)$ are used to identify different types of nodes. If location i is a farm, then $\delta_b(i) = 1$ and $\delta_d(i) = 1$. If location i is a market, then $\delta_b(i) = 0$ and $\delta_d(i) = 0$. If location i is a feedlot, then $\delta_b(i) = 0$ and $\delta_d(i) = 1$. The numbers of livestock infected by *Aedes* mosquitoes and *Culex* mosquitoes are denoted by $\beta_{12} S_{2i}(t) I_{1i}(t)/N_{1i}(t)$ and $\beta_{32} S_{2i}(t) I_{3i}(t)/N_{3i}(t)$, respectively. After the incubation period, $\varepsilon_2 E_{2i}(t)$ livestock transfer from exposed state to infected state. After the infection period, $\gamma_2 I_{2i}(t)$ livestock recover from RVF virus infection. The number of livestock deaths in compartment X is $d_2 X_{2i} N_{2i}(t)/K_2$ in which K_2 is the carrying capacity of livestock in each node. Change in the number of livestock in compartment X due to mobility is $\sum_{j=1,j\neq i}^{n} \omega_{2ji} X_{2j}(t) - \sum_{j=1,j\neq i}^{n} \omega_{2ij} X_{2i}(t)$ for livestock in compartments S, E, and R, and $p\sum_{j=1,j\neq i}^{n} \omega_{2ji} X_{2j}^{[m]}(t)$-$p\sum_{j=1,j\neq i}^{n} \omega_{2ij} X_{2i}^{[m]}(t)$ [63], $(0 < p < 1)$ for livestock in compartment I.

3.1.4 Human Population Model

$$S_{4i}(t+1) - S_{4i}(t) = -\beta_{14} S_{4i}(t) I_{1i}(t)/N_{1i}(t) - \beta_{24} S_{4i}(t) I_{2i}(t)/N_{2i}(t) - \beta_{34} S_{4i}(t) I_{3i}(t)/N_{3i}(t)$$
$$E_{4i}(t+1) - E_{4i}(t) = \beta_{14} S_{4i}(t) I_{1i}(t)/N_{1i}(t) + \beta_{24} S_{4i}(t) I_{2i}(t)/N_{2i}(t) + \beta_{34} S_{4i}(t) I_{3i}(t)/N_{3i}(t) - \varepsilon_4 E_{4i}(t)$$
$$I_{4i}(t+1) - I_{4i}(t) = \varepsilon_4 E_{4i}(t) - \gamma_4 I_{4i}(t)$$
$$R_{4i}(t+1) - R_{4i}(t) = \gamma_4 I_{4i}(t)$$

The number of humans in each node is constant because birth, death, mortality, and mobility of humans are not considered. The numbers of humans infected by *Aedes* mosquitoes, *Culex* mosquitoes, and livestock are $\beta_{14} S_{4i}(t) I_{1i}(t)/N_{1i}(t)$, $\beta_{24} S_{4i}(t) I_{2i}(t)/N_{2i}(t)$, and $\beta_{34} S_{4i}(t) I_{3i}(t)/N_{3i}(t)$, respectively. After the incubation period, $\varepsilon_4 E_{4i}(t)$ humans transfer

to infected compartment, and $\gamma_4 I_{4i}(t)$ humans recover from RVF virus infection after the infection period.

3.2 Case Study: Texas, the United States from 2005 to 2010

3.2.1 Networks in the Study Area

As a case study, various RVF virus introduction scenarios were tested using the model presented in Section 3.1 to determine hypothetical model outcomes (number of livestock cases and timing of the epidemic). Although the model accounts for exact locations when simulating RVF virus spread, that information is not reported or even discussed for ranches in areas smaller than county level. Exact farms and counties are well masked from the results. Texas cattle ranches were selected because of large cattle concentrations and available aggregate survey data for cattle movements in these areas [40].

A network with $3,526$ cattle farms, three livestock markets, and 92 cattle feedlots was constructed [117]. The cattle farms and livestock markets were located in one region and feedlots are located in another region. Each node was uniformly distributed in each county according to the total number of farms within that county [117]. The exact location of each farm was obscured because those data are not publicly available [99] due to confidentiality. The initial number of cattle in each farm is categorized as $0-9$, $10-19$, $20-49$, $50-99$, $100-199$, $200-499$, and more than 500 [117]. The initial number of susceptible cattle in each farm or feedlot for numerical simulation was assumed according to the number and histogram of cattle in each county in 2007 [117]. For cattle movement, if cattle were sold from one node to another, then a link was present between the nodes. Movement rate of cattle, ω_{2ij} shown in Table 3.2 was estimated based on aggregate movement rates from survey [40] and inversely proportional to the distance between source-destination pairs. Cattle movement rate refers to the average movement rate for all cattle at different ages, and movement rate of cattle in compartment I was assumed to be half the movement rate

Parameter	Range	Assumed most possible value	Dimension	Source
β_{12}	$(0.0021, 0.2762)$	0.1392	1/day	[22, 56, 59, 78, 96, 114, 115]
β_{21}	$(0.0021, 0.2429)$	0.1225	1/day	[22, 56, 59, 78, 96, 113]
β_{23}	$(0.0000, 0.3200)$	0.16	1/day	[56, 59, 78, 96, 113, 123]
β_{32}	$(0.0000, 0.096)$	0.04	1/day	[56, 59, 78, 96, 123]
β_{14}	$(0.001, 0.002)$	0.0015	1/day	Assume
β_{24}	$(0.00004, 0.00008)$	0.00006	1/day	Assume
β_{34}	$(0.0005, 0.001)$	0.000525	1/day	Assume
$1/\gamma_2$	$(2, 5)$	3.5	1/day	[42]
$1/\gamma_4$	$(4, 7)$	5.5	1/day	[84]
$1/d_1$	$(3, 60)$	31.5	days	[15, 83, 96]
$1/d_2$	$(360, 3600)$	1980	days	[97]
$1/d_3$	$(3, 60)$	31.5	days	[15, 83, 96]
b_1			1/day	[15, 83, 96]
b_2	d_2		1/day	[97]
b_3	weather dependent		1/day	[15, 83, 96]
$1/\epsilon_1$	$(4, 8)$	6	days	[114]
$1/\epsilon_2$	$(2, 6)$	4	days	[93]
$1/\epsilon_3$	$(4, 8)$	6	days	[114]
$1/\epsilon_4$	$(2, 6)$	4	days	[84]
μ_2	$(0.025, 0.1)$	0.0375	1/day	[42, 93]
q_1	$(0, 0.1)$	0.05	1/day	[45]
$1/\theta_1$	weather dependent		days	[96]
$1/\theta_3$	weather dependent		days	[52]
K_1	100000000		Assume	
K_2		1000000		Assume
K_3		100000000		Assume
p		$\frac{1}{2}$		Assume

Table 3.1: *Parameter ranges for numerical simulations.*

for cattle in compartments S, E, and R, namely, $p = \frac{1}{2}$.

Node i	Node j	Range	Source
farm	market	$60.7\% \ /(n_m(i) \times d_{ij})$	[40]
market	farm	$60.7\% \ /(n_f(i) \times d_{ij})$	[40]
farm	feedlot	$10.9\% \ /(n_{ffe}(i) \times d_{ij})$	[40]
market	feedlot	$10.9\% \ /(n_{mfe}(i) \times d_{ij})$	[40]
feedlot	farm	0	[40]
feedlot	market	0	[40]

Table 3.2: *Cattle movement rate ω_{2ij}, where $n_m(i)$=the number of markets connected to farm i, $n_f(i)$=the number of farms connected to market i, $n_{ffe}(i)$=the number of feedlots connected to farm i, $n_{mfe}(i)$=the number of feedlots connected to market i.*

For mosquito diffusion, if the distance between two farms was smaller than an assumed radius, two kilometers, then a link was present between the nodes in the network. The diffusion rates of *Aedes* and *Culex* mosquitoes are shown below [91].

$$\omega_{1ij} = \omega_{3ij} = \begin{cases} 0, & \text{if the nodes are disjoint,} \\ diff/d_{ij}^2, & \text{if two nodes share a border,} \end{cases}$$

where d_{ij} is the distance between the centers of node i and node j [91] and $diff$ is a diffusion-like parameter within the range $(830, 8300) m^2/\text{day}$ [91].

3.2.2 Parameters for Numerical Simulations

Vector competence varies within and between mosquito species [116]. Stochastic parameters were used to account for broad range of vector competence between *Aedes* and *Culex* species and individual variation within each species. PERT distribution has few constraints (minimum, maximum, and most likely value), similarly to triangular distribution applied in [124] to simulate West Nile virus epidemic. In the following simulations, PERT distributions were selected to generate stochastic parameters with ranges and the most likely values listed in Table 3.1. Any appropriate parameter distribution can be adapted into the model.

Egg laying rates of *Aedes* and *Culex* mosquitoes changing with moisture conditions as indicated in Equation (3.1) [52] are shown in Figure 3.2(a). Egg development rate of *Aedes* mosquitoes varying with temperature in Equation (3.2) [103] and that of *Culex* mosquitoes

in Equation (2.5) are in Figure 3.2(e) and Figure 3.2(b), respectively. Parameters for egg laying rates of *Aedes* mosquitoes and *Culex* mosquitoes, and parameters for egg development rate of *Culex* mosquitoes were derived from data concerning West Nile virus in 2010 in the Northern U.S. [52], and the parameters for egg development rate of *Aedes* mosquitoes are derived using the model for *Aedes* aegypti [103]. More precise parameters may be adopted as they become available. Egg laying rate of *Aedes* and *Culex* mosquitoes, egg development rate of *Culex* mosquitoes, and egg development rate of *Aedes* mosquitoes computed with climate data for the region where cattle farm and markets located in the study area of Texas from January 2005 to October 2010 are shown in Figure 3.2(c), Figure 3.2(d), and Figure 3.2(f), respectively. If temperature is too low, mosquito eggs will not develop into larvae and then adult mosquitoes. If temperature is too high, lifespan of the mosquitoes is shortened and the development rate decreases.

Moisture index is the difference between precipitation and evaporation, as shown in Equation (2.7). A lower moisture index corresponds to fewer adult mosquitoes because low moisture index represents a combination of low precipitation and high evaporation. Throughout the study time period, missing precipitation data from January 2005 to December 2010 [86] were assumed to be zero. Evaporation data were calculated using Equation (2.8) [69]. Parameters in Equations (2.5), (2.6), (3.1), and (3.2) are listed in Table 3.3, other parameters take the same values and meanings as corresponding parameters in Table 2.2 and the variables in Equations (3.1) and (3.2) share the same descriptions as those in Equations (2.5) and (2.6).

$$b_1(temp, prcp, T_d, t) = b_3(temp, prcp, T_d, t) = b_0 + \frac{Emax}{1 + exp[-\frac{Moisture(t) - Emean}{Evar}]}, \tag{3.1}$$

$$\theta_1(temp, t) = A_1 * \frac{(temp(t) + K)}{298.15} * \frac{exp[\frac{HA_1}{1.987} * (\frac{1}{298.15} - \frac{1}{temp(t)+K})]}{1 + exp[\frac{HH_1}{1.987} * (\frac{1}{TH_1} - \frac{1}{temp(t)+K})]}. \tag{3.2}$$

Although humans moved between nodes, they did not transmit virus between nodes, and the number of humans in each node (i.e., farm) was assumed to be fewer than 15.

Parameter	Description	Value	Source
A_1	parameter in Equation (3.2)	0.1546	[103]
HA_1	parameter in Equation (3.2)	$33,255.57$	[103]
HH_1	parameter in Equation (3.2)	$50,543.49$	[103]
TH_1	parameter in Equation (3.2)	301.67	[103]
b_0	minimum constant fecundity rate	0	[52]
$Emax$	maximum daily egg laying rate	20	[52]

Table 3.3: *Parameters in Equations (2.5), (2.6),* (3.1)*, and* (3.2).

3.3 Results and Discussions

A discrete-time compartmental mathematical model based on a network approach is presented. Rift Valley fever is transmitted by several species of mosquito vectors that have varying levels of vector competence. Therefore, modeling each genus and species combination requires information on vector competence, movement, and life stage development patterns, which are too complicated, whereas, considering only a single species or genus is inaccurate. Consequently, the species were loosely grouped as their genera and parameters were allowed to vary following PERT distributions. The distribution captured uncertainties in regards to inherent variability between species, as well as variability among individual mosquitoes. The mosquito parameters are modeled as functions of climate factors in order to reflect the impacts of weather and seasonality on mosquito population dynamics. Only *Aedes* and *Culex* genera mosquitoes that are competent vectors of RVF virus transmission were considered in the model.

Various networks were developed for mosquito diffusion and livestock movement, considering heterogeneity in both. In cattle movement network, different types of nodes are distinguished between sources, sinks, and transitions.

The easily solvable discrete-time model can be used to simulate networks with up to thousands of nodes. To use the model in any location, the initial populations, movement rates, parameter ranges, and climate factors in each location are needed to obtain epidemic curves.

Sixteen initial conditions shown in Table 3.4 in two regions of Texas from January 2005 to October 2010 were tested with the model to determine their impacts on the simulated and hypothetical spread of RVF virus. A farm with fewer than 10 cattle was identified as a small farm, while a farm with more than 500 cattle was identified as a large farm. Average results of 100 realizations for each scenario, starting in a small or large farm are presented qualitatively in Table 3.5, and quantitative numerical simulation results are shown in Table 3.6. If at least one cattle in a farm is infected, then the farm was defined to be infected. The outcome characteristics are classified as follows:

very small ($0 < A < 300$ or $0 < B < 320 \times 10^3$ or $0 < C < 3000$),

small ($300 \leqslant A < 350$ or $320 \times 10^3 \leqslant B < 350 \times 10^3$ or $3000 \leqslant C < 4000$),

average ($350 \leqslant A < 400$ or $350 \times 10^3 \leqslant B < 380 \times 10^3$ or $4000 \leqslant C < 4500$),

large ($400 \leqslant A < 600$ or $380 \times 10^3 \leqslant B < 400 \times 10^3$ or $4500 \leqslant C < 6000$),

very large ($A \geqslant 600$ or $B \geqslant 400 \times 10^3$ or $C \geqslant 6000$),

very short or really large ($0 < D < 700$ or $0 < E < 250$),

short ($700 \leqslant D < 1000$ or $250 \leqslant E < 300$),

medium ($1000 \leqslant D < 1200$ or $300 \leqslant E < 450$),

long ($1200 \leqslant D < 1300$ or $450 \leqslant E < 500$),

very long ($D \geqslant 1300$ or $E \geqslant 500$).

Here A represents the number of infected farms, B represents the cumulative number of infected cattle throughout simulation, C stands for the total number of infected cattle when the number of infected cattle farms is maximum, D stands for the time to peak number of infected farms, that is, the time it takes from the first day to the day on which the largest number of infected farms appears as shown in Figure 3.3, E represents epidemic duration, defined as the number of days with more than 60 infected cattle farms, F represents the peak number of farms with more than one infected human, and G represents the peak number of infected humans in a single farm in one day.

By choosing various initially infected nodes in extensive numerical simulations, the value

of each variable was different from the value for corresponding variable in Table 3.6 but similar trends were observed. At the time of the study, no specific mitigation strategies were applied; during an outbreak RVF virus control methods post detection are expected to modify simulation results.

Farm size	Quantity	*Aedes* eggs	*Aedes* mosquitoes	Infected *Culex* mosquitoes	Cattle
small	few	*Aedes*-egg-f-s	*Aedes*-f-s	*Culex*-f-s	Cattle-f-s
	many	*Aedes*-egg-m-s	*Aedes*-m-s	*Culex*-m-s	Cattle-m-s
large	few	*Aedes*-egg-f-l	*Aedes*-f-l	*Culex*-f-l	Cattle-f-l
	many	*Aedes*-egg-m-l	*Aedes*-m-l	*Culex*-m-l	Cattle-m-l

Table 3.4: *Sixteen different initial conditions.*

The suffix, l or s, (representing large or small farms) were removed from initial condition labels when comparing results with different initial infections in the same scale of initial location. Impacts of the RVF epidemic in terms of infected cattle depend on the number of the initial infections.

When initial condition of the outbreak was assumed to be *Aedes*-eggs-f (few *Aedes* eggs), simulations resulted in a larger cumulative number of infected cattle than the number of infected cattle obtained in the case of *Aedes*-eggs-m (many *Aedes* eggs). When initial condition of the outbreak was assumed to be *Aedes*-f (few adult *Aedes* mosquitoes), simulations resulted in a larger cumulative number of infected cattle than the number of infected cattle obtained in the case of *Aedes*-m (many adult *Aedes* mosquitoes). Similarly, fewer initial infected *Culex* mosquitoes (*Culex*-f) lead to larger cumulative number of infected cattle than the number of infected cattle obtained in the case of *Culex*-m throughout the simulation period. When initial condition of the outbreak was assumed to be Cattle-f (few cattle), simulations resulted in a larger cumulative number of infected cattle than the number of infected cattle obtained in the case of Cattle-m (many cattle).

The total number of infected humans and total number of farms with at least one infected

Farm size	Initial infection size	Outcome characteristics	Initial *Aedes* eggs infection	Initial adult *Aedes* infection	Initial *Culex* adult infection	Initial cattle infection
small	few (1)	A	average	small	very small	very small
		B	very large	very large	large	average
		C	very large	very large	average	very small
		D	very long	very long	long	medium
		E	medium	long	very long	short
	many ($\gg 1$)	A	very small	large	very large	average
		B	average	small	very small	small
		C	very small	small	average	very small
		D	short	short	short	short
		E	short	very short	very short	very short
large	few (1)	A	very small	very small	very small	small
		B	very large	large	average	very large
		C	very small	small	very small	average
		D	long	long	short	very long
		E	very long	medium	short	long
	many ($\gg 1$)	A	very large	very large	very large	very small
		B	very small	small	small	large
		C	average	large	average	small
		D	short	very short	very short	long
		E	very short	short	short	medium

Table 3.5: *Qualitative numerical simulation results of different scenarios with respect to infected cattle. The average number of infected farms in each day is in the range of* $[350, 400)$*, the average cumulative number of infected cattle during simulation is within the range* $[350 \times 10^3, 380 \times 10^3)$*, and the average time to peak is within* $[1000, 1200)$*.*

human remained fewer than one regardless of initial infection conditions, possibly because human population of each farm was assumed to be fewer than 15. Therefore, human infection was unlikely in this case, but the number of human infections should not be inferred or generalized to be similar in a more heavily populated region or where many more persons

Farm size	Initial infection size	Outcome characteristics	Initial *Aedes* eggs infection	Initial adult *Aedes* infection	Initial *Culex* adult infection	Initial cattle infection
small	few	A	359	319	267	183
		B	410×10^3	411×10^3	397×10^3	374×10^3
		C	16288	6369	4230	2557
		D	1596	1382	1205	1012
		E	444	471	592	291
		F	0	0	0	0
		G	0	0	0	0
	many	A	224	437	610	388
		B	364×10^3	335×10^3	313×10^3	343×10^3
		C	1772	3125	4433	2773
		D	701	701	700	701
		E	278	181	217	227
		F	0	0	0	0
		G	0	0	0	0
large	few	A	293	197	296	342
		B	407×10^3	382×10^3	354×10^3	413×10^3
		C	2907	3878	2459	4411
		D	1205	1204	711	1382
		E	557	443	278	467
		F	0	0	0	0
		G	0	0	0	0
	many	A	631	732	745	208
		B	315×10^3	321×10^3	332×10^3	385×10^3
		C	4251	4689	4428	3778
		D	700	655	608	1204
		E	226	260	276	449
		F	0	0	0	0
		G	0	0	0	0

Table 3.6: *Quantitative simulation results of different scenarios. The total number of farms is* 3526 *and the total number of cattle in all farms is* 303240.

are in direct contact with animals (e.g., slaughter plants). Temporal characteristics of RVF cases followed the general trend that fewer infected individuals in the initial introduction resulted in a delayed epidemic peak. When initial condition of the outbreak was assumed to be *Aedes*-eggs-f-s, simulations resulted in a peak 895 days later than the peak with initial starting condition of *Aedes*-eggs-m-s. When initial condition of the outbreak was assumed

to be *Aedes*-eggs-f-l, simulations resulted in a later peak than the peak under *Aedes*-eggs-m-l condition. When another pair of initial conditions were compared, the epidemic peak happened not earlier when few initially infected *Aedes* eggs were considered than when few initially infected *Aedes* adult mosquitoes were assumed. Similarly, the epidemic peak occurred not earlier when many initially infected *Aedes* eggs are considered than the one when many initially infected *Aedes* adult mosquitoes were assumed. When initial condition of the outbreak was assumed to be *Aedes*-f, simulations resulted in a later peak than the peak under *Aedes*-l condition. When initial condition of the outbreak was assumed to be *Culex*-f, simulations resulted in a later peak than the peak under *Culex*-l condition. Few initially infected cattle produced a later peak than the peak when many cattle are initially infected.

The original metapopulation model for RVF virus transmission presented in Section 3.1 was applied to a case study in two areas of Texas. The simulation results are helpful in understanding mechanisms of RVF virus transmission. Modeling each mosquito species individually required specific species information to parameterize the model, such as vector competence, which typically is not available or is based on assumptions from other species. Therefore, the model grouped competent mosquito vectors into two primary genera of RVF competent mosquitoes, *Aedes* and *Culex*. The PERT distribution allows for mosquito species of the same genera to be considered together and for individual variation within a single mosquito species by having a distribution with a most likely value and a range of possible values for each parameter. The distribution also allows the model to be easily applied to new environments where vector competence of mosquitoes remains uncharacterized. The model can accommodate various mosquito species of the same genus by adjusting the most likely values and the range of values to account for variation in vector competence between species. Moreover, the model is not limited to known mosquito vector species, and newly discovered competent vectors of RVF can be readily included in the model.

The model can be used to study not only local transmission between hosts and vectors,

but also trans-location transmission of RVF virus using the network approach. The roles of mosquitoes and livestock in RVF virus transmission can be studied independently because separate networks were built for mosquitoes and livestock. One infected farm node can spread the infection to other connected nodes; therefore, additional nodes can be infected over time. Temporal and spatial evolution of RVF virus and their driving forces can also be analyzed. The spread of RVF virus was estimated within farms, as well as among farms, markets, and feedlots. The goal of simulation analysis was to provide insights into possible pathways for rapid spread of RVF virus among farms and counties. Using cattle networks, the impact of cattle movement from trade can be investigated as newborn calves mature to weaning and on to harvest. Cattle farms are source nodes where cattle are born and raised for several months before being sold through markets, directly to feedlots, or directly to other farms as stockers or replacement females. Cattle on an infected farm may become infected and then carry the virus to livestock markets or other transition nodes before being sold to another farm, consequently introducing the virus to a new farm. On the other hand, infected cattle movement to feedlots (sink nodes) does not propagate the transmission because no further transfer of cattle from the nodes occurs except onto slaughter. Different mitigation strategies can be applied according to each node type (source, sink, and transition) within livestock movement network.

Discrete-time modeling is appealing because it describes the epidemic process, which is conceptualized as evolving through a set of discrete-time epochs instead of through a set of continuous-time epochs [75]. Typically infections or illnesses are reported at discrete-time (daily or weekly) [17, 75]. Outputs of discrete-time models can be easily compared with incidence data [17]. Moreover, numerical exploration of discrete-time models is more straightforward [17], thus can be easily implemented by non-mathematicians, which is an advantage in the public health world [17]. The presented discrete-time model allows for simulations of RVF outbreaks on small networks with few nodes and large-scale networks with thousands of nodes. The model was developed not only to be applied to the study area

of Texas, but also to any geographic region or habitat type of concerns without changing the model. To apply the model to a new study area, the modelers only need to adapt corresponding data into the model. Frequently changing a model to apply it to a new environment is time consuming and increases the probability of making mistakes.

In regard to simulation results, *Aedes* are the bridge between *Culex* and livestock beginning with *Aedes* egg infection. Infected *Aedes* eggs may hatch infected *Aedes* mosquitoes. Susceptible livestock become infected after being bitten by infected *Aedes* mosquitoes. *Culex* mosquitoes are amplifiers of RVF virus transmission and they acquire the infection after blood meals on infected livestock. In return, infected *Culex* feed on livestock and RVF virus infection is amplified. If more initially infected adult mosquitoes are present, whether *Aedes* or *Culex* mosquitoes, the rate of infection is faster, herd immunity is reached earlier, and the cumulative number of infected cattle is smaller because most recover before they diffuse to other farms to spread RVF virus, as shown in Figure 3.3. If most livestock infected by mosquitoes in a node recover before moving to other nodes, then the numbers of infected livestock and mosquitoes that transmit RVF virus to other nodes are reduced. Mosquito eggs do not hatch until their habitats, such as dambos (in Africa) or playas/ ponds/ sloughs (in Texas), are created by rainfall. Moreover, *Aedes* eggs require time to become adult *Aedes* mosquitoes, thus increasing the time necessary to reach the epidemic peak with initially infected *Aedes* eggs as compared to initially infected *Aedes* mosquitoes.

Cattle can be spreaders of virus because they are frequently bought and sold [11]. Infected cattle may infect a large number of mosquitoes via mosquito bites in a new location. In turn, infected mosquitoes can bite a large number of susceptible cattle and transmit the virus. Movement bans during an RVF outbreak may restrict further spatial spread of RVF. By interacting with mosquito vectors, very few infected cattle are able to indirectly infect a large number of susceptible cattle. The cumulative number of infected cattle produced by few initially infected cattle is greater than the cumulative number of infected cattle produced by a large number of initially infected cattle. Hence, regional authorities should be warned

and response planning should be initiated even if only few infected cattle are detected.

No human cases (integers) were present in the simulation results regardless of initial starting conditions because of small constant human population in each node of the study region. In high population areas, a large number of human cases may exist. Typically humans are exposed to fewer mosquitoes than cattle, especially in urban areas, resulting in lower probability of being infected by mosquitoes. The probability that humans are infected by cattle is also small in low population areas because the model does not account for contact with the virus via animal slaughter. Hence, the number of infected humans in each farm produced by simulations is fewer than one. Based on the deterministic mathematical model presented by [131], an introduction of RVF in the study area of Texas is primarily a concern for livestock farms but not as a human outbreak as recently occurred in South Africa. During previous outbreaks, many reported human cases were proceeded by livestock cases. In the U.S., humans still have the potential of being infected by mosquitoes and livestock, especially when many livestock cases are reported, thus the dynamics of human infection during an outbreak and factors affecting RVF virus transmission will also be studied in future models.

In conclusion, the general epidemiological trends of a smaller initial infection observed through various simulations with various initial starting locations are: (1) a larger total number of infected cattle, (2) a longer delay after introduction until the epidemic peak, and (3) a prolonged epidemic. If the infection remains small (and possibly undetected) for a longer duration, it expands geographically before the epidemic involves many cattle simultaneously. Therefore, an established and endemic condition can generate larger epidemic disease incidence after a long period of apparent hibernation.

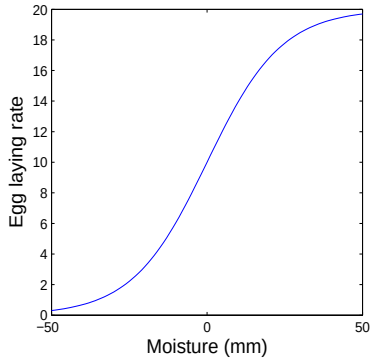

(a) The egg development rate of *Culex* mosquitoes with temperature

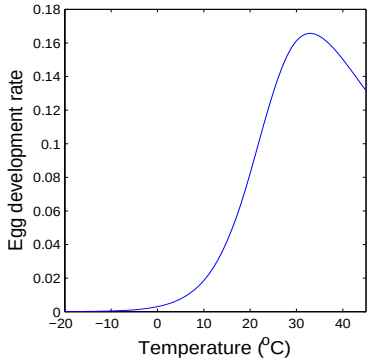

(b) The egg development rate of *Culex* mosquitoes with temperature

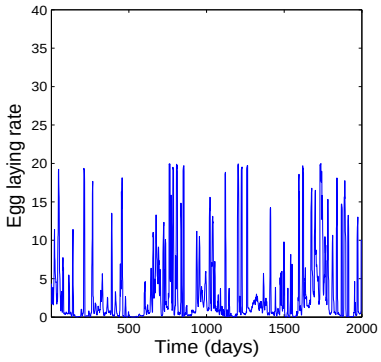

(c) The egg laying rates of *Aedes* and *Culex* mosquitoes in the nine counties in the south of Texas from January, 2005 to October, 2010

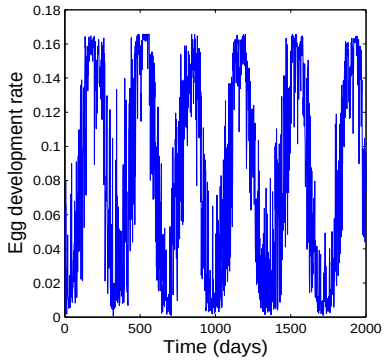

(d) The egg development rate of *Culex* mosquitoes in the nine counties in the south of Texas from January, 2005 to October, 2010

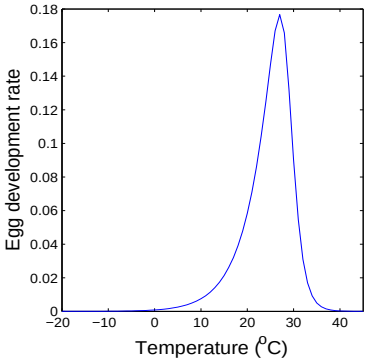

(e) The egg development rate of *Aedes* mosquitoes with temperature

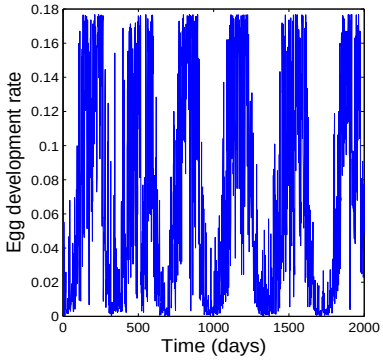

(f) The egg development rate of *Aedes* mosquitoes in the nine counties in the south of Texas from January, 2005 to October, 2010

Figure 3.2: *Relationships between egg laying rates, egg development rates of mosquitoes, and climate factors.*

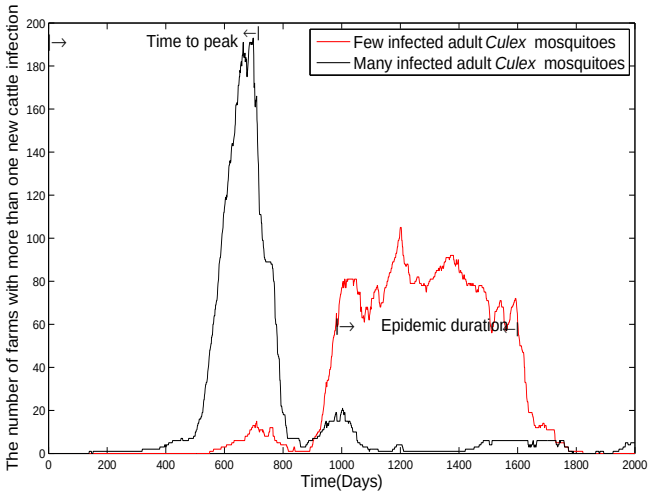

Figure 3.3: *Disease epidemic characteristics based on model outputs with different initial numbers of infected Culex* mosquitoes on a small farm. Time to peak infection is the time until the maximal number of cases is observed, and epidemic duration is the amount of time an epidemic persists.

Chapter 4

The Reproduction Number

A wide range of infectious diseases are both vertically and horizontally transmitted. Such diseases are spatially transmitted via multiple species in heterogeneous environments, typically described by complex metapopulation models. The reproduction number, defined as the average number of secondary cases produced by one infectious individual in a naive population is a critical metric in predicting whether the disease can invade the metapopulation system. This chapter presents R_0 for a generic disease vertically and horizontally transmitted among multiple species on heterogeneous networks in which nodes are locations, and links reflect outgoing or incoming movement flows. The expression of R_0 is the spectral radius of a matrix reduced in size with respect to the original next generation matrix and is easily adaptable to specific infectious diseases, affording insights into disease intervention.

The metapopulation model for vertically and horizontally transmitted diseases was gradually formulated from two species, two-node network models. Metapopulations consisting of discrete, well-mixed subpopulations were considered and the assumption was made that individuals move between different nodes and the disease can be transmitted within a node. All sojourn times were assumed to be exponentially distributed, and vertical transmission was restricted to the egg stage with exponential duration. The reproduction number is shown to be a function of vertical and horizontal transmission parameters, and the lower bound is the R_0 for horizontal transmission. As an application, R_0 and its bounds for RVF zoonosis in which livestock, mosquitoes, and humans are involved, are derived. By com-

puting R_0 for various scenarios through numerical simulations, results showed that R_0 is affected by livestock movement rates only when parameters are heterogeneous across nodes.

This chapter is organized as follows. Section 4.1 reviews the next generation matrix approach used to derive an explicit expression of R_0, and presents the general metapopulation model beginning with two species, two-node network models, as well as computation of R_0. In Section 4.2, the R_0 formula is applied to the RVF metapopulation model, computing R_0 and its bounds. The impacts of livestock movement, heterogeneities of parameters, and size of a network on R_0 are also studied through simulations. Section 4.3 provides a summary and discussion on analytical and numerical results.

4.1 The Reproduction Number for Diseases with Vertical and Horizontal Transmission

One frequently used method computes R_0 as the spectral radius of the next generation matrix [36, Chapter 5], [118]. For ease of computation, only compartments corresponding to infected and asymptomatically infected compartments are considered [38]. First, the original nonlinear system of ODEs is decomposed into two column vectors $\mathscr{F} = (\mathscr{F}_i)$ and $\mathscr{V} = (\mathscr{V}_i)$, where $\mathscr{F}_i$ is the i^{th} row of $\mathscr{F}$ representing the rate at which new infections appear in compartment i, and $\mathscr{V}_i$ is the i^{th} row of $\mathscr{V}$. Moreover, $\mathscr{V}_i = \mathscr{V}_i^- - \mathscr{V}_i^+$, where $\mathscr{V}_i^-$ represents the rate at which individuals transfer out of compartment i, and $\mathscr{V}_i^+$ is the rate at which individuals transfer into compartment i [118] with the assumption that the number of infected and asymptomatically infected compartments is m. Jacobian matrices F denoting transmission, and V denoting transition [38] are defined as:

$$F = [\frac{\partial \mathscr{F}_i(x^0)}{\partial x_j}], \quad V = [\frac{\partial \mathscr{V}_i(x^0)}{\partial x_j}], \tag{4.1}$$

where x^0 represents the disease free equilibrium (DFE), and x_j is the number or proportion of infected individuals in compartment j, where $j = 1, \cdots, m$.

The spectral radius of a matrix A is denoted by $\rho(A)$. The reproduction number is defined as $\rho(FV^{-1})$ [37]. To understand entries of FV^{-1}, called the next generation matrix,

consider the consequence of an infected individual introduced into compartment k in a population at DFE [118]. The (i, j) entry of F represents the rate at which new infected individuals in compartment i are produced by infected individuals in compartment j [118]. The (j, k) entry of V^{-1} represents the average time that an infected individual remains in compartment j [118]. Hence, the (i, k) entry of FV^{-1} represents the expected number of new infections in compartment i, resulting from the infected individual originally introduced into compartment k [118], where $i, k = 1, \cdots, m$. Note that matrix F is nonnegative and V is proven to be a nonsingular M-matrix [118]. An $n \times n$ matrix A is an M-matrix if it can be expressed in the form $A = sI - B$, such that matrix B is non-negative, and $s \geqslant \rho(B)$ [95].

Next, computational procedures for finding R_0 using the next generation matrix method for SEIR compartmental models were illustrated assuming a disease is transmittable within a species and between different species, and movement rates for all species are independent of disease status. Daily time steps were used in all models.

4.1.1 Models for Two Species in Two Nodes

Presented here are two applications of a simplified system for a disease involving two species in a two-node network with movement between the two nodes. In the first example, R_0 was computed while assuming only horizontal transmission is occurring. In the second example, the first model was extended by introducing vertical transmission into one species. The reproduction number was then computed.

R_0 for Two Species with Only Horizontal Transmission

Below, a compartmental model for an infectious disease incorporating four compartments $(J = S, E, I, R)$, two species $(k = 1, 2)$, two nodes $(i = 1, 2)$, and only horizontal transmis-

sion is presented. Differential equations representing the dynamic behavior are:

$$\begin{aligned}
\frac{dS_{ki}}{dt} &= r_{ki} - \beta_{1ki}S_{ki}I_{1i}/N_{1i} - \beta_{2ki}S_{ki}I_{2i}/N_{2i} - d_{ki}S_{ki} \\
&\quad + \sum_{j=1,j\neq i}^{2} \omega_{kji}S_{kj} - \sum_{j=1,j\neq i}^{2} \omega_{kij}S_{ki} \\
\frac{dE_{ki}}{dt} &= \beta_{1ki}S_{ki}I_{1i}/N_{1i} + \beta_{2ki}S_{ki}I_{2i}/N_{2i} - \varepsilon_{ki}E_{ki} - d_{ki}E_{ki} \\
&\quad + \sum_{j=1,j\neq i}^{2} \omega_{kji}E_{kj} - \sum_{j=1,j\neq i}^{2} \omega_{kij}E_{ki} \\
\frac{dI_{ki}}{dt} &= \varepsilon_{ki}E_{ki} - \gamma_{ki}I_{ki} - d_{ki}I_{ki} + \sum_{j=1,j\neq i}^{2} \omega_{kji}I_{kj} - \sum_{j=1,j\neq i}^{2} \omega_{kij}I_{ki} \\
\frac{dR_{ki}}{dt} &= \gamma_{ki}I_{ki} - d_{ki}R_{ki} + \sum_{j=1,j\neq i}^{2} \omega_{kji}R_{kj} - \sum_{j=1,j\neq i}^{2} \omega_{kij}R_{ki}.
\end{aligned} \tag{4.2}$$

The number of newborn individuals of species k in node i per day is denoted by r_{ki}. The number of species k individuals in node i of compartment J is denoted by J_{ki}, and the total number of species k individuals in node i is $N_{ki} = S_{ki} + E_{ki} + I_{ki} + R_{ki}$. Total individuals of species k infected daily in node i by species 1 and species 2 are $\beta_{1ki}S_{ki}I_{1i}/N_{1i}$ and $\beta_{2ki}S_{ki}I_{2i}/N_{2i}$, respectively. The number of deaths from each compartment J per day is $d_{ki}J_{ki}$. After the incubation period, $\varepsilon_{ki}E_{ki}$ individuals transfer to infected compartment daily. Following the infection period, $\gamma_{ki}I_{ki}$ individuals recover from the infection each day. Movement rates for species k individuals in compartment J in and out of node i are $\sum_{j=1,j\neq i}^{2} \omega_{kji}J_{kj}$ and $\sum_{j=1,j\neq i}^{2} \omega_{kij}J_{ki}$, respectively.

Species k quantity in compartment J and the total number in node i at DFE are denoted by J_{ki}^0 and N_{ki}^0, respectively. At DFE, $S_{1i}^0 = N_{1i}^0$, and $S_{2i}^0 = N_{2i}^0$, as $E_{1i}^0 = I_{1i}^0 = R_{1i}^0 = E_{2i}^0 = I_{2i}^0 = R_{2i}^0 = 0$. The proof for existence and uniqueness of DFE is a special case of the model for Theorem 1, which determines the existence of a unique solution $[N_{1i}^0 \quad N_{2i}^0]^T$.

Equations related to exposed and infected compartments are ordered:

$$\frac{d}{dt}\begin{bmatrix} E_{11} & E_{12} & E_{21} & E_{22} & I_{11} & I_{12} & I_{21} & I_{22} \end{bmatrix}^T = \mathscr{F}_H - \mathscr{V}_H, \text{ where}$$

$$\mathscr{F}_H = \begin{bmatrix} \beta_{211} S_{11} I_{21}/N_{21} + \beta_{111} S_{11} I_{11}/N_{11} \\ \beta_{212} S_{12} I_{22}/N_{22} + \beta_{112} S_{12} I_{12}/N_{12} \\ \beta_{121} S_{21} I_{11}/N_{11} + \beta_{221} S_{21} I_{21}/N_{21} \\ \beta_{122} S_{22} I_{12}/N_{12} + \beta_{222} S_{22} I_{22}/N_{22} \\ 0 \\ 0 \\ 0 \\ 0 \end{bmatrix},$$

$$\mathscr{V}_H = \begin{bmatrix} d_{11}E_{11} + \varepsilon_{11}E_{11} + \omega_{112}E_{11} - \omega_{121}E_{12} \\ d_{12}E_{12} + \varepsilon_{12}E_{12} + \omega_{121}E_{12} - \omega_{112}E_{11} \\ d_{21}E_{21} + \varepsilon_{21}E_{21} + \omega_{212}E_{21} - \omega_{221}E_{22} \\ d_{22}E_{22} + \varepsilon_{22}E_{22} + \omega_{221}E_{22} - \omega_{212}E_{21} \\ -\varepsilon_{11}E_{11} + d_{11}I_{11} + \gamma_{11}I_{11} + \omega_{112}I_{11} - \omega_{121}I_{12} \\ -\varepsilon_{12}E_{12} + d_{12}I_{12} + \gamma_{12}I_{12} + \omega_{121}I_{12} - \omega_{112}I_{11} \\ -\varepsilon_{21}E_{21} + d_{21}I_{21} + \gamma_{21}I_{21} + \omega_{212}I_{21} - \omega_{221}I_{22} \\ -\varepsilon_{22}E_{22} + d_{22}I_{22} + \gamma_{22}I_{22} + \omega_{221}I_{22} - \omega_{212}I_{21} \end{bmatrix}.$$

By (4.1), Jacobian matrices for this model are:

$$F_H = \begin{bmatrix} 0_{4\times4} & Z \\ 0 & 0_{4\times4} \end{bmatrix}, \quad V_H = \begin{bmatrix} \oplus_{k=1}^{2} Y_k & 0 \\ -\oplus_{k=1}^{2} (\oplus_{i=1}^{2} \varepsilon_{ki}) & \oplus_{k=1}^{2} X_k \end{bmatrix}, \tag{4.3}$$

where the symbol $\bigoplus$ represents the direct sum of matrices, i.e., $A \bigoplus B = \begin{bmatrix} A & 0 \\ 0 & B \end{bmatrix}$ for matrices A and B. The subscript of the zero blocks, 4×4, indicates the size of the block. Matrices Z, Y_k, and X_k are:

$$Z = \begin{bmatrix} \beta_{111}\frac{S_{11}^0}{N_{11}^0} & 0 & \beta_{211}\frac{S_{11}^0}{N_{21}^0} & 0 \\ 0 & \beta_{112}\frac{S_{12}^0}{N_{12}^0} & 0 & \beta_{212}\frac{S_{12}^0}{N_{22}^0} \\ \beta_{121}\frac{S_{21}^0}{N_{11}^0} & 0 & \beta_{221}\frac{S_{21}^0}{N_{21}^0} & 0 \\ 0 & \beta_{122}\frac{S_{22}^0}{N_{12}^0} & 0 & \beta_{222}\frac{S_{22}^0}{N_{22}^0} \end{bmatrix},$$

$$Y_1 = \begin{bmatrix} d_{11} + \varepsilon_{11} + \omega_{112} & -\omega_{121} \\ -\omega_{112} & d_{12} + \varepsilon_{12} + \omega_{121} \end{bmatrix}, \tag{4.4}$$

$$Y_2 = \begin{bmatrix} d_{21} + \varepsilon_{21} + \omega_{212} & -\omega_{221} \\ -\omega_{212} & d_{22} + \varepsilon_{22} + \omega_{221} \end{bmatrix}, \tag{4.5}$$

$$X_1 = \begin{bmatrix} d_{11} + \gamma_{11} + \omega_{112} & -\omega_{121} \\ -\omega_{112} & d_{12} + \gamma_{12} + \omega_{121} \end{bmatrix}, \tag{4.6}$$

$$X_2 = \begin{bmatrix} d_{21} + \gamma_{21} + \omega_{212} & -\omega_{221} \\ -\omega_{212} & d_{22} + \gamma_{22} + \omega_{221} \end{bmatrix}. \tag{4.7}$$

Because matrices Y_1, Y_2, X_1, and X_2 are all invertible, by direct calculation:

$$V_H^{-1} = \begin{bmatrix} \oplus_{k=1}^{2} Y_k^{-1} & 0 \\ \oplus_{k=1}^{2} L_k & \oplus_{k=1}^{2} X_k^{-1} \end{bmatrix},$$

where $L_k = X_k^{-1}(\oplus_{i=1}^{2}\varepsilon_{ki})Y_k^{-1}$. The spectral radius of the next generation matrix $F_H V_H^{-1}$ is:

$$\rho(F_H V_H^{-1}) = \rho(\begin{bmatrix} 0_{4\times4} & Z \\ 0 & 0_{4\times4} \end{bmatrix} \begin{bmatrix} \oplus_{k=1}^{2} Y_k^{-1} & 0 \\ \oplus_{k=1}^{2} L_k & \oplus_{k=1}^{2} X_k^{-1} \end{bmatrix}) = \rho(Z(\oplus_{k=1}^{2} L_k)).$$

Therefore,

$$R_0^H := \rho(F_H V_H^{-1}) = \rho(Z(\oplus_{k=1}^{2} L_k)), \tag{4.8}$$

where R_0^H is R_0 for horizontal transmission.

R_0 for Two Species with Vertical Transmission in One Species

The model for species 2 (Equation (4.2) with $k = 2$) remains while extending the model for species 1 by incorporating vertical transmission. The model for species 1 is:

$$\begin{aligned}
\frac{dP_{1i}}{dt} &= r_{1i} - b_1 q_{1i} I_{1i} - \theta_{1i} P_{1i} \\
\frac{dQ_{1i}}{dt} &= b_{1i} q_{1i} I_{1i} - \theta_{1i} Q_{1i} \\
\frac{dS_{1i}}{dt} &= \theta_{1i} P_{1i} - \beta_{11i} S_{1i} I_{1i}/N_{1i} - \beta_{21i} S_{1i} I_{2i}/N_{2i} - d_{1i} S_{1i} \\
&\quad + \sum_{j=1, j\neq i}^{2} \omega_{1ji} S_{1j} - \sum_{j=1, j\neq i}^{2} \omega_{1ij} S_{1i} \\
\frac{dE_{1i}}{dt} &= \beta_{11i} S_{1i} I_{1i}/N_{1i} + \beta_{21i} S_{1i} I_{2i}/N_{2i} - \varepsilon_{1i} E_{1i} - d_{1i} E_{1i} \\
&\quad + \sum_{j=1, j\neq i}^{2} \omega_{1ji} E_{1j} - \sum_{j=1, j\neq i}^{2} \omega_{1ij} E_{1i} \\
\frac{dI_{1i}}{dt} &= \theta_{1i} Q_{1i} + \varepsilon_{1i} E_{1i} - \gamma_{1i} I_{1i} - d_{1i} I_{1i} + \sum_{j=1, j\neq i}^{2} \omega_{1ji} I_{1j} - \sum_{j=1, j\neq i}^{2} \omega_{1ij} I_{1i} \\
\frac{dR_{1i}}{dt} &= \gamma_{1i} I_{1i} - d_{1i} R_{1i} + \sum_{j=1, j\neq i}^{2} \omega_{1ji} R_{1j} - \sum_{j=1, j\neq i}^{2} \omega_{1ij} R_{1i}
\end{aligned} \tag{4.9}$$

The number of eggs laid by species 1 per day is denoted by r_{1i}, including $b_{1i}q_{1i}I_{1i}$ infected eggs, and $r_{1i} - b_{1i}q_{1i}I_{1i}$ uninfected eggs. After the development period, $\theta_{1i}P_{1i}$ eggs develop into susceptible adults, and $\theta_{1i}Q_{1i}$ eggs develop into infected adults daily. Interpretations of other terms are the same as corresponding terms described in Section 4.1.1.

At DFE, $Q_{1i}^0 = E_{1i}^0 = I_{1i}^0 = R_{1i}^0 = E_{2i}^0 = I_{2i}^0 = R_{2i}^0 = 0$, $S_{1i}^0 = N_{1i}^0$, and $S_{2i}^0 = N_{2i}^0$. Since this model is also a special case of the model for Theorem 1, a unique solution $[N_{1i}^0 \quad N_{2i}^0]^T$ exists. In the second model, equations related to exposed and infected compartments are ordered:

$$\frac{d}{dt}\left[\begin{array}{cccccccccc} Q_{11} & Q_{12} & E_{11} & E_{12} & E_{21} & E_{22} & I_{11} & I_{12} & I_{21} & I_{22} \end{array}\right]^T = \mathscr{F} - \mathscr{V},$$

where

$$\mathscr{F} = \begin{bmatrix} b_{11}q_{11}I_{11} \\ b_{12}q_{12}I_{12} \\ \beta_{211}S_{11}I_{21}/N_{21} + \beta_{111}S_{11}I_{11}/N_{11} \\ \beta_{212}S_{12}I_{22}/N_{22} + \beta_{112}S_{12}I_{12}/N_{12} \\ \beta_{121}S_{21}I_{11}/N_{11} + \beta_{221}S_{21}I_{21}/N_{21} \\ \beta_{122}S_{22}I_{12}/N_{12} + \beta_{222}S_{22}I_{22}/N_{22} \\ 0 \\ 0 \\ 0 \\ 0 \end{bmatrix},$$

and

$$\mathscr{V} = \begin{bmatrix} \theta_{11}Q_{11} \\ \theta_{12}Q_{12} \\ d_{11}E_{11} + \varepsilon_{11}E_{11} + \omega_{112}E_{11} - \omega_{121}E_{12} \\ d_{12}E_{12} + \varepsilon_{12}E_{12} + \omega_{121}E_{12} - \omega_{112}E_{11} \\ d_{21}E_{21} + \varepsilon_{21}E_{21} + \omega_{212}E_{21} - \omega_{221}E_{22} \\ d_{22}E_{22} + \varepsilon_{22}E_{22} + \omega_{221}E_{22} - \omega_{212}E_{21} \\ -\theta_{11}Q_{11} - \varepsilon_{11}E_{11} + d_{11}I_{11} + \gamma_{11}I_{11} + \omega_{112}I_{11} - \omega_{121}I_{12} \\ -\theta_{12}Q_{12} - \varepsilon_{12}E_{12} + d_{12}I_{12} + \gamma_{12}I_{12} + \omega_{121}I_{12} - \omega_{112}I_{11} \\ -\varepsilon_{21}E_{21} + d_{21}I_{21} + \gamma_{21}I_{21} + \omega_{212}I_{21} - \omega_{221}I_{22} \\ -\varepsilon_{22}E_{22} + d_{22}I_{22} + \gamma_{22}I_{22} + \omega_{221}I_{22} - \omega_{212}I_{21} \end{bmatrix}.$$

By (4.1), Jacobian matrices for this model are:

$$F = \begin{bmatrix} 0_{2\times 2} & U_{2\times 8} \\ 0_{8\times 2} & F_H \end{bmatrix}, \quad V = \begin{bmatrix} \oplus_{i=1}^{2}\theta_{1i} & 0_{2\times 8} \\ W_{8\times 2} & V_H \end{bmatrix}.$$

Here F_H and V_H are the matrices in (4.3) and

$$U = \begin{bmatrix} 0_{2\times 4} & \bigoplus_{i=1}^{2} b_{1i}q_{1i} & 0_{2\times 2} \end{bmatrix}, \quad W = \begin{bmatrix} 0_{4\times 2} \\ -\bigoplus_{i=1}^{2} \theta_{1i} \\ 0_{2\times 2} \end{bmatrix}.$$

Matrix V^{-1} and the next generation matrix FV^{-1} are:

$$V^{-1} = \begin{bmatrix} \bigoplus_{i=1}^{2} \theta_{1i}^{-1} & 0 \\ -V_H^{-1}W(\bigoplus_{i=1}^{2} \theta_{1i}^{-1}) & V_H^{-1} \end{bmatrix}, \quad FV^{-1} = \begin{bmatrix} -UV_H^{-1}W(\bigoplus_{i=1}^{2} \theta_{1i}^{-1}) & UV_H^{-1} \\ -F_HV_H^{-1}W(\bigoplus_{i=1}^{2} \theta_{1i}^{-1}) & F_HV_H^{-1} \end{bmatrix}.$$

Since $\mathcal{M}^{-1}(FV^{-1})\mathcal{M} = \begin{bmatrix} 0 & UV_H^{-1} \\ 0 & F_HV_H^{-1} - W(\bigoplus_{i=1}^{2} \theta_{1i}^{-1})UV_H^{-1} \end{bmatrix}$,

where $\mathcal{M} = \begin{bmatrix} I_{2\times 2} & 0 \\ W(\bigoplus_{i=1}^{2} \theta_{1i}^{-1}) & I_{8\times 8} \end{bmatrix}$,

$$R_0 = \rho(FV^{-1}) = \rho(F_HV_H^{-1} - W(\bigoplus_{i=1}^{2} \theta_{1i}^{-1})UV_H^{-1}). \tag{4.10}$$

R_0 is a function of vertical and horizontal transmission parameters. Since $F_HV_H^{-1}$ and $-W(\bigoplus_{i=1}^{2} \theta_{1i}^{-1})UV_H^{-1}$ are both nonnegative matrices, by Theorem 7,

$$R_0 \geqslant \rho(F_HV_H^{-1}). \tag{4.11}$$

4.1.2 R_0 for Multiple Species in a General Network Model

The models presented in Section 4.1.1 are generalized to describe dynamics of diseases transmitted among h species in node i ($i = 1, \cdots, n$). Suppose a disease is transmitted by species k ($k = 1, \cdots, h$) vertically and horizontally if $1 \leqslant k \leqslant g$ and only horizontally

otherwise. Dynamical behavior is given by the system with $4hn+2gn$ differential equations:

$$\begin{aligned}
\frac{dP_{ki}}{dt} &= [r_{ki} - b_{ki}q_{ki}I_{ki} - \theta_{ki}P_{ki}]\delta(k) \\
\frac{dQ_{ki}}{dt} &= [b_{ki}q_{ki}I_{ki} - \theta_{ki}Q_{ki}]\delta(k) \\
\frac{dS_{ki}}{dt} &= \theta_{ki}P_{ki}\delta(k) + r_{ki}(1-\delta(k)) - \sum_{m=1}^{h}\beta_{mki}S_{ki}I_{mi}/N_{mi} - d_{ki}S_{ki} + \sum_{j=1,j\neq i}^{n}\omega_{kji}S_{kj} \\
&\quad - \sum_{j=1,j\neq i}^{n}\omega_{kij}S_{ki} \\
\frac{dE_{ki}}{dt} &= \sum_{m=1}^{h}\beta_{mki}S_{ki}I_{mi}/N_{mi} - \varepsilon_{ki}E_{ki} - d_{ki}E_{ki} + \sum_{j=1,j\neq i}^{n}\omega_{kji}E_{kj} - \sum_{j=1,j\neq i}^{n}\omega_{kij}E_{ki} \\
\frac{dI_{ki}}{dt} &= \theta_{ki}Q_{ki}\delta(k) + \varepsilon_{ki}E_{ki} - \gamma_{ki}I_{ki} - d_{ki}I_{ki} + \sum_{j=1,j\neq i}^{n}\omega_{kji}I_{kj} - \sum_{j=1,j\neq i}^{n}\omega_{kij}I_{ki} \\
\frac{dR_{ki}}{dt} &= \gamma_{ki}I_{ki} - d_{ki}R_{ki} + \sum_{j=1,j\neq i}^{n}\omega_{kji}R_{kj} - \sum_{j=1,j\neq i}^{n}\omega_{kij}R_{ki}.
\end{aligned} \tag{4.12}$$

Daily number of species k individuals infected by species m is $\beta_{mki}S_{ki}I_{mi}/N_{mi}$. Daily numbers of species k individuals in compartment J moving in and out of node i are $\sum_{j=1,j\neq i}^{n}\omega_{kji}J_{kj}$ and $\sum_{j=1,j\neq i}^{n}\omega_{kij}J_{ki}$, respectively. Other terms in the above equations have the same meanings as corresponding terms in Equations (4.2) and (4.9) except $\delta(k)$ defined below, which is used to differentiate the horizontally-transmitting species and the species exhibiting both types of transmission.

$$\delta(k) = \begin{cases} 1 & \text{for} \quad 1 \leq k \leq g, \\ 0 & \text{for} \quad g+1 \leq k \leq h. \end{cases}$$

To compute R_0 using the next generation matrix approach, matrices $\mathscr{F}$ and $\mathscr{V}$ must be found, omitted here due to large size. In determining Jacobian matrices F and V, infected variables are ordered by compartment, species, and node index, i.e.,

$$Q_{11}, \cdots, Q_{1n}, \cdots, Q_{g1}, \cdots, Q_{gn}, E_{11}, \cdots, E_{1n}, \cdots, E_{h1}, \cdots, E_{hn}, I_{11}, \cdots, I_{1n}, \cdots, I_{h1}, \cdots, I_{hn}.$$

At DFE, $Q_{ki} = E_{ki} = I_{ki} = R_{ki} = 0$, and $S_{ki} = N_{ki}$.

Theorem 1. *For the model presented in system of equations (4.12),a unique nonnegative solution for total number of species k individuals in node i at DFE exists.*

Proof. To solve the total number of species k individuals in each node at DFE, the following system of equations must be solved.

$$\mathcal{W}\begin{bmatrix} N_{k1}^* & \cdots & N_{kn}^* \end{bmatrix}^T = \begin{bmatrix} r_{k1} & \cdots & r_{kn} \end{bmatrix}^T, \tag{4.13}$$

where

$$\mathcal{W} = \begin{bmatrix} d_{k1} + \sum_{j=2}^{n} \omega_{k1j} & -\omega_{k21} & \cdots & -\omega_{kn1} \\ -\omega_{k12} & d_{k2} + \sum_{j=1,j\neq 2}^{n} \omega_{k2j} & \cdots & -\omega_{kn2} \\ \cdots & \cdots & \cdots & \cdots \\ -\omega_{k1n} & -\omega_{k2n} & \cdots & d_{kn} + \sum_{j=1}^{n-1} \omega_{knj} \end{bmatrix}.$$

The variable vector $\begin{bmatrix} N_{k1}^* \cdots N_{kn}^* \end{bmatrix}^T$ is to be solved. Matrix $\mathcal{W}$ is a diagonal dominant matrix of its column entries [23], i.e., $\mathcal{W}_{ii} \geqslant \sum_{i=1,i\neq j}^{n} \mathcal{W}_{ij}$, for all i, where $\mathcal{W}_{ij}$ is the (i,j) entry of $\mathcal{W}$. By Theorem 1 in page 654 of [23], $\mathcal{W}$ is invertible. Moreover, by Theorem 9, $\mathcal{W}^{-1}$ is nonnegative. Thus, a unique nonnegative solution for the system of equations (4.13) exists:

$$\begin{bmatrix} N_{k1}^* & \cdots & N_{kn}^* \end{bmatrix}^T = \begin{bmatrix} N_{k1}^0 & \cdots & N_{kn}^0 \end{bmatrix}^T = \mathcal{W}^{-1} \begin{bmatrix} r_{k1} & \cdots & r_{kn} \end{bmatrix}^T.$$

□

Since incorporating multiple species in multiple nodes leads to matrices F and V growing very large, the computation of R_0 is simplified by decomposing the matrices into blocks, deriving block upper or lower triangular matrices as follows:

$$F = \begin{bmatrix} 0_{gn\times gn} & U_{gn\times 2hn} \\ 0_{2hn\times gn} & F_H \end{bmatrix}, \quad V = \begin{bmatrix} \bigoplus_{k=1}^{g}(\bigoplus_{i=1}^{n} \theta_{ki}) & 0_{gn\times 2hn} \\ W_{2hn\times gn} & V_H \end{bmatrix},$$

where

$$F_H = \begin{bmatrix} 0_{hn\times hn} & Z_{hn\times hn} \\ 0_{hn\times hn} & 0_{hn\times hn} \end{bmatrix}, \quad V_H = \begin{bmatrix} \bigoplus_{k=1}^{h} Y_k & 0_{hn\times hn} \\ -\bigoplus_{k=1}^{h}(\bigoplus_{i=1}^{n} \varepsilon_{ki}) & \bigoplus_{k=1}^{h} X_k \end{bmatrix},$$

$$U = \begin{bmatrix} 0_{gn\times hn} & \bigoplus_{k=1}^{g}(\bigoplus_{i=1}^{n} b_{ki}q_{ki}) & 0_{gn\times(h-g)n} \end{bmatrix}, \quad W = \begin{bmatrix} 0_{hn\times gn} \\ -\bigoplus_{k=1}^{g}(\bigoplus_{i=1}^{n} \theta_{ki}) \\ 0_{(h-g)n\times gn} \end{bmatrix}.$$

The block matrix Z in F_H is written into an $h \times h$ block matrix $Z = (Z_{km})$ and its (k, m) entry is an $n \times n$ diagonal matrix $Z_{km} = \bigoplus_{i=1}^{n}(\beta_{mki}\frac{S_{ki}^0}{N_{mi}^0})$. Matrices Y_k and X_k are:

$$Y_k = \begin{bmatrix} \zeta_{k1} & -\omega_{k21} & \cdots & -\omega_{kn1} \\ -\omega_{k12} & \zeta_{k2} & \cdots & -\omega_{kn2} \\ \cdots & \cdots & \cdots & \cdots \\ -\omega_{k1n} & \cdots & \cdots & \zeta_{kn} \end{bmatrix}, \quad \text{and} \quad X_k = Y_k + \bigoplus_{i=1}^{n}(\gamma_{ki} - \varepsilon_{ki}), \tag{4.14}$$

where $\zeta_{ki} = d_{ki} + \varepsilon_{ki} + \sum_{j=1, j\neq i}^{n} \omega_{kij}$. Since matrices Y_k and X_k are invertible, according to Theorem 9, V_H and V are invertible. By direct calculation:

$$V_H^{-1} = \begin{bmatrix} \oplus_{k=1}^{h} Y_k^{-1} & 0 \\ \oplus_{k=1}^{h} L_k & \oplus_{k=1}^{h} X_k^{-1} \end{bmatrix}, \quad V^{-1} = \begin{bmatrix} \bigoplus_{k=1}^{g}(\bigoplus_{i=1}^{n} \theta_{ki}^{-1}) & 0_{gn\times 2hn} \\ -V_H^{-1}W(\bigoplus_{k=1}^{g}(\bigoplus_{i=1}^{n} \theta_{ki}^{-1})) & V_H^{-1} \end{bmatrix}, \tag{4.15}$$

where $L_k = X_k^{-1}(\oplus_{i=1}^{n}\varepsilon_{ki})Y_k^{-1}$. Similar to the derivation in Section 4.1.1, R_0 is:

$$R_0 = \rho(FV^{-1}) = \rho(F_H V_H^{-1} - W(\bigoplus_{k=1}^{g}(\bigoplus_{i=1}^{n} \theta_{ki}^{-1}))UV_H^{-1}). \tag{4.16}$$

Moreover, (4.11) still holds. If the lower bound $\rho(F_H V_H^{-1}) > 1$, the conclusion can be made that a network may be invaded without computing the upper bound or the exact value of R_0.

The term $F_H V_H^{-1}$ is related to horizontal transmission, and $-W(\bigoplus_{k=1}^{g}(\bigoplus_{i=1}^{n} \theta_{ki}^{-1}))UV_H^{-1}$ is related to vertical transmission, making R_0 a function of vertical and horizontal transmission parameters. Generally, R_0 depends on demographic, disease, and movement factors, proving too complicated to compute or analyze [11]. The complexity of computing R_0 using Equation (4.16) depends on a specific model for a certain disease. For the general model, only the formula of R_0 in Equation (4.16) and its lower bound in Inequality (4.11) can be provided.

In the following section, Equation (4.16) is applied to an RVF virus transmission metapopulation model. Then, based on assumptions for the RVF model, R_0 is computed using Equation (4.16) and lower and upper bounds are derived, providing insights into the role of model parameters on R_0.

4.2 Applying R_0 Formula to an Rift Valley Fever Metapopulation Model

The explicit expression of R_0 in Equation (4.16) was applied to an RVF metapopulation model to study the roles of parameters and networks on R_0.

4.2.1 The Network-based Rift Valley Fever Metapopulation Model

In this section, the general model in system of equations (4.12) in Section 4.1.2 was applied to study the dynamics of RVF virus transmission with $h = 4$, $g = 1$. *Aedes* and *Culex* mosquito vectors, as well as livestock and human hosts were considered. The RVF model is less complex than the general model presented in Equations (4.12). Here, the assumption is made that only livestock can move in and out of nodes, and all mosquitoes do not recover. Disease-induced mortality for livestock and humans and carrying capacity for mosquitoes and humans were considered. Due to lack of transmission by humans or direct intra-species transmission, this RVF model contains fewer infection terms than those in the general model. The full model is described by Equations (2.14), (2.15), (4.17), and (4.18) and relative parameters are in Table 4.1. The descriptions of parameters are the same as corresponding parameters in Table 2.1 and are omitted here. Parameter w_{2ij} is livestock movement rate from node i to node j, and r_{2i} is the number of livestock born daily in node i ($i = 1, \cdots, n$). This model is slightly different from the model in Chapter 2. The number of species k individuals ($k = 1, 2, 3, 4$) from node i in compartment J is represented by J_{ki}, where $k = 1$ (resp. 2, 3, 4) represents *Aedes* mosquitoes (resp. livestock, *Culex* mosquitoes, and humans). Daily numbers of newborn *Aedes* mosquitoes, *Culex* mosquitoes, and humans are $b_{ki}N_{ki}$. A node index is added at the end of the subscript of a parameter only when referring to a parameter for a specific node. For example, β_{12i} represents the contact rate from *Aedes* mosquitoes ($k = 1$) to livestock ($k = 2$) in node i.

Livestock Population Model

$$
\begin{aligned}
\frac{dS_{2i}}{dt} &= r_{2i} - \beta_{12i}S_{2i}I_{1i}/N_{1i} - \beta_{32i}S_{2i}I_{3i}/N_{3i} - d_{2i}S_{2i} + \sum_{j=1,j\neq i}^{n}\omega_{2ji}S_{2j} \\
&\quad - \sum_{j=1,j\neq i}^{n}\omega_{2ij}S_{2i} \\
\frac{dE_{2i}}{dt} &= \beta_{12i}S_{2i}I_{1i}/N_{1i} + \beta_{32i}S_{2i}I_{3i}/N_{3i} - \varepsilon_{2i}E_{2i} - d_{2i}E_{2i} \\
&\quad + \sum_{j=1,j\neq i}^{n}\omega_{2ji}E_{2j} - \sum_{j=1,j\neq i}^{n}\omega_{2ij}E_{2i} \\
\frac{dI_{2i}}{dt} &= \varepsilon_{2i}E_{2i} - \gamma_{2i}I_{2i} - \mu_{2i}I_{2i} - d_{2i}I_{2i} + \sum_{j=1,j\neq i}^{n}\omega_{2ji}I_{2j} - \sum_{j=1,j\neq i}^{n}\omega_{2ij}I_{2i} \\
\frac{dR_{2i}}{dt} &= \gamma_{2i}I_{2i} - d_{2i}R_{2i} + \sum_{j=1,j\neq i}^{n}\omega_{2ji}R_{2j} - \sum_{j=1,j\neq i}^{n}\omega_{2ij}R_{2i} \\
\frac{dN_{2i}}{dt} &= r_{2i} - \mu_{2i}I_{2i} - d_{2i}N_{2i} + \sum_{j=1,j\neq i}^{n}\omega_{2ji}N_{2j} - \sum_{j=1,j\neq i}^{n}\omega_{2ij}N_{2i}
\end{aligned}
\tag{4.17}
$$

Human Population Model

$$
\begin{aligned}
\frac{dS_{4i}}{dt} &= b_{4i}N_{4i} - \beta_{14i}S_{4i}I_{1i}/N_{1i} - \beta_{24i}S_{4i}I_{2i}/N_{2i} - \beta_{34i}S_{4i}I_{3i}/N_{3i} - d_{4i}S_{4i}N_{4i}/K_4 \\
\frac{dE_{4i}}{dt} &= \beta_{14i}S_{4i}I_{1i}/N_{1i} + \beta_{24i}S_{4i}I_{2i}/N_{2i} + \beta_{34i}S_{4i}I_{3i}/N_{3i} - \varepsilon_{4i}E_{4i} - d_{4i}E_{4i}N_{4i}/K_4 \\
\frac{dI_{4i}}{dt} &= \varepsilon_{4i}E_{4i} - \gamma_{4i}I_{4i} - \mu_{4i}I_{4i} - d_{4i}I_{4i}N_{4i}/K_4 \\
\frac{dR_{4i}}{dt} &= \gamma_{4i}I_{4i} - d_{4i}R_{4i}N_{4i}/K_4 \\
\frac{dN_{4i}}{dt} &= b_{4i}N_{4i} - \mu_{4i}I_{4i} - d_{4i}N_{4i}N_{4i}/K_4
\end{aligned}
\tag{4.18}
$$

4.2.2 The Calculation of R_0 for an Rift Valley Fever Model

The explicit expression of R_0 in Equation (4.16) is applied to the RVF metapopulation model, lower and upper bounds of R_0 are derived based on the above assumptions in Section 4.2.1.

Parameter	Range or Value	Dimension	Source
β_{12}	$(0.0021, 0.2762)$	1/day	[22, 56, 59, 78, 96, 114, 115]
β_{21}	$(0.0021, 0.2429)$	1/day	[22, 56, 59, 78, 96, 113]
β_{23}	$(0.0000, 0.3200)$	1/day	[56, 59, 78, 96, 113, 123]
β_{32}	$(0.0000, 0.096)$	1/day	[56, 59, 78, 96, 123]
β_{14}		1/day	
β_{24}		1/day	
β_{34}		1/day	
$1/\gamma_2$	$(2, 5)$	days	[42]
$1/\gamma_4$	$(4, 7)$	days	[84]
$1/d_1$	$(3, 60)$	days	[15, 83, 96]
$1/d_2$	$(360, 3600)$	days	[97]
$1/d_3$	$(3, 60)$	days	[15, 83, 96]
$1/d_4$		days	
b_1		1/day	[15, 83, 96]
b_3		1/day	[15, 83, 96]
b_4		1/day	
$1/\epsilon_1$	$(4, 8)$	days	[114]
$1/\epsilon_2$	$(2, 6)$	days	[93]
$1/\epsilon_3$	$(4, 8)$	days	[114]
$1/\epsilon_4$	$(2, 6)$	days	[84]
μ_2	$(0.025, 0.1)$	1/day	[42, 93]
q_1	$(0, 0.1)$	1/day	[45]
$1/\theta_1$	$(5, 15)$	days	[96]
$1/\theta_3$	$(5, 15)$	days	[96]
K_1	10000		
K_3	10000		
K_4	100000		
r_{2i}	1	1/day	[84]
ω_{2ij}	$(0, \frac{1}{n})$	1/day	

Table 4.1: *Parameters in the model omitting the node index.*

Explicit Expression of R_0 for an Rift Valley Fever Model

First, a check must be made to verify whether a unique solution N_{ki}^0 exists. At DFE, $E_{ki}^0 = I_{ki}^0 = R_{ki}^0 = 0$. By computation, $S_{ki}^0 = N_{ki}^0 = \frac{b_{ki}K_k}{d_{ki}}$ for $k = 1, 3, 4$, where K_k is the carrying capacity of species k. This model is a special case of the model for Theorem 1, which generates a unique nonnegative solution for the total number of livestock in node i at DFE denoted by: $\begin{bmatrix} N_{21}^0 & \cdots & N_{2n}^0 \end{bmatrix}^T$.

By (4.1), Jacobian matrices for the RVF model are:

$$F = \begin{bmatrix} 0_{n\times n} & U_{n\times 8n} \\ 0_{8n\times n} & F_H \end{bmatrix}, \quad V = \begin{bmatrix} \oplus_{i=1}^n \theta_{1i} & 0_{n\times 8n} \\ W_{8n\times n} & V_H \end{bmatrix}.$$

Each component of the R_0 formula is computed as follows:

$$F_H = \begin{bmatrix} 0_{4n\times 4n} & Z_{4n\times 4n} \\ 0_{4n\times 4n} & 0_{4n\times 4n} \end{bmatrix}, \quad V_H = \begin{bmatrix} \bigoplus_{k=1}^4 Y_k & 0_{4n\times 4n} \\ -(\oplus_{k=1}^4(\oplus_{i=1}^n \varepsilon_{ki}))_{4n\times 4n} & \bigoplus_{k=1}^4 X_k \end{bmatrix}. \tag{4.19}$$

$$U = \begin{bmatrix} 0_{n\times 4n} & \oplus_{i=1}^n (b_{1i}q_{1i}) & 0_{n\times 3n} \end{bmatrix}, \quad W = \begin{bmatrix} 0_{4n\times n} \\ -(\oplus_{i=1}^n \theta_{1i}) \\ 0_{3n\times n} \end{bmatrix}. \tag{4.20}$$

$$Z = \begin{bmatrix} 0 & Z_{12} & 0 & 0 \\ Z_{21} & 0 & Z_{23} & 0 \\ 0 & Z_{32} & 0 & 0 \\ Z_{41} & Z_{42} & Z_{43} & 0 \end{bmatrix}, \tag{4.21}$$

$$Z_{12} = \oplus_{i=1}^n \beta_{21i}\frac{S_{1i}^0}{N_{2i}^0}, \quad Z_{21} = \oplus_{i=1}^n \beta_{12i}\frac{S_{2i}^0}{N_{1i}^0}, \quad Z_{23} = \oplus_{i=1}^n \beta_{32i}\frac{S_{2i}^0}{N_{3i}^0}, \quad Z_{32} = \oplus_{i=1}^n \beta_{23i}\frac{S_{3i}^0}{N_{2i}^0},$$
$$Z_{41} = \oplus_{i=1}^n \beta_{14i}\frac{S_{4i}^0}{N_{1i}^0}, \quad Z_{42} = \oplus_{i=1}^n \beta_{24i}\frac{S_{4i}^0}{N_{2i}^0}, \quad Z_{43} = \oplus_{i=1}^n \beta_{34i}\frac{S_{4i}^0}{N_{3i}^0}.$$

The matrices V_H^{-1} and V^{-1} are in Equation (4.15) with g=1 and h=4, respectively. Below, matrices Y_k and X_k relate to *Aedes* mosquitoes, livestock, *Culex* mosquitoes, and humans with $k = 1, 2, 3, 4$, respectively.

$$Y_1 = \oplus_{i=1}^n (\tfrac{d_{1i}N_{1i}^0}{K_1} + \varepsilon_{1i}), \quad X_1 = Y_1 - \oplus_{i=1}^n \varepsilon_{1i},$$
$$Y_3 = \oplus_{i=1}^n (\tfrac{d_{3i}N_{3i}^0}{K_3} + \varepsilon_{3i}), \quad X_3 = Y_3 - \oplus_{i=1}^n \varepsilon_{3i},$$
$$Y_4 = \oplus_{i=1}^n (\tfrac{d_{4i}N_{4i}^0}{K_4} + \varepsilon_{4i}), \quad X_4 = Y_4 - \oplus_{i=1}^n \varepsilon_{4i},$$

$$Y_2 = \begin{bmatrix} \zeta_{21} & -\omega_{221} & \cdots & -\omega_{2n1} \\ -\omega_{212} & \zeta_{22} & \cdots & -\omega_{2n2} \\ \cdots & \cdots & \cdots & \cdots \\ -\omega_{21n} & -\omega_{22n} & \cdots & \zeta_{2n} \end{bmatrix}, \quad X_2 = Y_2 + \oplus_{i=1}^{n}(\gamma_{2i} + \mu_{2i} - \varepsilon_{2i}).$$

The reproduction number can be computed by plugging the above terms into Equation (4.16). Typically, R_0 for a metapopulation model is complicated [9], deriving some bounds on the value of R_0 can be helpful [9]. In the following section, lower and upper bounds for R_0 are derived.

Deriving Lower and Upper Bounds for R_0

Bounds of R_0 are derived in many articles, including the following examples. Gao and Ruan presented bounds of R_0 for an SIS patch model [48] investigating effects of media coverage and human movement on the spread of infectious diseases, as well as a malaria model [49]. Hsieh, Driessche, and Wang [58] derived bounds of R_0, describing the relationship between the reproduction numbers for the isolated i^{th} patch and for the system. Salmani and van den Driessche [104] derived bounds for an SEIRS patch model. Arino [9] presented bounds of R_0 for patch models considering multiple species. The reproduction number for an averaging process of mixed individuals or groups is estimated to be smaller than or equal to the reproduction number before mixing [3]. Bounds of R_0 were derived for an RVF metapopulation model in this section.

Theorem 2. *Consider the model in Equations* (2.14), (2.15), (4.17), *and* (4.18), *then*

$$\rho(F_H V_H^{-1}) \leqslant R_0 \leqslant \rho(F_H V_H^{-1}) + \max_i(q_{1i}). \tag{4.22}$$

Proof. The left inequality is the same as (4.11). The right inequality is to be proven to hold. By (4.15) and (4.20),

$$-W(\oplus_{i=1}^{n}\theta_{1i}^{-1})UV_H^{-1} = \begin{bmatrix} 0_{4n\times 4n} & 0_{4n\times 4n} \\ \mathcal{Y} & \mathcal{Z} \end{bmatrix}, \text{ where}$$

$$\mathcal{Y} = \begin{bmatrix} X_1^{-1}(\oplus_{i=1}^{n}(b_{1i}q_{1i}\varepsilon_{1i}))Y_1^{-1} & 0_{n\times 3n} \\ 0_{3n\times n} & 0_{3n\times 3n} \end{bmatrix}, \quad \mathcal{Z} = \begin{bmatrix} (\oplus_{i=1}^{n}(b_{1i}q_{1i}))X_1^{-1} & 0_{n\times 3n} \\ 0_{3n\times n} & 0_{3n\times 3n} \end{bmatrix}.$$

Matrices X_1 and X_1^{-1} are diagonal matrices and the nonzero eigenvalues of $-W(\oplus_{i=1}^{n}\theta_{1i}^{-1})UV_H^{-1}$ are diagonal entries of $(\oplus_{i=1}^{n}(b_{1i}q_{1i}))X_1^{-1}$. Hence, $-W(\oplus_{i=1}^{n}\theta_{1i}^{-1})UV_H^{-1} = \mathcal{P}\mathcal{D}\mathcal{P}^{-1}$ for some $\mathcal{P}$. Here

$$\mathcal{D} = \begin{bmatrix} 0_{4n\times 4n} & 0_{4n\times 4n} \\ 0_{4n\times 4n} & \mathcal{Q} \end{bmatrix}, \quad \mathcal{Q} = \begin{bmatrix} 0_{3n\times 3n} & 0_{3n\times n} \\ 0_{n\times 3n} & (\oplus_{i=1}^{n}(b_{1i}q_{1i}))X_1^{-1} \end{bmatrix}.$$

From linear algebra, each column of $\mathcal{P}$ can be chosen as an eigenvector of $-W(\oplus_{i=1}^{n}\theta_{1i}^{-1})UV_H^{-1}$. By direct calculation,

$$\mathcal{P} = \begin{bmatrix} \mathcal{H}_{4n\times 4n} & 0 \\ \mathcal{J}_{4n\times 4n} & \mathcal{L}_{4n\times 4n} \end{bmatrix}, \quad \text{where} \quad \mathcal{H} = \begin{bmatrix} (\oplus_{i=1}^{n}(b_{1i}q_{1i}))X_1^{-1} & 0_{n\times 3n} \\ 0_{3n\times n} & I_{3n\times 3n} \end{bmatrix},$$
$$\mathcal{L} = \begin{bmatrix} 0_{n\times 3n} & I_{n\times n} \\ I_{3n\times 3n} & 0_{3n\times n} \end{bmatrix}, \quad \mathcal{J} = \begin{bmatrix} -(\oplus_{i=1}^{n}(b_{1i}q_{1i}\varepsilon_{1i}))X_1^{-1}Y_1^{-1} & 0_{n\times 3n} \\ 0_{3n\times n} & 0_{3n\times 3n} \end{bmatrix}.$$

Since $F_HV_H^{-1} - W(\oplus_{i=1}^{n}\theta_{1i}^{-1})UV_H^{-1} = \mathcal{P}(\mathcal{P}^{-1}F_HV_H^{-1}\mathcal{P} + \mathcal{D})\mathcal{P}^{-1}$,

$$\rho(FV^{-1}) = \rho(F_HV_H^{-1} - W(\oplus_{i=1}^{n}\theta_{1i}^{-1})UV_H^{-1}) = \rho(\mathcal{P}^{-1}F_HV_H^{-1}\mathcal{P} + \mathcal{D}). \tag{4.23}$$

Matrix $\mathcal{P}^{-1}F_HV_H^{-1}\mathcal{P}$ is to be proven to be a nonnegative matrix. By calculation,

$$\mathcal{P}^{-1} = \begin{bmatrix} \mathcal{H}^{-1} & 0 \\ -\mathcal{L}^{-1}\mathcal{J}\mathcal{H}^{-1} & \mathcal{L}^{-1} \end{bmatrix}, \ \mathcal{H}^{-1} = \begin{bmatrix} (\oplus_{i=1}^{n}\frac{1}{b_{1i}q_{1i}})X_1 & 0_{n\times 3n} \\ 0_{3n\times n} & I_{3n\times 3n} \end{bmatrix}, \ \mathcal{L}^{-1} = \begin{bmatrix} 0_{3n\times n} & I_{3n\times 3n} \\ I_{n\times n} & 0_{n\times 3n} \end{bmatrix}.$$

By direct checking, $\mathcal{H}^{-1}$, $\mathcal{L}^{-1}$, and $-\mathcal{L}^{-1}\mathcal{J}\mathcal{H}^{-1}$ are all nonnegative matrices. Hence, $\mathcal{P}^{-1}$ is a nonnegative matrix. Next, matrix $F_HV_H^{-1}\mathcal{P}$ is to be proven to be a nonnegative matrix.

$$F_HV_H^{-1}\mathcal{P} = \begin{bmatrix} Z(\oplus_{k=1}^{4}L_k)\mathcal{H} + Z(\oplus_{k=1}^{4}X_k^{-1})\mathcal{J} & Z(\oplus_{k=1}^{4}X_k^{-1})\mathcal{L} \\ 0 & 0 \end{bmatrix},$$

where $Z(\oplus_{k=1}^{4}X_k^{-1})\mathcal{L}$ is a nonnegative matrix and $L_k = X_k^{-1}(\oplus_{i=1}^{n}\varepsilon_{ki})Y_k^{-1}$. Furthermore, the only possible negative entries of $Z(\oplus_{k=1}^{4}L_k)\mathcal{H} + Z(\oplus_{k=1}^{4}X_k^{-1})\mathcal{J}$ are in its $(2,1)$ and $(4,1)$ blocks. But the block in $(2,1)$-entry is

$$Z_{21}X_1^{-1}(\oplus_{i=1}^{n}\varepsilon_{1i})Y_1^{-1}(\oplus_{i=1}^{n}(b_{1i}q_{1i}))X_1^{-1} + Z_{21}X_1^{-1}(-\oplus_{i=1}^{n}(b_{1i}q_{1i}\varepsilon_{1i}))X_1^{-1}Y_1^{-1} = 0.$$

By assumption, X_1 and Y_1 are both diagonal matrices. The last equality follows $X_1^{-1}Y_1^{-1} = Y_1^{-1}X_1^{-1}$. Similarly, the block in $(4,1)$-entry is

$$Z_{41}X_1^{-1}(\oplus_{i=1}^{n}\varepsilon_{1i})Y_1^{-1}(\oplus_{i=1}^{n}(b_{1i}q_{1i}))X_1^{-1} + Z_{41}X_1^{-1}(-\oplus_{i=1}^{n}(b_{1i}q_{1i}\varepsilon_{1i}))X_1^{-1}Y_1^{-1} = 0.$$

Hence, $F_H V_H^{-1}\mathcal{P}$ is a nonnegative matrix. This proves the claim. By Theorem 2 in [32],

$$\rho(FV^{-1}) \leq \rho(\mathcal{P}^{-1}F_H V_H^{-1}\mathcal{P}) + \rho(\mathcal{D}) = \rho(F_H V_H^{-1}) + \rho(\mathcal{D}). \tag{4.24}$$

Since $X_1 = \oplus_{i=1}^n \frac{d_{1i}N_{1i}^0}{K_1}$ and $N_{1i}^0 = \frac{b_{1i}K_1}{d_{1i}}$,

$$\rho(\mathcal{D}) = \rho(-W(\oplus_{i=1}^n \theta_{1i}^{-1})UV_H^{-1}) = \rho((\oplus_{i=1}^n (b_{1i}q_{1i}))X_1^{-1}) = \rho(\oplus_{i=1}^n q_{1i}) \leqslant \max_i(q_{1i}).$$

Therefore,

$$\rho(F_H V_H^{-1}) \leq R_0 = \rho(FV^{-1}) \leq \rho(F_H V_H^{-1}) + \max_i(q_{1i}).$$

□

The difference between the lower and upper bounds is $\max_i(q_{1i})$ with lower bound, $\rho(F_H V_H^{-1})$, computed by Equation (4.28).

Theorem 3. *For the model in Equations* (2.14), (2.15), (4.17), *and* (4.18), *assume* $\varepsilon_{2i} = \varepsilon_2$ *for all* i, *then*

$$\sqrt{\min_i(\chi_i)\rho(X_2^{-1}Y_2^{-1})} \leqslant R_0 \leqslant \sqrt{\max_i(\chi_i)\rho(X_2^{-1}Y_2^{-1})} + \max_i(q_{1i}), \tag{4.25}$$

where

$$\chi_i = \frac{\varepsilon_{1i}\varepsilon_2\beta_{12i}\beta_{21i}}{b_{1i}(b_{1i}+\varepsilon_{1i})} + \frac{\varepsilon_2\varepsilon_{3i}\beta_{32i}\beta_{23i}}{b_{3i}(b_{3i}+\varepsilon_{3i})}. \tag{4.26}$$

Proof. By Equations (4.15) and (4.19),

$$F_H V_H^{-1} = \begin{bmatrix} Z(\oplus_{k=1}^4 L_k) & Z(\oplus_{k=1}^4 X_k^{-1}) \\ 0 & 0 \end{bmatrix}.$$

Then

$$R_0^H = \rho(F_H V_H^{-1}) = \rho(Z(\oplus_{k=1}^4 L_k)). \tag{4.27}$$

By Equation (4.21),

$$Z(\oplus_{k=1}^4 L_k) = \begin{bmatrix} 0 & Z_{12}L_2 & 0 & 0 \\ Z_{21}L_1 & 0 & Z_{23}L_3 & 0 \\ 0 & Z_{32}L_2 & 0 & 0 \\ Z_{41}L_1 & Z_{42}L_2 & Z_{43}L_3 & 0 \end{bmatrix} =: \begin{bmatrix} 0 & \mathcal{T}_1 & 0 & 0 \\ \mathcal{T}_2 & 0 & \mathcal{T}_3 & 0 \\ 0 & \mathcal{T}_4 & 0 & 0 \\ \mathcal{T}_5 & \mathcal{T}_6 & \mathcal{T}_7 & 0 \end{bmatrix}.$$

To compute the eigenvalues of $Z(\oplus_{k=1}^{4} L_k)$, first the characteristic polynomial of $Z(\oplus_{k=1}^{4} L_k)$ is calculated:

$$
\begin{aligned}
|\lambda I_{4n} - Z(\oplus_{k=1}^{4} L_k)| &= \begin{vmatrix} \lambda I_n & -\mathcal{T}_1 & 0 & 0 \\ -\mathcal{T}_2 & \lambda I_n & -\mathcal{T}_3 & 0 \\ 0 & -\mathcal{T}_4 & \lambda I_n & 0 \\ -\mathcal{T}_5 & -\mathcal{T}_6 & -\mathcal{T}_7 & \lambda I_n \end{vmatrix} = \lambda^n \begin{vmatrix} \lambda I_n & -\mathcal{T}_1 & 0 \\ -\mathcal{T}_2 & \lambda I_n & -\mathcal{T}_3 \\ 0 & -\mathcal{T}_4 & \lambda I_n \end{vmatrix} \\
&= \lambda^n \left| \begin{bmatrix} I_n & \lambda \mathcal{T}_2^{-1} & 0 \\ 0 & I_n & 0 \\ 0 & 0 & I_n \end{bmatrix} \begin{bmatrix} \lambda I_n & -\mathcal{T}_1 & 0 \\ -\mathcal{T}_2 & \lambda I_n & -\mathcal{T}_3 \\ 0 & -\mathcal{T}_4 & \lambda I_n \end{bmatrix} \right| = \lambda^n \left| \begin{bmatrix} 0 & -\mathcal{T}_1 + \lambda^2 \mathcal{T}_2^{-1} & -\lambda \mathcal{T}_2^{-1} \mathcal{T}_3 \\ -\mathcal{T}_2 & \lambda I_n & -\mathcal{T}_3 \\ 0 & -\mathcal{T}_4 & \lambda I_n \end{bmatrix} \right| \\
&= \lambda^n |\mathcal{T}_2| \begin{vmatrix} -\mathcal{T}_1 + \lambda^2 \mathcal{T}_2^{-1} & -\lambda \mathcal{T}_2^{-1} \mathcal{T}_3 \\ -\mathcal{T}_4 & \lambda I_n \end{vmatrix} = \lambda^n |\mathcal{T}_2| \left| \begin{bmatrix} -\mathcal{T}_1 + \lambda^2 \mathcal{T}_2^{-1} & -\lambda \mathcal{T}_2^{-1} \mathcal{T}_3 \\ -\mathcal{T}_4 & \lambda I_n \end{bmatrix} \begin{bmatrix} I_n & \lambda \mathcal{T}_4^{-1} \\ 0 & I_n \end{bmatrix} \right| \\
&= \lambda^n |\mathcal{T}_2| \begin{vmatrix} -\mathcal{T}_1 + \lambda^2 \mathcal{T}_2^{-1} & -\lambda(\mathcal{T}_1 \mathcal{T}_4^{-1} - \lambda^2 \mathcal{T}_2^{-1} \mathcal{T}_4^{-1} + \mathcal{T}_2^{-1} \mathcal{T}_3) \\ -\mathcal{T}_4 & 0 \end{vmatrix} \\
&= \lambda^n |\mathcal{T}_2| \begin{vmatrix} -\lambda(\mathcal{T}_1 \mathcal{T}_4^{-1} - \lambda^2 \mathcal{T}_2^{-1} \mathcal{T}_4 + \mathcal{T}_2^{-1} \mathcal{T}_3) & \mathcal{T}_1 - \lambda^2 \mathcal{T}_2^{-1} \\ 0 & \mathcal{T}_4 \end{vmatrix} \\
&= \lambda^n |\mathcal{T}_2| |\mathcal{T}_4| \left| -\lambda(\mathcal{T}_1 \mathcal{T}_4^{-1} - \lambda^2 \mathcal{T}_2^{-1} \mathcal{T}_4^{-1} + \mathcal{T}_2^{-1} \mathcal{T}_3) \right| \\
&= \lambda^{2n} |\mathcal{T}_2| |\mathcal{T}_4| \left| \lambda^2 \mathcal{T}_2^{-1} \mathcal{T}_4^{-1} - (\mathcal{T}_1 \mathcal{T}_4^{-1} + \mathcal{T}_2^{-1} \mathcal{T}_3) \right| \\
&= \lambda^{2n} |\mathcal{T}_2| |\mathcal{T}_4| |\mathcal{T}_2^{-1}| |\mathcal{T}_4^{-1}| \left| \lambda^2 I_n - (\mathcal{T}_4 \mathcal{T}_2 \mathcal{T}_1 \mathcal{T}_4^{-1} + \mathcal{T}_4 \mathcal{T}_3) \right| \\
&= \lambda^{2n} \left| \lambda^2 I_n - (\mathcal{T}_4 \mathcal{T}_2 \mathcal{T}_1 \mathcal{T}_4^{-1} + \mathcal{T}_4 \mathcal{T}_3) \right|.
\end{aligned}
$$

Matrix $Z(\oplus_{k=1}^{4} L_k)$ has $2n$ zero eigenvalues. The spectral radius of $Z(\oplus_{k=1}^{4} L_k)$ is the square root of the spectral radius of $\mathcal{T}_4 \mathcal{T}_2 \mathcal{T}_1 \mathcal{T}_4^{-1} + \mathcal{T}_4 \mathcal{T}_3$. By Equation (4.27),

$$
\rho(F_H V_H^{-1}) = \sqrt{\rho(\mathcal{T}_4 \mathcal{T}_2 \mathcal{T}_1 \mathcal{T}_4^{-1} + \mathcal{T}_4 \mathcal{T}_3)} = \sqrt{\rho(\mathcal{T}_4 (\mathcal{T}_2 \mathcal{T}_1 + \mathcal{T}_3 \mathcal{T}_4) \mathcal{T}_4^{-1})} = \sqrt{\rho(\mathcal{T}_2 \mathcal{T}_1 + \mathcal{T}_3 \mathcal{T}_4)}. \tag{4.28}
$$

Recall that Z_{21}, Z_{12}, X_1, Y_1, Z_{23}, Z_{32}, Y_3, X_3 are all diagonal matrices. By the assumption that $\varepsilon_{2i} = \varepsilon_2$, for all i,

$$
\begin{aligned}
\mathcal{T}_2 \mathcal{T}_1 &= (\oplus_{i=1}^{n} \varepsilon_{1i} \varepsilon_2) Z_{21} X_1^{-1} Y_1^{-1} Z_{12} X_2^{-1} Y_2^{-1} = (\oplus_{i=1}^{n} \frac{\varepsilon_2 \varepsilon_{1i} \beta_{12i} \beta_{21i}}{b_{1i}(b_{1i} + \varepsilon_{1i})}) X_2^{-1} Y_2^{-1}, \\
\mathcal{T}_3 \mathcal{T}_4 &= (\oplus_{i=1}^{n} \varepsilon_2 \varepsilon_{3i}) Z_{23} X_3^{-1} Y_3^{-1} Z_{32} X_2^{-1} Y_2^{-1} = (\oplus_{i=1}^{n} \frac{\varepsilon_2 \varepsilon_{3i} \beta_{32i} \beta_{23i}}{b_{3i}(b_{3i} + \varepsilon_{3i})}) X_2^{-1} Y_2^{-1}.
\end{aligned}
$$

By the definition of χ_i in (4.26),

$$
\min_i(\chi_i) \rho(X_2^{-1} Y_2^{-1}) \leqslant \rho(\mathcal{T}_2 \mathcal{T}_1 + \mathcal{T}_3 \mathcal{T}_4) \leqslant \max_i(\chi_i) \rho(X_2^{-1} Y_2^{-1}).
$$

Therefore,

$$\sqrt{\min_i(\chi_i)\rho(X_2^{-1}Y_2^{-1})} \leqslant \rho(F_H V_H^{-1}) \leqslant \sqrt{\max_i(\chi_i)\rho(X_2^{-1}Y_2^{-1})}.$$

According to Theorem 2,

$$\sqrt{\min_i(\chi_i)\rho(X_2^{-1}Y_2^{-1})} \leqslant R_0 \leqslant \sqrt{\max_i(\chi_i)\rho(X_2^{-1}Y_2^{-1})} + \max_i(q_{1i}).$$

□

The difference between the lower bound and the upper bound in a network with heterogeneous corresponding parameters across nodes is larger than that in Inequality (4.22).

Corollary 1. *Suppose for all i, birth and incubation rates in mosquitoes and livestock, contact rates between livestock and mosquitoes are homogeneous for different nodes, i.e.,*

$$b_{1i} = b_1,\ b_{3i} = b_3,\ \varepsilon_{1i} = \varepsilon_1,\ \varepsilon_{2i} = \varepsilon_2,\ \varepsilon_{3i} = \varepsilon_3,\ \beta_{12i} = \beta_{12},\ \beta_{21i} = \beta_{21},\ \beta_{23i} = \beta_{23},\ \beta_{32i} = \beta_{32}. \tag{4.29}$$

Then

$$\sqrt{\chi\rho(X_2^{-1}Y_2^{-1})} \leqslant R_0 \leqslant \sqrt{\chi\rho(X_2^{-1}Y_2^{-1})} + \max_i(q_{1i}). \tag{4.30}$$

where

$$\chi = \frac{\varepsilon_1\varepsilon_2\beta_{12}\beta_{21}}{b_1(b_1+\varepsilon_1)} + \frac{\varepsilon_2\varepsilon_3\beta_{32}\beta_{23}}{b_3(b_3+\varepsilon_3)}. \tag{4.31}$$

Proof. By the conditions in (4.29) and (4.34),

$$\begin{aligned}\frac{\min_i(\chi_i)}{\max_i(d_{2i}+\varepsilon_{2i})\max_i(d_{2i}+\gamma_{2i}+\mu_{2i})} &= \frac{\chi}{(d_2+\varepsilon_2)(d_2+\gamma_2+\mu_2)} \\ &= \frac{\max_i(\chi_i)}{\min_i(d_{2i}+\varepsilon_{2i})\min_(d_{2i}+\gamma_{2i}+\mu_{2i})}.\end{aligned}$$

Corollary follows Theorem 4. □

Theorem 4. *Under the condition of Theorem 3, R_0 can be estimated by the following inequality:*

$$\sqrt{\frac{\min_i(\chi_i)}{\max_i(d_{2i}+\varepsilon_2)\max_i(d_{2i}+\gamma_{2i}+\mu_{2i})}} \leqslant R_0$$

$$\leqslant \sqrt{\frac{\max_i(\chi_i)}{\min_i(d_{2i}+\varepsilon_2)\min_i(d_{2i}+\gamma_{2i}+\mu_{2i})}} + \max_i(q_{1i}). \tag{4.32}$$

Proof. According to Theorem 8,

$$\frac{1}{\max_i(d_{2i}+\varepsilon_{2i})\max_i(d_{2i}+\gamma_{2i}+\mu_{2i})} \leqslant \rho(X_2^{-1}Y_2^{-1}) \leqslant \frac{1}{\min_i(d_{2i}+\varepsilon_{2i})\min_i(d_{2i}+\gamma_{2i}+\mu_{2i})}. \tag{4.33}$$

By Theorem 3,

$$\sqrt{\frac{\min_i(\chi_i)}{\max_i(d_{2i}+\varepsilon_{2i})\max_i(d_{2i}+\gamma_{2i}+\mu_{2i})}} \leqslant R_0$$
$$\leqslant \sqrt{\frac{\max_i(\chi_i)}{\min_i(d_{2i}+\varepsilon_{2i})\min_(d_{2i}+\gamma_{2i}+\mu_{2i})}} + \max_i(q_{1i}).$$

□

If the differences between $\min_i(\chi_i)$ and $\max_i(\chi_i)$, $\min_i(d_{2i}+\varepsilon_2)$ and $\max_i(d_{2i}+\varepsilon_2)$, $\min_i(d_{2i}+\gamma_{2i}+\mu_{2i})$ and $\max_i(d_{2i}+\gamma_{2i}+\mu_{2i})$ are large, then the difference between the lower bound and the upper bound may be large. However, the scalar lower and upper bounds are more easily computed. Moreover, if the lower bound is greater than one, the conclusion can be drawn that the network may be invaded without computing R_0 or its upper bound.

Corollary 2. *Based on the condition for Corollary 1, the assumption is further made that for all i, the death rate, mortality rate, and recovery rate in livestock, and transovarial transmission rate in Aedes mosquitoes are homogeneous for all nodes, i.e.,*

$$d_{2i} = d_2, \quad \mu_{2i} = \mu_2, \quad \gamma_{2i} = \gamma_2, \quad q_{1i} = q_1. \tag{4.34}$$

Consequently,

$$\sqrt{\frac{\chi}{(d_2+\varepsilon_2)(d_2+\gamma_2+\mu_2)}} \leqslant R_0 \leqslant \sqrt{\frac{\chi}{(d_2+\varepsilon_2)(d_2+\gamma_2+\mu_2)}} + q_1. \tag{4.35}$$

Proof. By the assumptions in (4.29), $\min_i(\chi_i) = \max_i(\chi_i) = \chi$. Corollary follows Theorem 3. □

In this case, the lower and upper bounds of R_0 correspond to the bounds for homogeneous populations presented in [131] and are tight. Clearly, R_0 for horizontal transmission,

$$R_0^H = \sqrt{\frac{\varepsilon_2}{(d_2+\varepsilon_2)(d_2+\gamma_2+\mu_2)}\left[\frac{\varepsilon_1\beta_{12}\beta_{21}}{b_1(b_1+\varepsilon_1)}+\frac{\varepsilon_3\beta_{32}\beta_{23}}{b_3(b_3+\varepsilon_3)}\right]}, \tag{4.36}$$

does not depend on livestock movement rates. Only bounds for R_0 can theoretically be obtained. Based on numerical simulation results, the conjecture is made that given the conditions for Corollary 2, R_0 does not depend on livestock movement rates.

The bounds for R_0 in inequalities (4.35) can be interpreted biologically as follows. The lower bound, R_0^H, is R_0 for horizontal transmission because $R_0^H = \rho\,(F_H V_H^{-1})$, where $\rho(F_H V_H^{-1})$ represents the spectral radius of the next generation matrix for horizontal transmission $F_H V_H^{-1}$. The upper bound is given by the sum of R_0^H and a second term that is only related to vertical transmission, i.e., from mothers to their offspring in the *Aedes* mosquito population.

R_0^H includes *Aedes*-livestock interaction and *Culex*-livestock interaction. R_0^H for interaction between *Aedes* and livestock is represented by:

$$R_0^{H(A-L)} = \sqrt{\frac{\varepsilon_2}{(d_2+\varepsilon_2)(d_2+\gamma_2+\mu_2)}\frac{\varepsilon_1\beta_{12}\beta_{21}}{b_1(b_1+\varepsilon_1)}},$$

and $R_0^{H(A-L)}$ can be rewritten as:

$$R_0^{H(A-L)} = \sqrt{\left[\frac{\beta_{12}}{d_1\frac{N_1^0}{K_1}}\frac{\varepsilon_1}{(d_1\frac{N_1^0}{K_1}+\varepsilon_1)}\right]\left[\frac{\beta_{21}}{(d_2+\gamma_2+\mu_2)}\frac{\varepsilon_2}{(d_2+\varepsilon_2)}\right]}, \tag{4.37}$$

which is a product of four terms. Each infected *Aedes* mosquito can infect $\frac{\beta_{12}}{d_1\frac{N_1^0}{K_1}}$ susceptible livestock throughout its lifetime. Similarly, each infected livestock can infect $\frac{\beta_{21}}{d_2+\gamma_2+\mu_2}$ susceptible *Aedes* mosquitoes during its lifetime. The probability of *Aedes* mosquitoes and livestock surviving through incubation period to the point where they become infectious is $\frac{\varepsilon_1}{d_1\frac{N_1^0}{K_1}+\varepsilon_1}$ and $\frac{\varepsilon_2}{d_2+\varepsilon_2}$, respectively. Therefore, $R_0^{H(A-L)}$ is geometric mean of the average number of secondary livestock infections produced by one *Aedes* mosquito vector in the first square bracket in (4.37), and average number of secondary *Aedes* mosquito vector infections produced by one livestock host in the second square bracket in (4.37).

Similarly, R_0^H due to interaction between *Culex* and livestock is represented by:

$$R_0^{H(C-L)} = \sqrt{\frac{\varepsilon_2}{(d_2+\varepsilon_2)(d_2+\gamma_2+\mu_2)}\frac{\varepsilon_3\beta_{32}\beta_{23}}{b_3(b_3+\varepsilon_3)}},$$

and it can be rewritten as $R_0^{H(C-L)}$ as:

$$R_0^{H(C-L)} = \sqrt{\left[\frac{\beta_{32}}{d_3\frac{N_3^0}{K_3}}\frac{\varepsilon_3}{(d_3\frac{N_3^0}{K_3}+\varepsilon_3)}\right]\left[\frac{\beta_{23}}{(d_2+\gamma_2+\mu_2)}\frac{\varepsilon_2}{(d_2+\varepsilon_2)}\right]}, \tag{4.38}$$

which is also a product of four terms. Each infected *Culex* mosquito can infect $\frac{\beta_{32}}{d_3\frac{N_3^0}{K_3}}$ susceptible livestock throughout its lifetime. Similarly, each infected livestock can infect $\frac{\beta_{23}}{d_2+\gamma_2+\mu_2}$ susceptible *Culex* mosquitoes. The probability of *Culex* mosquitoes surviving through the incubation period to the point where they become infectious is $\frac{\varepsilon_3}{d_3\frac{N_3^0}{K_3}+\varepsilon_3}$. Similarly, the probability of livestock surviving through the incubation period to the point where they become infectious is $\frac{\varepsilon_2}{d_2+\varepsilon_2}$. Therefore, $R_0^{H(C-L)}$ is the geometric mean of average number of secondary livestock infections produced by one *Culex* mosquito vector in the first square bracket in (4.38), and average number of secondary *Culex* mosquito vector infections produced by one livestock in the second square bracket in (4.38).

The expression (4.36) for R_0^H can be rewritten as $R_0^H = \sqrt{(R_0^{H(A-L)})^2 + (R_0^{H(C-L)})^2}$, which increases with the increase of each of the four terms in $R_0^{H(A-L)}$ and $R_0^{H(C-L)}$. The square root is due to the vector-host-vector viral transmission path [46, 57, 98]. The dependence of R_0^H on $R_0^{H(A-L)}$ and $R_0^{H(C-L)}$ is shown in Figure 4.1.

Tightness of Bounds for R_0

A 100-node network with heterogeneous corresponding parameters among nodes was built to study the tightness of bounds. Disease parameters were uniformly distributed for each node during 100 runs within their respective ranges, given in Table 4.1. Then, R_0 was numerically computed according to Equation (4.16). Lower and upper bounds of R_0 were computed according to Inequality (4.22) in Theorem 2. The reproduction number for horizontal transmission was computed according to Equation (4.28). The lower bound of R_0

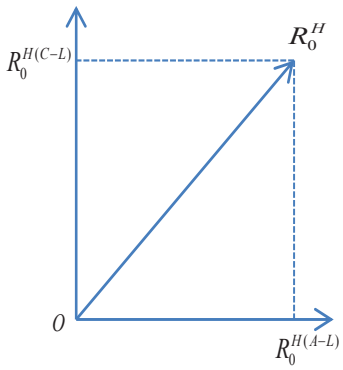

Figure 4.1: *The interpretation of* R_0^H.

(denoted by R_0^L) versus R_0 in each run was shown in Figure 4.2(a), and the upper bound of R_0 (denoted by R_0^U) versus R_0 in each run was shown in Figure 4.2(b). In each run, the upper bound was slightly greater and the lower bound was slightly smaller than R_0. With the same network and the same set of parameters, the lower and upper bounds of R_0 were computed using Inequality (4.25). The lower bound versus exact R_0 was shown in Figure 4.3(*a*), and the upper bound versus exact R_0 was shown in Figure 4.3(b). The bounds obtained by Inequality (4.25) in Theorem 3 are less tight than those obtained by Inequality (4.22) in Theorem 2, as $\rho(F_H V_H^{-1})$ is estimated by computing the spectral radius of a smaller size matrix. The bounds obtained by Inequality (4.32) in Theorem 4 can be even looser because $\rho(X_2^{-1}Y_2^{-1})$ is estimated by scalars.

The above bounds are for heterogeneous networks. The bounds in Corollary 2 (see Inequality (4.35)) apply to homogeneous networks in which the difference between the lower bound and the upper bound is the largest transovarial transmission rate of *Aedes* mosquitoes across nodes.

4.2.3 Assessing Roles of Parameters on R_0

As an example, a two-node network demonstrates how bounds of R_0 alter with livestock movement rates, if parameters d_{2i}, γ_{2i}, and μ_{2i} are heterogeneous, i.e., at least one of the inequalities $d_{2i} \neq d_{2j}$, $\gamma_{2i} \neq \gamma_{2j}$, $\mu_{2i} \neq \mu_{2j}$ holds for different i and j. In this example, Y_2

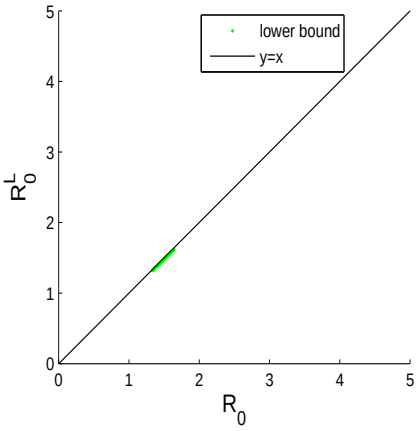

(a) The reproduction number and its lower bound with heterogeneous parameters

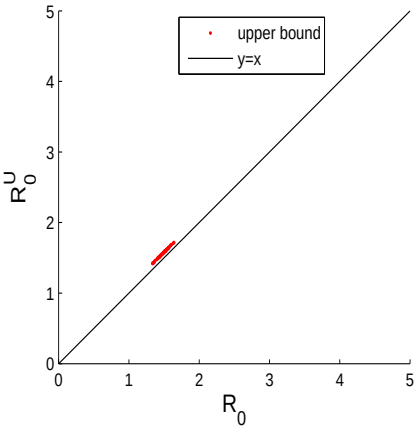

(b) The reproduction number and its upper bound with heterogeneous parameters

Figure 4.2: *The reproduction number and its lower and upper bounds computed using Theorem 2 for* 100 *simulation runs on* 100*-node heterogeneous networks.*

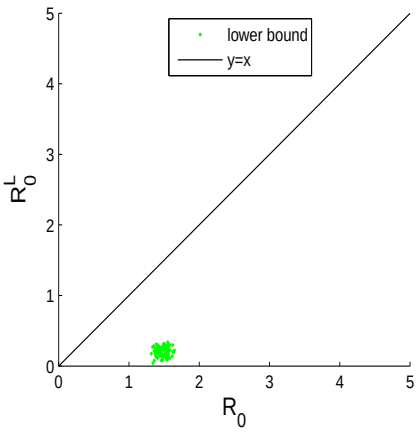

(a) The reproduction number and its lower bound with heterogeneous parameters

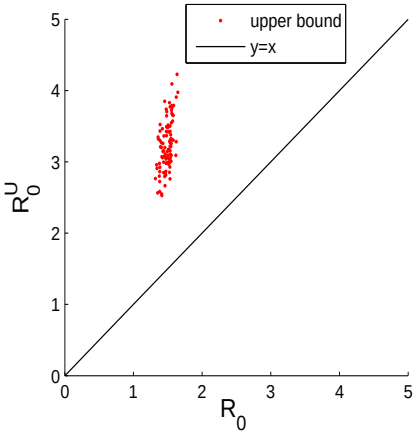

(b) The reproduction number and its upper bound with heterogeneous parameters

Figure 4.3: *The reproduction number and its lower and upper bounds computed using Theorem 3 for* 100 *simulation runs on* 100*-node heterogeneous networks.*

corresponds to the matrix in Equation (4.4) and $X_2 = Y_2 + \oplus_{i=1}^{2}(\gamma_{2i} + \mu_{2i} - \varepsilon_{2i})$. Since X_2, Y_2 are both diagonal dominant matrices, by Theorem 9, Y_2^{-1} and X_2^{-1} are both nonnegative matrices.

According to Proposition 4.3 in [49], $\rho(X_2^{-1}Y_2^{-1})$ is decreasing in ω_{212} if

$$\omega_{212}(a_2 - a_1) > (a_1c_1 - a_2c_2) - (a_2 - a_1)\omega_{221}$$

and increasing otherwise, where $a_1 = d_{21} + \varepsilon_{21}, a_2 = d_{22} + \varepsilon_{22}$, $c_1 = d_{21} + \gamma_{21} + \mu_{21}$ and $c_2 = d_{22} + \gamma_{22} + \mu_{22}$. In the case that $a_1 = a_2$, $\rho(X_2^{-1}Y_2^{-1})$ is decreasing in ω_{212} if $c_2 > c_1$ and increasing otherwise. If $a_1 \neq a_2$, $\omega_{212}^* := \frac{a_1c_1 - a_2c_2}{a_2 - a_1} - \omega_{221}$ is a critical point of $\rho(X_2^{-1}Y_2^{-1})$. Moreover, $\rho(X_2^{-1}Y_2^{-1})$ reaches the maximum value at ω_{212}^* if $a_2 > a_1$ and the minimum value at ω_{212}^* otherwise.

To evaluate the impact of networks with corresponding homogeneous parameters across all nodes on the value of R_0 computed using Equation (4.16), three networks with three, four, and 100 nodes were constructed, respectively. Simulation runs with varying livestock movement rates and parameters in assumptions (4.29) and (4.34) held constant and homogeneous across nodes showed that R_0 is not affected by livestock movement rates during 100 runs per network. Moreover, values and bounds of R_0 obtained through numerical simulations were identical for networks with three, four, and 100 nodes. Extensive numerical simulation results showed that R_0 does not depend on livestock movement rates or the number of nodes in a network when (4.29) and (4.34) hold.

Scenarios (see Table 4.2) were run 100 times for each four-node network to study the impact of livestock movement rates on R_0. During 100 realizations for each scenario, livestock movement rates were increased while keeping remaining parameters constant and homogeneous across all nodes. In Scenario 1, contact rates β_{12}, β_{21}, β_{23}, and β_{32} for node i were set larger than respective parameters for node j $(i > j,\ i, j = 1, 2, 3, 4)$. During each run, R_0 increased while increasing livestock movement rates from node j to node i, ω_{2ji}, and decreased while increasing livestock movement rates from node i to node j, ω_{2ij}, as shown in Figures 4.4(a) and 4.4(b), respectively. In Scenario 2, under setting $d_{2i} > d_{2j}$, R_0 decreased when ω_{2ji} increased, and increased when ω_{2ij} increased, as demonstrated in Figures 4.5(a) and 4.5(b), respectively. With livestock recovery rates $\gamma_{2i} > \gamma_{2j}$ in Scenario 3, R_0 decreased when ω_{2ji} increased, and increased when ω_{2ij} increased, as shown in Figures 4.6(a) and

No.	parameter	livestock movement rates	R_0
1	$\beta_{12i} > \beta_{12j}$, $\beta_{21i} > \beta_{21j}$, $\beta_{23i} > \beta_{23j}$, $\beta_{32i} > \beta_{32j}$	ω_{2ji} increases	increases
		ω_{2ij} increases	decreases
2	$d_{2i} > d_{2j}$	ω_{ji}^2 increases	decreases
		ω_{2ij} increases	increases
3	$\gamma_{2i} > \gamma_{2j}$	ω_{2ji} increases	decreases
		ω_{2ij} increases	increases
4	$\mu_{2i} > \mu_{2j}$	ω_{2ji} increases	decreases
		ω_{2ij} increases	increases

Table 4.2: *Different scenarios for numerical simulations on four-node networks. Other parameters are kept the same and homogeneous across all nodes during all realizations. The superscripts* $i, j = 1, 2, 3, 4$ *and* $i > j$.

4.6(b), respectively. Similarly, with livestock mortality rates $\mu_{2i} > \mu_{2j}$ in Scenario 4, R_0 decreased when ω_{2ji} increased, and increased with larger ω_{2ij}, as illustrated in Figures 4.7(a) and 4.7(b), respectively. Tuning the parameters in above scenarios yielded R_0 from below one to above one. As a consequence, livestock movement rates are important in leading to epidemic outbreak or epidemic burnout.

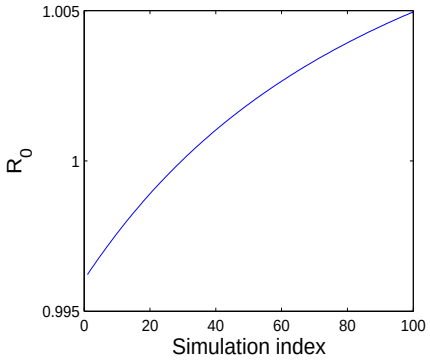

(a) As the livestock movement rate from node j to node i (ω_{2ji}) increases when $\beta_{12i} > \beta_{12j}$, $\beta_{21i} > \beta_{21j}$, $\beta_{23i} > \beta_{23j}$, and $\beta_{23i} > \beta_{23j}$, R_0 increases.

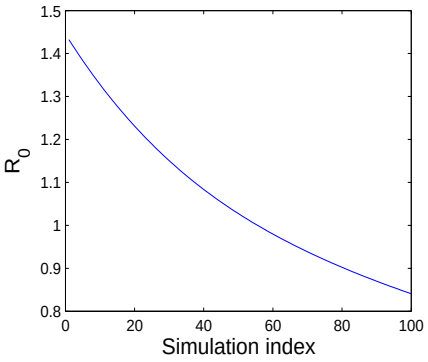

(b) As the livestock movement rate from node i to node j (ω_{2ij}) increases when $\beta_{12i} > \beta_{12j}$, $\beta_{21i} > \beta_{21j}$, $\beta_{23i} > \beta_{23j}$, and $\beta_{23i} > \beta_{23j}$, R_0 decreases.

Figure 4.4: *The reproduction number for four-node networks with different contact rates during* 100 *runs.*

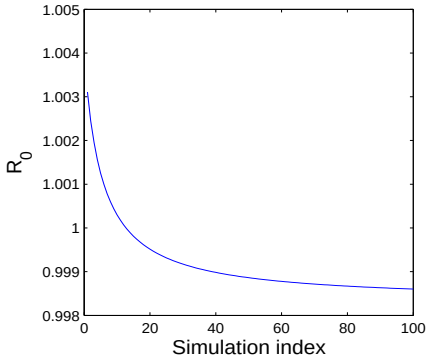

(a) As the livestock movement rate from node j to node i (ω_{2ji}) increases when $d_{2i} > d_{2j}$, R_0 decreases.

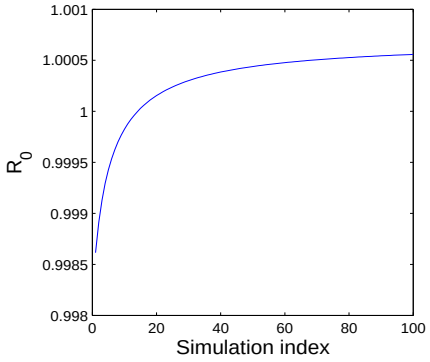

(b) As the livestock movement rate from node i to node j (ω_{2ij}) increases when $d_{2i} > d_{2j}$, R_0 increases.

Figure 4.5: *The reproduction number for four-node networks with different livestock death rates during* 100 *runs.*

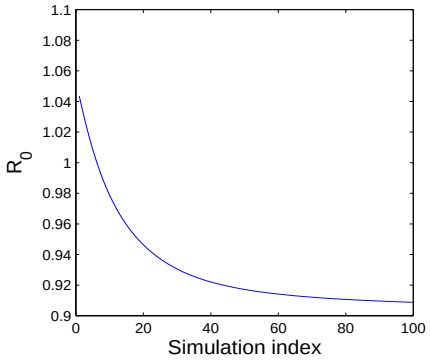

(a) As the livestock movement rate from node j to node i (ω_{2ji}) increases when $\gamma_{2i} > \gamma_{2j}$, R_0 decreases.

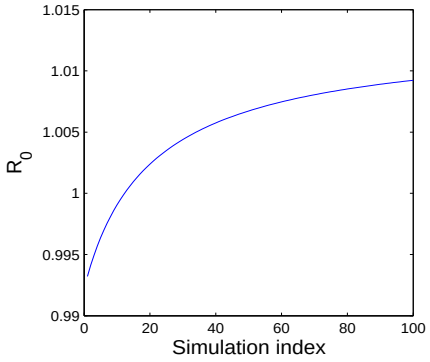

(b) As the livestock movement rate from node i to node j (ω_{2ij}) increases when $\gamma_{2i} > \gamma_{2j}$, R_0 increases.

Figure 4.6: *The reproduction number for four-node networks with different livestock recovery rates during* 100 *runs.*

4.3 Results and Discussions

Proposed here is an explicit expression of R_0, which is formulated as a function of vertical and horizontal transmission parameters shown in Equation (4.16). This formula facilitates computing R_0 for many diseases that involve both vertical and horizontal transmission by replacing the spectral radius of the original next generation matrix with that of a smaller size

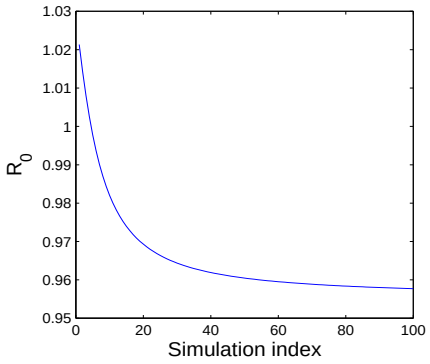

(a) As the livestock movement rate from node j to node i (ω_{2ji}) increases when $\mu_{2i} > \mu_{2j}$, R_0 decreases.

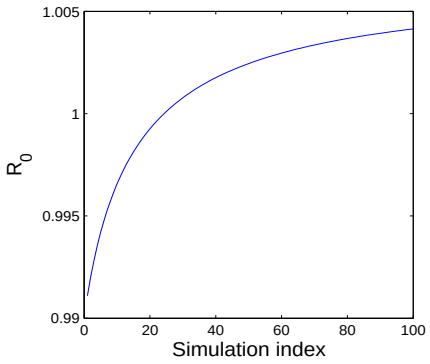

(b) As the livestock movement rate from node i to node j (ω_{2ij}) increases when $\mu_{2i} > \mu_{2j}$, R_0 increases.

Figure 4.7: *The reproduction number for four-node networks with different livestock mortality rates during* 100 *runs.*

matrix. The lower bound of R_0 equals R_0 for horizontal transmission. Equation (4.16) was applied to the RVF model, deriving R_0 and its lower and upper bounds. Tightness of various bounds was compared, and the role of livestock movement rates and disease parameters on R_0 was analyzed through numerical simulations.

The reproduction number for an RVF metapopulation model relates to R_0 for horizontal transmission involving *Aedes*-livestock interaction, and *Culex*-livestock interaction, and vertical transmission parameters. Different bounds of R_0 for heterogeneous networks were provided by Theorems 2, 3, and 4, with decreasing tightness and increasing ease. For homogeneous networks, R_0 for horizontal transmission in Equation (4.36) and bounds of R_0 given by Corollary 2 are proven to be independent of livestock movement rates and equal to corresponding terms for homogeneous populations presented in [131]. The lower bound is R_0 for horizontal transmission and the upper bound is the sum of R_0 for horizontal transmission and the largest transovarial transmission rate of *Aedes* mosquitoes among nodes.

Typically, networks in the real world are heterogeneous. Rates of livestock death, incubation, mortality, recovery, and contact with mosquitoes may vary in different nodes due to climate, public health facilities, environment, and/or type of nodes (e.g., death rates of

livestock in feedlots are higher than those in livestock premises). Variations in weather may affect values of some mosquito parameters, e.g., rainfall affects mosquito birth rates, and temperature affect mosquito incubation rates. Even if weather conditions are homogeneous across all nodes, various genera and/or species of mosquitoes may exhibit different rates of incubation, contact, birth, and/or death. Numerical simulations showed livestock movement rates between different nodes only affect R_0 when the network is spatially heterogeneous regarding parameters. Changing livestock movement rates on heterogeneous networks resulted in R_0 varying between values below and above the critical value one. When other parameters remained homogeneous and constant, increasing livestock movement rates from nodes with smaller contact rates to those with larger contact rates increased R_0. If livestock movement rates were increased from nodes with smaller livestock death rates (or recovery rates, or mortality rates) to nodes with larger livestock death rates (or recovery rates, or mortality rates), R_0 decreased. This observation helps us better envision effective mitigation strategies in executing movement bans between some nodes and in some directions.

Whatever heterogeneity exists between nodes, the same mathematical model in Equations (4.12), and the explicit expression of R_0 in (4.16), are applicable. The formula for R_0 presented in this chapter can be applied to numerous diseases aside from RVF.

This work on RVF computes R_0 accurately by taking into account vertical transmission, which is important but ignored by modelers. This research simplified the derivation of R_0 by computing the spectral radius of a smaller size matrix than the original next generation matrix. Bounds of R_0 facilitate the estimation of R_0 for an RVF metapopulation model. Simulation results of livestock movement rates and parameters are helpful in developing efficient mitigation strategies for RVF.

Chapter 5

The Extinction Threshold

The reproduction number of deterministic models is an essential quantity to predict whether an epidemic will spread or die out. The extinction threshold for infectious diseases is a term used to explain the point at which a disease may extinct, contributing crucial knowledge of mitigation, control, and elimination of infectious diseases. Relationships between basic reproduction numbers of two network-based vector-host models, and extinction thresholds of corresponding CTMC models are derived under some assumptions. Numerical simulation results for malaria and RVF transmission on heterogeneous networks are in agreement with analytical results without any assumptions, reinforcing the relationships may always exist and proposing a mathematical problem of proving existence of the relationships in general. Moreover, numerical simulations show that R_0 does not monotonically increase or decrease with the extinction threshold. Key parameters in predicting uncertainty of extinction thresholds are identified using Latin Hypercube Sampling/Partial Rank Correlation Coefficient. Consistent trends of extinction probability observed through numerical simulations provide novel insights into mitigation strategies to increase the disease extinction probability. Research findings may improve understandings of thresholds for disease persistence in order to control vector-borne diseases.

This chapter is organized as follows. Section 5.1 reviews the branching process for deriving E_0. Section 5.2 calculates R_0 for a deterministic vector-host model in which transmission dynamics of vectors are described by an SI model and transmission dynamics of hosts are

described by an SIS model. Relationships between E_0 of corresponding CTMC model and R_0 are analyzed. In Section 5.3, an analogue of results in Section 5.2 is obtained for a model in which transmission dynamics of vectors are described by an SEI model and transmission dynamics of hosts are described by an SEIR model. Local transmission and trans-location transmission due to proximity for vector-borne diseases are both considered in Sections 5.2 and 5.3. In Section 5.4, the relationships derived in Sections 5.2 and 5.3 are numerically shown to hold without any assumptions for simplified malaria and RVF metapopulation models. The sensitivity test determines key parameters in predicting uncertainty of extinction probability. Relationships between varying parameters and extinction probabilities are explored through extensive simulations for homogeneous populations and a two-node network. Section 5.5 provides a summary and discussion of mathematical derivations and simulation results.

5.1 Computing E_0 using Branching Process

In this section we review the multitype branching process approximation used to derive E_0 for corresponding CTMC models.

Calculating the probability of disease extinction is one of the most interesting applications of the branching process which may lead to disease extinction or persistence. We are interested in conditions under which a disease may become extinct and the probability for this event to occur. First, we review the approach of using branching process to compute extinction threshold and extinction probability for multi-type infections.

The rest of this section refers to [4, 92]. Let $\overrightarrow{X}(t) = (X_1(t), \cdots, X_n(t))^T : t \in (0, \infty)$ be a set of discrete-valued vector random variables. The assumptions are made that the number of infections produced by type i is independent of the number of infections produced by any other types and individuals of type i have identical probability generating function (pgf). Let $\{X_{ji}\}_{j=1}^{n}$ be offspring random variables for type i, where X_{ji} is the number of infected individuals of type j produced by individuals of type i. The probability that one

individual of type i produces x_j infected individuals of type j is given as

$$P_i(x_1, \cdots, x_n) = \text{Prob}\{X_{1i} = x_1, \cdots, X_{ni} = x_n\}.$$

The offspring pgf array $(g_1, \cdots, g_n) : [0,1]^n \to [0,1]^n$, is defined as

$$g_i(w_1, \cdots, w_n) = \sum_{x_n=0}^{\infty} \cdots \sum_{x_1=0}^{\infty} P_i(x_1, \cdots, x_n) w_1^{x_1} \cdots w_n^{x_n}. \tag{5.1}$$

Note that a trivial fixed point of $(g_1, \cdots, g_n)$ always exists at $\mathbf{1} = (1, \cdots, 1)$.

The nonnegative expectation matrix of offspring distribution is denoted by $M = [m_{ij}]_{n\times n}$, where $m_{ji} := \frac{\partial g_i}{\partial w_j}|_{x=1} < \infty$ represents the expected number of infected individuals of type j produced by an individual of type i.

The *extinction threshold*, E_0, is defined as the spectral radius of the expectation matrix, denoted by $\rho(M)$.

Recall that (B_0) and (B_1) assumptions in [92] are as follows:

(B_0) g_i is not simple. Here, a function is called simple if it is linear without constant terms.

(B_1) Matrix M is irreducible.

If $E_0 > 1$, under assumptions (B_0) and (B_1), the pgf has at most one fixed point in $(0,1)^n$, denoted by $w^* = (w_1^*, \cdots, w_n^*)$, if extinction array w^* in $(0,1)^n$ exists. In the following, extinction array only refers to $w^* \in (0,1)^n$. If $I_j(0) = i_j$, then disease extinction probability, denoted by P_E, is

$$P_E = \lim_{t\to\infty} \text{Prob}\{\overrightarrow{I}(t) = 0\} = w_1^{*i_1} \cdots w_n^{*i_n} < 1. \tag{5.2}$$

If $E_0 \leq 1$, then

$$P_E = \lim_{t\to\infty} \text{Prob}\{\overrightarrow{I}(t) = 0\} = 1.$$

5.2 SI Vector Model and SIS Host Metapopulation Model

In this section, a deterministic vector-host model in which disease transmission dynamics of vectors are described by an SI model, while transmission dynamics of hosts are described by

an SIS model. The reproduction number and extinction threshold for corresponding CTMC model are analytically related.

5.2.1 The Reproduction Number

The model for vectors consists of compartment G representing susceptible vectors, and compartment J representing infected vectors. Disease dynamics of hosts are modeled by an SIS model.

$$\begin{aligned}
\frac{\mathrm{d}G_i}{\mathrm{d}t} &= \eta_i - \beta_i G_i I_i/N_i - \sum_{j=1,j\neq i}^{n} \omega_{ji} G_i I_j/N_j - \mu_i G_i \\
\frac{\mathrm{d}J_i}{\mathrm{d}t} &= \beta_i G_i I_i/N_i + \sum_{j=1,j\neq i}^{n} \omega_{ji} G_i I_j/N_j - \mu_i J_i \\
\frac{\mathrm{d}S_i}{\mathrm{d}t} &= \psi_i + \gamma_i I_i - \alpha_i S_i J_i/N_i - \sum_{j=1,j\neq i}^{n} \sigma_{ji} S_i J_j/N_i - d_i S_i \\
\frac{\mathrm{d}I_i}{\mathrm{d}t} &= \alpha_i S_i J_i/N_i + \sum_{j=1,j\neq i}^{n} \sigma_{ji} S_i J_j/N_i - \gamma_i I_i - d_i I_i
\end{aligned} \tag{5.3}$$

The recruitment rate of vectors (resp. hosts) in node i is η_i (resp. ψ_i) for all $i = 1, \cdots, n$. The rate of new infections in vectors in node i produced by local hosts and hosts in other nodes are $\beta_i G_i I_i/N_i$ and $\sum_{j=1,j\neq i}^{n} \omega_{ji} G_i I_j/N_j$, respectively. The death rates of susceptible and infected vectors in node i are μG_i and μJ_i, respectively. The rate of host infection in node i produced by local vectors and vectors in other nodes are $\alpha_i S_i J_i/N_i$ and $\sum_{j=1,j\neq i}^{n} \sigma_{ji} S_i J_j/N_i$, respectively. Death rates of susceptible and infected hosts in node i are $d_i S_i$ and $d_i I_i$, respectively. The recovery rate for hosts in node i is $\gamma_i I_i$.

The system of ODEs only consisting of compartments J_i and I_i is:

$$\frac{d}{dt}\begin{bmatrix} J_1 & \cdots & J_n & I_1 & \cdots & I_n \end{bmatrix}^T = \mathscr{F} - \mathscr{V}.$$

A unique solution at DFE, represented by $(G_i^0, 0, N_i^0, 0)$ exists, where $G_i^0 = \frac{\eta_i}{\mu_i}$ and $N_i^0 = \frac{\psi_i}{d_i}$. The Jacobian matrices F and V defined in (4.1) for this model are

$$F = \begin{bmatrix} 0 & \mathcal{A} \\ \mathcal{B} & 0 \end{bmatrix}, \quad V = \begin{bmatrix} \Lambda_1 & 0 \\ 0 & \Lambda_2 \end{bmatrix},$$

where

$$\mathcal{A} = \begin{bmatrix} \hat{\beta}_1 & \hat{\omega}_{21} & \cdots & \hat{\omega}_{n1} \\ \hat{\omega}_{12} & \hat{\beta}_2 & \cdots & \hat{\omega}_{n2} \\ \cdots & \cdots & \ddots & \cdots \\ \hat{\omega}_{1n} & \hat{\omega}_{2n} & \cdots & \hat{\beta}_n \end{bmatrix}, \quad \mathcal{B} = \begin{bmatrix} \alpha_1 & \sigma_{21} & \cdots & \sigma_{n1} \\ \sigma_{12} & \alpha_2 & \cdots & \sigma_{n2} \\ \cdots & \cdots & \ddots & \cdots \\ \sigma_{1n} & \alpha_2 & \cdots & \alpha_n \end{bmatrix}, \tag{5.4}$$

$$\Lambda_1 = \text{diag}(\mu_1, \cdots, \mu_n), \quad \Lambda_2 = \text{diag}(d_1 + \gamma_1, \cdots, d_n + \gamma_n). \tag{5.5}$$

Here

$$\hat{\beta}_i = \frac{\beta_i G_i^0}{N_i^0} \quad \text{and} \quad \hat{\omega}_{ij} = \frac{\omega_{ij} G_j^0}{N_i^0}.$$

The notation $\text{diag}(\mu_1, \cdots, \mu_n)$ represents the diagonal matrix with diagonal entries $\mu_1, \cdots, \mu_n$. To calculate R_0, the following lemma is proved first.

Lemma 1. *Let A_1, A_2 be square matrices of the same size and $A = \begin{bmatrix} 0 & A_1 \\ A_2 & 0 \end{bmatrix}$, then $\rho(A) = \sqrt{\rho(A_2 A_1)}$.*

Proof. For any $\lambda \neq 0$,

$$|\lambda I - A| = \begin{vmatrix} \lambda I & -A_1 \\ -A_2 & \lambda I \end{vmatrix} = \begin{vmatrix} \lambda I & -A_1 \\ 0 & \lambda I - \frac{A_2 A_1}{\lambda} \end{vmatrix} = |\lambda^2 I - A_2 A_1|. \tag{5.6}$$

Therefore, $\rho(A) = \sqrt{\rho(A_2 A_1)}$ if $\rho(A_2 A_1) \neq 0$.

If $\rho(A_2 A_1) = 0$, we assume that $\rho(A) \neq 0$. Then there exists a $\lambda' \neq 0$ such that $|\lambda' I - A| = 0$. By (5.6), $|\lambda'^2 I - A_2 A_1| = 0$ for a nonzero λ', contradicting the assumption that $\rho(A_2 A_1) = 0$. Therefore, $\rho(A) = \sqrt{\rho(A_2 A_1)}$. □

A direct calculation gives $FV^{-1} = \begin{bmatrix} 0 & \mathcal{A}\Lambda_2^{-1} \\ \mathcal{B}\Lambda_1^{-1} & 0 \end{bmatrix}$. By Lemma 1, we have the following proposition:

Proposition 1. *The reproduction number of the model (5.3) is*

$$R_0 = \sqrt{\rho(\mathcal{B}\Lambda_1^{-1}\mathcal{A}\Lambda_2^{-1})}. \tag{5.7}$$

Description	State transition	Rate
Host birth	$(S,I,G,J) \to (S+1,I,G,J)$	ψ
Death of S	$(S,I,G,J) \to (S-1,I,G,J)$	dS
Host local infection	$(S,I,G,J) \to (S-1,I+1,G,J)$	$\alpha SJ/N$
Host infection by J_j	$(S,I,G,J) \to (S-1,I+1,G,J)$	$\sigma_{ji}S_iJ_j/N_i$
Host recovery	$(S,I,G,J) \to (S+1,I-1,G,J)$	γI
Death of I	$(S,I,G,J) \to (S,I-1,G,J)$	dI
Vector birth	$(S,I,G,J) \to (S,I,G+1,J)$	η
Death of G	$(S,I,G,J) \to (S,I,G-1,J)$	μG
Vector local infection	$(S,I,G,J) \to (S,I,G-1,J+1)$	$\beta GI/N$
Vector infection by I_j	$(S,I,G,J) \to (S,I,G-1,J+1)$	$\omega_{ji}G_iI_j/N_j$
Death of J	$(S,I,G,J) \to (S,I,G,J-1)$	μJ

Table 5.1: *State transitions and rates for corresponding continuous-time Markov chain for deterministic model* (5.3) *omitting node index* i.

5.2.2 The Threshold for Extinction Probability

In this section, we compute E_0 for corresponding CTMC of model (5.3). See Table 5.1 for state transitions and rates.

The pgfs are

$$g_i(w_1,\cdots,w_n,u_1,\cdots,u_n) = \begin{cases} \frac{\alpha_i w_i u_i + \sum_{j=1,j\neq i}^{n} \sigma_{ij} w_i u_j + \mu_i}{\alpha_i + \sum_{j=1,j\neq i}^{n} \sigma_{ij} + \mu_i}, & \text{if } 1 \le i \le n, \\ \frac{\hat{\beta}_k u_k w_k + \sum_{j=1,j\neq k}^{n} \hat{\omega}_{kj} u_k w_j + d_k + \gamma_k}{\hat{\beta}_k + \sum_{j=1,j\neq k}^{n} \hat{\omega}_{kj} + d_k + \gamma_k}, & \text{if } n+1 \le i \le 2n, \end{cases}$$

where $j = 1,\cdots,n$, the index $k = i-n$ for $n+1 \le i \le 2n$, w_i represents $I_{V_i} = 1, I_{H_i} = 0$, and u_i represents $I_{H_i} = 1, I_{V_i} = 0$ for $i = 1,\cdots,n$.

The expectation matrix M is:

$$M = \begin{bmatrix} \Lambda_3\Lambda_4 & \mathcal{A}\Lambda_5 \\ \mathcal{B}\Lambda_4 & \Lambda_6\Lambda_5 \end{bmatrix}, \tag{5.8}$$

where $\mathcal{A}, \mathcal{B}$ are the same as those in (5.4), and

$$\Lambda_3 = \text{diag}(\alpha_1 + \sum_{i\neq 1}\sigma_{1i},\cdots,\alpha_n + \sum_{i\neq n}\sigma_{ni}), \quad \Lambda_4 = \text{diag}(\frac{1}{C_1},\cdots,\frac{1}{C_n}),$$
$$\Lambda_6 = \text{diag}(\hat{\beta}_1 + \sum_{i\neq 1}\hat{\omega}_{1i},\cdots,\hat{\beta}_n + \sum_{i\neq n}\hat{\omega}_{ni}), \quad \Lambda_5 = \text{diag}(\frac{1}{D_1},\cdots,\frac{1}{D_n}),$$
$$C_i = \alpha_i + \sum_{j\neq i}\sigma_{ij} + \mu_i, \quad D_i = \hat{\beta}_i + \sum_{j\neq i}\hat{\omega}_{ij} + d_i + \gamma_i, \quad \text{for } i = 1,\cdots,n.$$

Note that if both $\mathcal{A}$ and $\mathcal{B}$ are positive matrices, then the assumptions (B_0) and (B_1) in [92] hold for this model.

Lemma 2. *Let A_1, A_2 be nonnegative square matrices of identical size, such that $\rho(A_2A_1)$ is an eigenvalue of A_2A_1 and Λ, Λ' be nonnegative diagonal matrices such that $0 \leq k_1 I \leq \begin{bmatrix} \Lambda & 0 \\ 0 & \Lambda' \end{bmatrix} \leq k_2 I$ for some real numbers k_1, k_2. Then the spectral radius of $B = \begin{bmatrix} \Lambda & A_1 \\ A_2 & \Lambda' \end{bmatrix}$ satisfies that*

$$\sqrt{\rho(A_2A_1)} + k_1 \leq \rho(B) \leq \sqrt{\rho(A_2A_1)} + k_2.$$

Proof. Since $0 \leq \begin{bmatrix} k_1 I & A_1 \\ A_2 & k_1 I \end{bmatrix} \leq B \leq \begin{bmatrix} k_2 I & A_1 \\ A_2 & k_2 I \end{bmatrix}$, by Theorem 4 in [130],

$$\rho(\begin{bmatrix} k_1 I & A_1 \\ A_2 & k_1 I \end{bmatrix}) \leq \rho(B) \leq \rho(\begin{bmatrix} k_2 I & A_1 \\ A_2 & k_2 I \end{bmatrix}). \tag{5.9}$$

By hypothesis and (5.6), $\rho(\begin{bmatrix} 0 & A_1 \\ A_2 & 0 \end{bmatrix})$ is an eigenvalue of $\begin{bmatrix} 0 & A_1 \\ A_2 & 0 \end{bmatrix}$. Following the fact that $|\lambda' + k| < \lambda + k$ for any $k > 0$, if $|\lambda'| < \lambda$, then

$$\rho(\begin{bmatrix} k_1 I & A_1 \\ A_2 & k_1 I \end{bmatrix}) = \rho(\begin{bmatrix} 0 & A_1 \\ A_2 & 0 \end{bmatrix}) + k_1 = \sqrt{\rho(A_2A_1)} + k_1.$$

Similarly, $\rho(\begin{bmatrix} k_2 I & A_1 \\ A_2 & k_2 I \end{bmatrix}) = \sqrt{\rho(A_2A_1)} + k_2$. Lemma follows (5.9) and Lemma 1. □

Remark 1. *If both A_1 and A_2 are positive matrices, then $\rho(A_2A_1)$ is an eigenvalue of A_2A_1 by Perron-Frobenius theorem.*

By Lemma 2, we have the following proposition:

Proposition 2. *The extinction threshold of model (5.3) satisfies that*

$$\min_{1\leq i\leq n}\left(\frac{\alpha_i + \sum_{j=1,j\neq i}^{n} \sigma_{ij}}{C_i}, \frac{\hat{\beta}_i + \sum_{j=1,j\neq i}^{n} \hat{\omega}_{ij}}{D_i}\right) + \sqrt{\rho(\mathcal{B}\Lambda_5\mathcal{A}\Lambda_4)} \leq E_0$$
$$\leq \max_{1\leq i\leq n}\left(\frac{\alpha_i + \sum_{j=1,j\neq i}^{n} \sigma_{ij}}{C_i}, \frac{\hat{\beta}_i + \sum_{j=1,j\neq i}^{n} \hat{\omega}_{ij}}{D_i}\right) + \sqrt{\rho(\mathcal{B}\Lambda_5\mathcal{A}\Lambda_4)}.$$

5.2.3 Relationships between R_0 and E_0

To obtain a theoretical relationship between R_0 in (5.7) and E_0, the assumption is made that

$$\frac{\mu_i}{C_i} = k_1 \quad \text{and} \quad \frac{d_i + \gamma_i}{D_i} = k_2, \quad \forall\, i = 1, \cdots, n \tag{5.10}$$

for constant numbers $k_1, k_2 \in [0, 1]$ throughout this section. The assumption can be interpreted biologically as: the probability of natural death is identical for vectors from each node, and the probability of natural death is identical for hosts from each node. The assumption shall be removed for numerical simulations in Section 5.4.1.

Theorem 5. *Under the assumption (5.10),*

(1) If $R_0 \leq \frac{1-k_2}{1-\sqrt{k_1 k_2}} \leq 1$ *or* $E_0 \leq \frac{1-k_2}{1-\sqrt{k_1 k_2}} \leq 1$, *then* $R_0 \leq E_0$;

(2) If $R_0 \geq \frac{1-k_1}{1-\sqrt{k_1 k_2}} \geq 1$ *or* $E_0 \geq \frac{1-k_1}{1-\sqrt{k_1 k_2}} \geq 1$, *then* $R_0 \geq E_0$.

Proof. Under the assumption (5.10), $\Lambda_1\Lambda_4 = k_1 I$, $\Lambda_3\Lambda_4 = (1-k_1)I$, $\Lambda_2\Lambda_5 = k_2 I$, and $\Lambda_6\Lambda_5 = (1-k_2)I$, where I is the identity matrix. Therefore, M in (5.8) can be rewritten as:

$$M = \begin{bmatrix} 0 & k_2 \mathcal{A}\Lambda_2^{-1} \\ k_1 \mathcal{B}\Lambda_1^{-1} & 0 \end{bmatrix} + \begin{bmatrix} (1-k_1)I & 0 \\ 0 & (1-k_2)I \end{bmatrix}.$$

Without loss of generality, we assume that $k_1 < k_2$. By Lemma 2 and (5.7),

$$R_0\sqrt{k_1 k_2} + 1 - k_2 \leq E_0 \leq R_0\sqrt{k_1 k_2} + 1 - k_1. \tag{5.11}$$

Following (5.11),

$$R_0(1-\sqrt{k_1 k_2}) - (1-k_1) \leq R_0 - E_0 \leq R_0(1-\sqrt{k_1 k_2}) - (1-k_2),$$
$$\frac{1}{\sqrt{k_1 k_2}}(E_0(1-\sqrt{k_1 k_2}) - (1-k_1)) \leq R_0 - E_0 \leq \frac{1}{\sqrt{k_1 k_2}}(E_0(1-\sqrt{k_1 k_2}) - (1-k_2)).$$

Theorem follows the above two inequalities. □

Corollary 3. *If further assumption is made that* $k_1 = k_2$ *besides assumption (5.10), then* $R_0 \leq 1$ *if and only if* $E_0 \leq 1$. *Moreover,* $|R_0 - 1| \geq |E_0 - 1|$.

Proof. By Theorem 5 (1), if $R_0 \leq 1$, then $R_0 \leq E_0$. Assuming that $E_0 > 1$, by Theorem 5 (2), $R_0 \geq E_0$, which is a contradiction. Conversely, if $E_0 > 1$, then $R_0 \leq 1$ following a similar argument. Hence, $R_0 \leq 1$ if and only if $E_0 \leq 1$. The proof for $|R_0 - 1| \geq |E_0 - 1|$ directly follows Theorem 5. □

5.3 SEI Vector Model and SEIR Host Metapopulation Model

A deterministic model in which vectors are divided into compartments S, E, and I, and hosts are classified into compartments S, E, I, and R is presented. The reproduction number for this model and the extinction threshold for corresponding CTMC model are connected.

5.3.1 The Reproduction Number

The following model extends the model in Section 5.2.1 by adding compartment Z for exposed vectors, and compartment E for exposed hosts. Other terms have identical meanings as corresponding terms in model (5.3). The rates at which exposed vectors and exposed hosts in node i transfer to infected compartments are $\varphi_i Z_i$ and $\varepsilon_i E_i$, respectively.

$$
\begin{aligned}
\frac{\mathrm{d}G_i}{\mathrm{d}t} &= \eta_i - \beta_i G_i I_i/N_i - \sum_{j=1, j\neq i}^{n} \omega_{ji} G_i I_j/N_j - \mu_i G_i \\
\frac{\mathrm{d}Z_i}{\mathrm{d}t} &= \beta_i G_i I_i/N_i + \sum_{j=1, j\neq i}^{n} \omega_{ji} G_i I_j/N_j - \varphi_i Z_i - \mu_i Z_i \\
\frac{\mathrm{d}J_i}{\mathrm{d}t} &= \varphi_i Z_i - \mu_i J_i \\
\frac{\mathrm{d}S_i}{\mathrm{d}t} &= \psi_i - \alpha_i S_i J_i/N_i - \sum_{j=1, j\neq i}^{n} \sigma_{ji} S_i J_j/N_i - d_i S_i \\
\frac{\mathrm{d}E_i}{\mathrm{d}t} &= \alpha_i S_i J_i/N_i + \sum_{j=1, j\neq i}^{n} \sigma_{ji} S_i J_j/N_i - \varepsilon_i E_i - d_i E_i \\
\frac{\mathrm{d}I_i}{\mathrm{d}t} &= \varepsilon_i E_i - \gamma_i I_i - d_i I_i \\
\frac{\mathrm{d}R_i}{\mathrm{d}t} &= \gamma_i I_i - d_i R_i
\end{aligned}
\tag{5.12}
$$

Compartments related to infected and asymptomatically infected are Z_i, E_i, J_i, and I_i, $i = 1, \cdots, n$. The unique solution at DFE is $(G_i^0, 0, 0, N_i^0, 0, 0, 0)$, where G_i^0 and N_i^0 are the same as corresponding terms in Section 5.2.1. The above system of ODEs including these compartments can be rewritten as:

$$\frac{d}{dt}\left[\begin{array}{cccccccccccc} Z_1 & \cdots & Z_n & E_1 & \cdots & E_n & J_1 & \cdots & J_n & I_1 & \cdots & I_n \end{array}\right]^T = \mathscr{F} - \mathscr{V}.$$

The Jacobian matrices F and V at DFE are

$$F = \begin{bmatrix} 0 & 0 & 0 & \mathcal{A} \\ 0 & 0 & \mathcal{B} & 0 \\ 0 & 0 & 0 & 0 \\ 0 & 0 & 0 & 0 \end{bmatrix}, \quad V = \begin{bmatrix} \Lambda_7 & 0 & 0 & 0 \\ 0 & \Lambda_8 & 0 & 0 \\ -\Lambda_9 & 0 & \Lambda_1 & 0 \\ 0 & -\Lambda_{10} & 0 & \Lambda_2 \end{bmatrix},$$

where Λ_1 and Λ_2 are given in (5.5); matrices $\mathcal{A}$ and $\mathcal{B}$ are in Equation (5.4); and

$$\Lambda_7 = \text{diag}(\varphi_1 + \mu_1, \cdots, \varphi_n + \mu_n), \quad \Lambda_8 = \text{diag}(\varepsilon_1 + d_1, \cdots, \varepsilon_n + d_n),$$

$$\Lambda_9 = \text{diag}(\varphi_1, \cdots, \varphi_n), \quad \Lambda_{10} = \text{diag}(\varepsilon_1, \cdots, \varepsilon_n).$$

By a direct calculation,

$$FV^{-1} = \begin{bmatrix} 0 & \mathcal{A}\Lambda_2^{-1}\Lambda_{10}\Lambda_8^{-1} & 0 & \mathcal{A}\Lambda_2^{-1} \\ \mathcal{B}\Lambda_1^{-1}\Lambda_9\Lambda_7^{-1} & 0 & \mathcal{B}\Lambda_1^{-1} & 0 \\ 0 & 0 & 0 & 0 \\ 0 & 0 & 0 & 0 \end{bmatrix}.$$

Following Lemma 1, the following proposition is obtained:

Proposition 3. *The reproduction number of the model (5.12) is*

$$R_0 = \sqrt{\rho(\mathcal{B}\Lambda_1^{-1}\Lambda_9\Lambda_7^{-1}\mathcal{A}\Lambda_2^{-1}\Lambda_{10}\Lambda_8^{-1})}. \tag{5.13}$$

5.3.2 The Threshold for Extinction Probability

State transitions and rates for corresponding CTMC of model (5.12) are listed in Table 5.2. The pgfs are:

$$g_i(w_1, \cdots, w_{2n}, u_1, \cdots, u_{2n}) = \begin{cases} \frac{\varphi_i u_i + \mu_i}{\varphi_i + \mu_i}, & \text{if } 1 \le i \le n, \\ \frac{\varepsilon_k u_i + d_k}{\varepsilon_k + d_k}, & \text{if } n+1 \le i \le 2n, \\ \frac{\alpha_p u_p w_{p+n} + \sum_{j=1, \neq p}^{n} \sigma_{pj} u_p w_{j+n} + \mu_p}{\alpha_p + \sum_{j=1, \neq p}^{n} \sigma_{pj} + \mu_p}, & \text{if } 2n+1 \le i \le 3n, \\ \frac{\hat{\beta}_q u_{q+n} w_q + \sum_{j=1, j\neq q}^{n} \hat{\omega}_{qj} u_{q+n} w_j + d_q + \gamma_q}{\hat{\beta}_q + \sum_{j=1, j\neq q}^{n} \hat{\omega}_{qj} + d_q + \gamma_q}, & \text{if } 3n+1 \le i \le 4n, \end{cases}$$

Description	State transition $a \to b$	Rate $P(a,b)$
Host birth	$(S,E,I,R,G,Z,J) \to (S{+}1,E,I,R,G,Z,J)$	ψ
Death of S	$(S,E,I,R,G,Z,J) \to (S{-}1,E,I,R,G,Z,J)$	dS
Death of E	$(S,E,I,R,G,Z,J) \to (S,E{-}1,I,R,G,Z,J)$	dE
Death of I	$(S,E,I,R,G,Z,J) \to (S,E,I{-}1,R,G,Z,J)$	dI
Death of R	$(S,E,I,R,G,Z,J) \to (S,E,I,R{-}1,G,Z,J)$	dR
Host local infection	$(S,E,I,R,G,Z,J) \to (S-1,E+1,I,R,G,Z,J)$	$\alpha SJ/N$
Host infection by J_j	$(S,E,I,R,G,Z,J) \to (S-1,E+1,I,R,G,Z,J)$	$\sigma_{ji}SJ_j/N$
Host recovery	$(S,E,I,R,G,Z,J) \to (S,E,I-1,R+1,G,Z,J)$	γI
Host Latent to infectious	$(S,E,I,R,G,Z,J) \to (S,E-1,I+1,R,G,Z,J)$	εE
Vector birth	$(S,E,I,R,G,Z,J) \to (S,E,I,R,G{+}1,Z,J)$	η
Death of G	$(S,E,I,R,G,Z,J) \to (S,E,I,R,G{-}1,Z,J)$	μG
Death of Z	$(S,E,I,R,G,Z,J) \to S,E,I,R,G,Z-1,J)$	μZ
Death of J	$(S,E,I,R,G,Z,J) \to (S,E,I,R,G,Z,J{-}1)$	μJ
Vector local infection	$(S,E,I,R,G,Z,J) \to (S,E,I,R,G-1,Z+1,J)$	$\beta GI/N$
Vector infection by I_j	$(S,E,I,R,G,Z,J) \to (S,E,I,R,G-1,Z+1,J)$	$\omega_{ji}GI_j/N_j$
Vector Latent to infectious	$(S,E,I,R,G,Z,J) \to (S,E,I,R,G,Z-1,J+1)$	φZ

Table 5.2: *State transitions and rates for corresponding continuous-time Markov chain for deterministic model* (5.12) *omitting node index* i.

where w_i represents only $Z_i = 1$, w_{i+n} represents $E_i = 1$, u_i represents $J_i = 1$, and u_{i+n} represents $I_i = 1$ for $i = 1, \cdots, n$. The indexes $k = i - n$ for $1 \le i \le n$, $p = i - 2n$ for $n + 1 \le i \le 2n$, and $q = i - 3n$ for $3n + 1 \le i \le 4n$.

The expectation matrix M is:

$$M = \begin{bmatrix} 0 & 0 & 0 & \mathcal{A}\Lambda_5 \\ 0 & 0 & \mathcal{B}\Lambda_4 & 0 \\ \Lambda_9\Lambda_7^{-1} & 0 & I - \Lambda_1\Lambda_4 & 0 \\ 0 & \Lambda_{10}\Lambda_8^{-1} & 0 & I - \Lambda_2\Lambda_5 \end{bmatrix}.$$

Similarly, the assumptions (B_0) and (B_1) in [92] hold for this model if both $\mathcal{A}$ and $\mathcal{B}$ are positive matrices. By Lemmas 1 and 2, as well as Remark 1, we have the following proposition:

Proposition 4. *The extinction threshold of the model (5.12) satisfies that*

$$\begin{aligned} &\sqrt[4]{\rho(\Lambda_{10}\Lambda_8^{-1}\mathcal{B}\Lambda_4\Lambda_9\Lambda_7^{-1}\mathcal{A}\Lambda_5)} + \min_{1\le i\le n}\left(\frac{\alpha_i+\sum_{j\neq i}\sigma_{ij}}{C_i}, \frac{\hat{\beta}_i+\sum_{j\neq i}\hat{\omega}_{ij}}{D_i}\right) \le E_0 \\ &\le \sqrt[4]{\rho(\Lambda_{10}\Lambda_8^{-1}\mathcal{B}\Lambda_4\Lambda_9\Lambda_7^{-1}\mathcal{A}\Lambda_5)} + \max_{1\le i\le n}\left(\frac{\alpha_i+\sum_{j\neq i}\sigma_{ij}}{C_i}, \frac{\hat{\beta}_i+\sum_{j\neq i}\hat{\omega}_{ij}}{D_i}\right). \end{aligned}$$

5.3.3 Relationships between R_0 and E_0

In this section, the assumption (5.10) holds and $k_1 < k_2$. Under the assumption (5.10), by Lemma 2,

$$\begin{aligned} &\sqrt[4]{k_1k_2\rho(\Lambda_{10}\Lambda_8^{-1}\mathcal{B}\Lambda_1^{-1}\Lambda_9\Lambda_7^{-1}\mathcal{A}\Lambda_2^{-1})} + 1 - k_2 \le E_0 \\ &\le \sqrt[4]{k_1k_2\rho(\Lambda_{10}\Lambda_8^{-1}\mathcal{B}\Lambda_1^{-1}\Lambda_9\Lambda_7^{-1}\mathcal{A}\Lambda_2^{-1})} + 1 - k_1. \end{aligned} \tag{5.14}$$

Recall that, for any square matrices A, B with the same size, $\rho(AB) = \rho(BA)$. By this property,

$$\rho(\Lambda_{10}\Lambda_8^{-1}\mathcal{B}\Lambda_4\Lambda_9\Lambda_7^{-1}\mathcal{A}\Lambda_2^{-1}) = \rho(\mathcal{B}\Lambda_4\Lambda_9\Lambda_7^{-1}\mathcal{A}\Lambda_2^{-1}\Lambda_{10}\Lambda_8^{-1}). \tag{5.15}$$

By (5.13), (5.14) and (5.15),

$$\sqrt{R_0}\sqrt[4]{k_1k_2} + 1 - k_2 \le E_0 \le \sqrt{R_0}\sqrt[4]{k_1k_2} + 1 - k_1.$$

Hence,

$$\sqrt{R_0}(1-\sqrt[4]{k_1k_2})-(1-k_1)\leq\sqrt{R_0}-E_0\leq\sqrt{R_0}(1-\sqrt[4]{k_1k_2})-(1-k_2),$$
$$\frac{1}{\sqrt[4]{k_1k_2}}(E_0(1-\sqrt[4]{k_1k_2})-(1-k_1))\leq\sqrt{R_0}-E_0\leq\frac{1}{\sqrt[4]{k_1k_2}}(E_0(1-\sqrt[4]{k_1k_2})-(1-k_2)).$$

Similarly, the following theorem is derived.

Theorem 6. *Under assumption* (5.10),

(1) If $\sqrt{R_0}\leq\frac{1-k_2}{1-\sqrt[4]{k_1k_2}}\leq 1$ *or* $E_0\leq\frac{1-k_2}{1-\sqrt[4]{k_1k_2}}\leq 1$, *then* $\sqrt{R_0}\leq E_0$;

(2) If $\sqrt{R_0}\geq\frac{1-k_1}{1-\sqrt[4]{k_1k_2}}\geq 1$ *or* $E_0\geq\frac{1-k_1}{1-\sqrt[4]{k_1k_2}}\geq 1$, *then* $\sqrt{R_0}\geq E_0$.

Corollary 4. *If a further assumption is made that* $k_1=k_2$ *besides assumption (5.10), then* $\sqrt{R_0}\leq 1$ *if and only if* $E_0\leq 1$. *Furthermore,* $|\sqrt{R_0}-1|\geq|E_0-1|$.

Proof. The proof is similar to that of Corollary 3. □

5.4 Numerical Results

General relationships between R_0 and E_0 for two models on heterogeneous networks were numerically demonstrated. Significant parameters for predicting the uncertainly in E_0 were determined by Latin Hypercube Sampling/Partial Rank Correlation Coefficient (LHS/PRCC) analysis. Finally, trends of parameters varying with extinction arrays were summarized.

5.4.1 Numerical Results on Relations between R_0 and E_0

Model (5.3) was applied to study thresholds for malaria transmission through numerical simulations on a four-node network. Five thousand realizations with parameters uniformly distributed within ranges listed in Table 5.3 on a four-node network gave rise to R_0 ranging from 0.7668 to 63.8111 and E_0 from 0.8965 to 1.9140. The ranges of R_0 and E_0 varied with the number of nodes on a network and the assumed ranges of vector (host) recruitment rates, while fixing ranges of other parameters. The values of R_0 were sorted from small to large values in Figures 5.1(a) and 5.1(b), and E_0 were ranked from small values to large

Parameter	Description	Range	Dimension	Source
α	Contact rate: mosquitoes to humans	$0.010 - 0.27$	1/day	[26]
β	Contact rate: humans to mosquitoes	$0.072 - 0.64$	1/day	[26]
μ	Per capita death rate for mosquitoes	$0.020 - 0.27$	1/day	[26]
d	Per capita death rate for humans	$0.000027 - 0.00014$	1/day	[26]
γ	Per capita recovery rate for humans	$0.0014 - 0.0017$	1/day	[26]
η	Mosquito recruitment rate	$1 - 5$	1/day	Assume
ψ	Human recruitment rate	$1 - 60$	1/day	Assume

Table 5.3: *Parameters of the malaria metapopulation model.*

values in Figures 5.1(c) and 5.1(d). The largest value of E_0 was 0.9980 when all values of R_0 were smaller than one and $R_0 \leq E_0$, as shown in Figure 5.1(a). The smallest value of E_0 was 1.003 when all values of R_0 were greater than one and $R_0 \geq E_0$, as shown in Figure 5.1(b). The largest value of R_0 was 0.9947 when all values of E_0 were smaller than one, as shown in Figure 5.1(c). The smallest value of R_0 was 1.006 when all values of E_0 were greater than one, as shown in Figure 5.1(d). The value of E_0 did not monotonically increase with the increase of R_0, as shown in Figures 5.1(a) and 5.1(b). Similarly, R_0 fluctuated as E_0 increased, as shown in Figures 5.1(c) and 5.1(d).

Model (5.12) was applied to numerically examine relationships between R_0 and E_0 for RVF on a four-node network. See Table 5.4 for descriptions and ranges of parameters. Five thousand realizations produced R_0 ranging between 0.2289 and 54.5086 and E_0 from 0.6757 to 1.9763. The values of R_0 were ordered from small to large magnitudes in Figures 5.2(a) and 5.2(b), and the values of E_0 were ordered from small to large values in Figures 5.2(c) and 5.2(d). The largest value of E_0 was 1 when all values of R_0 were smaller than one, and $\sqrt{R_0} \leq E_0$, as shown in Figure 5.2(a). The smallest value of E_0 was 1.005 when all values of R_0 were greater than one, and $\sqrt{R_0} \geq E_0$, as shown in Figure 5.2(b). The largest value

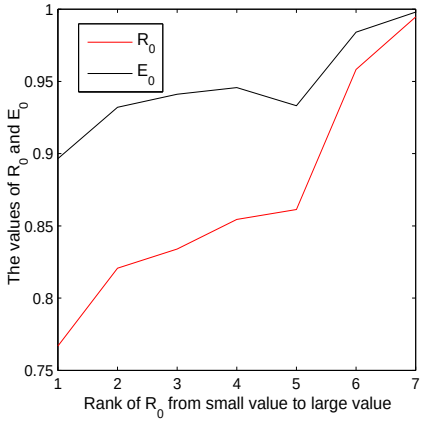

(a) When $R_0 \leq 1$, $R_0 \leq E_0$.

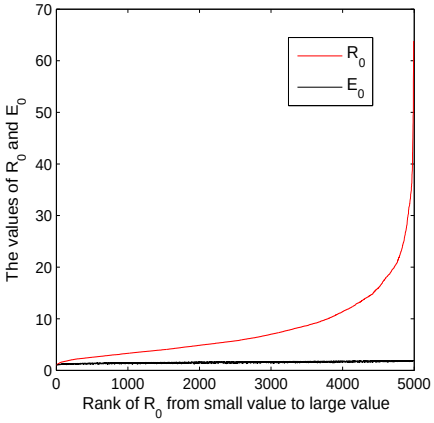

(b) When $R_0 \geq 1$, $R_0 \geq E_0$.

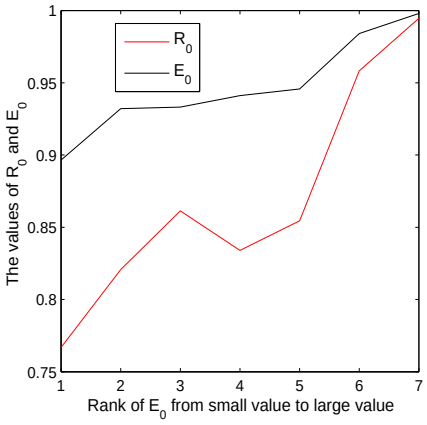

(c) When $E_0 \leq 1$, $R_0 \leq E_0$.

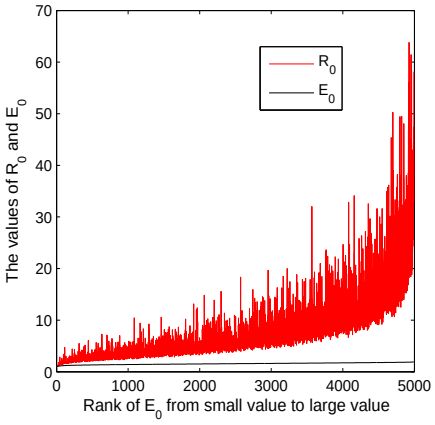

(d) When $E_0 \geq 1$, $R_0 \geq E_0$.

Figure 5.1: *Relationships between R_0 and E_0 for a malaria model.*

Parameter	Description	Range	Dimension	Source
α	Contact rate: mosquito to livestock	$0.0021 - 0.2762$	1/day	[22, 56, 59, 78, 96, 114, 115]
β	Contact rate: livestock to mosquitoes	$0 - 0.32$	1/day	[22, 56, 59, 78, 96, 113]
$1/\mu$	Longevity of mosquitoes	$3 - 60$	1/day	[15, 83, 96]
$1/d$	Longevity of livestock	$360 - 3600$	1/day	[97]
$1/\gamma$	Recover rate in livestock	$2 - 5$	1/day	[42]
$1/\varphi$	Incubation period in mosquitoes	$4 - 8$	days	[114]
$1/\epsilon$	Incubation period in livestock	$2 - 6$	days	[93]
η	Mosquito recruitment rate	$1 - 500$	1/day	Assume
ψ	Livestock recruitment rate	$1 - 10$	1/day	Assume

Table 5.4: *Parameters of the Rift Valley fever metapopulation model.*

of R_0 was 0.9998 when all values of E_0 were smaller than one, and $\sqrt{R_0} \geq E_0$, as shown in Figure 5.2(c). The smallest value of R_0 was 1.008 when all values of E_0 were greater than one, and $\sqrt{R_0} \geq E_0$, as shown in Figure 5.2(d). When R_0 increased, E_0 did not always increase, as shown in Figures 5.2(a) and 5.2(b). Similarly, R_0 fluctuated as E_0 increased, as shown in Figures 5.2(c) and 5.2(d).

5.4.2 Sensitivity Analysis

Latin Hypercube Sampling/Partial Rank Correlation Coefficient (LHS/PRCC) analysis [80] was employed to identify key parameters whose uncertainties contribute to predict uncertainty of E_0 for Model (5.12) and parameters were ranked by their significances. The parameters shown to be significant with large PRCC values (> 0.5) or small p-values (< 0.05) [51] by the sensitivity test with 5000 sets of parameter values, were listed in Table 5.5. The magnitude of PRCC value quantitatively represents contribution to the prediction for the imprecision of E_0, and a negative sign indicates that the parameter is inversely proportional to the magnitude of E_0. The closer PRCC value is to $+1$ or -1, the more the parameter

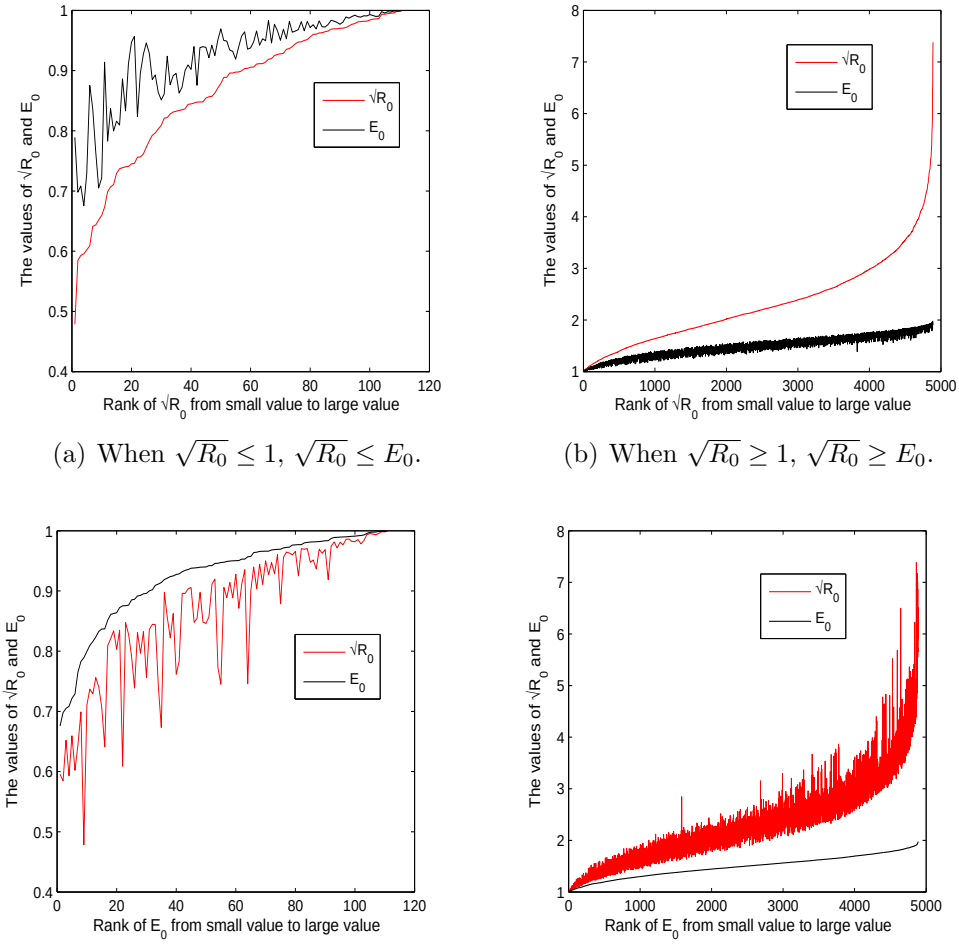

(a) When $\sqrt{R_0} \leq 1$, $\sqrt{R_0} \leq E_0$.

(b) When $\sqrt{R_0} \geq 1$, $\sqrt{R_0} \geq E_0$.

(c) When $E_0 \leq 1$, $\sqrt{R_0} \leq E_0$.

(d) When $E_0 \geq 1$, $\sqrt{R_0} \geq E_0$.

Figure 5.2: *Relationships between R_0 and E_0 for Rift Valley fever model.*

impacts the outcome of E_0.

5.4.3 Trends of Extinction Array with Varying Parameters

Consistent trends of w^* were observed by numerical simulations for homogeneous populations and a two-node network for Model (5.12). Table 5.6 listed three different values for each parameter and corresponding extinction array for homogeneous populations as an example. Table 5.7 showed trends of extinction array by varying one parameter at a time, keeping other parameters fixed and $E_0 > 1$ for homogeneous populations and a two-node

Parameter	PRCC	p-value
$1/\mu$	0.8061	< 0.001
β	0.6039	< 0.001
η	0.5785	< 0.001
α	0.5649	< 0.001
$1/\gamma$	0.5524	< 0.001
ψ	-0.5036	< 0.001
$1/d$	-0.4660	< 0.001
$1/\varphi$	-0.0284	< 0.05

Table 5.5: *Sensitivity testing results based on Latin Hypercube Sampling/Partial Rank Correlation Coefficient for Model* (5.12) *for homogeneous populations. Only significant parameters are shown.*

network. If at least one entry of extinction array increases and others remain constant, then we define that the array increases. The extinction array w^* decreased with the increase of contact rates from local vectors and vectors in other nodes to local hosts, contact rates from local hosts and hosts in other nodes to local vectors, death rates of hosts, recruitment rates of vectors, and incubation rates of vectors and hosts, whereas, w^* increased with the increase of vector death rates, host recovery rates, and host recruitment rates.

5.5 Discussions

The reproduction number, R_0, for deterministic vector-host models and thresholds for extinction probabilities, E_0 for corresponding CTMC models were analytically and numerically connected. For Model (5.3), mathematical analysis showed that $R_0 \leq 1$, if and only if $E_0 \leq 1$, and $|R_0 - 1| \geq |E_0 - 1|$ under certain assumptions. Numerical simulations for a malaria model on heterogeneous networks with different number of nodes showed that Corollary 3 holds without any assumptions. For Model (5.12), analytical results show that $\sqrt{R_0} < 1$ if and only if $E_0 < 1$, and $|\sqrt{R_0} - 1| \geq |E_0 - 1|$ by the same assumption in (5.10). Extensive numerical simulation results for an RVF model on networks with various number of nodes showed that Corollary 4 holds without any assumptions.

Conjecture 1. *Theorems 3, 4 and Corollary 3, 4 hold without assumption* (5.10)*, i.e.,*

Changing parameter	$(w_1^*, w_2^*, u_1^*, u_2^*)$
$\alpha = 0.0601$	$(0.9965, 0.9978, 0.9961, 0.9978)$
$\alpha = 0.0766$	$(0.8648, 0.9212, 0.8467, 0.9212)$
$\alpha = 0.0781$	$(0.8546, 0.9158, 0.8352, 0.9158)$
$\beta = 0.0639$	$(0.9158, 0.9824, 0.9046, 0.9824)$
$\beta = 0.1026$	$(0.6623, 0.8967, 0.6173, 0.8966)$
$\beta = 0.1426$	$(0.5448, 0.8224, 0.4841, 0.8223)$
$\mu = 1/60$	$(0.1955, 0.4961, 0.1419, 0.4956)$
$\mu = 1/59$	$(0.1996, 0.5016, 0.1453, 0.5110)$
$\mu = 1/56$	$(0.2127, 0.5188, 0.1565, 0.5182)$
$d = 1/3477$	$(0.4621, 0.7398, 0.3904, 0.7395)$
$d = 1/3370$	$(0.4554, 0.7312, 0.3828, 0.7310)$
$d = 1/3311$	$(0.4518, 0.7265, 0.3787, 0.7262)$
$\gamma = 1/5$	$(0.4247, 0.6877, 0.3480, 0.6874)$
$\gamma = 1/4$	$(0.4698, 0.7491, 0.3992, 0.7488)$
$\gamma = 1/3$	$(0.5451, 0.8226, 0.4845, 0.8224)$
$\epsilon = 1/6$	$(0.4700, 0.7493, 0.3994, 0.7489)$
$\epsilon = 1/4$	$(0.4698, 0.7491, 0.3992, 0.7488)$
$\epsilon = 1/2$	$(0.4697, 0.7489, 0.3990, 0.7488)$
$\varphi = 1/8$	$(0.5494, 0.7784, 0.4293, 0.7782)$
$\varphi = 1/7$	$(0.5312, 0.7715, 0.4218, 0.7712)$
$\varphi = 1/6$	$(0.5119, 0.7643, 0.4142, 0.7641)$
$\eta = 19$	$(0.5412, 0.8195, 0.4801, 0.8193)$
$\eta = 76$	$(0.5264, 0.8069, 0.4632, 0.8066)$
$\eta = 482$	$(0.2907, 0.3169, 0.1961, 0.3162)$
$\psi = 1$	$(0.4698, 0.7491, 0.3992, 0.7488)$
$\psi = 2$	$(0.6859, 0.9123, 0.6553, 0.9122)$
$\psi = 3$	$(0.9219, 0.9838, 0.9115, 0.9838)$

Table 5.6: *The extinction array changes with one parameter within the range at a time for homogeneous populations, while keeping other parameters fixed and $E_0 > 1$ for model (5.12). Fixed parameters are: $\alpha = 0.2$, $\beta = 0.19$, $\mu = 1/30$, $d = 1/3600$, $\gamma = 1/4$, $\epsilon = 1/2$, $\varphi = 1/4$, $\eta = 100$, $\psi = 1$ in this example. Same trends are obtained with various sets of fixed parameters.*

Increasing parameter	$(w_1^*, \cdots, w_n^*, u_1^*, \cdots, u_n^*)$
α_i, β_i, d_i, ε_i, φ_i, η_i, σ_{ij}, ω_{ij} $(i, j = 1, \cdots, n, i \neq j)$	decreases
μ_i, γ_i, ψ_i $(i = 1, \cdots, n)$	increases

Table 5.7: *Summary of trends for extinction array changing with one parameter at a time, while keeping other parameters fixed and $E_0 > 1$ for Model (5.12) for homogeneous populations and a two-node network throughout various simulations.*

$R_0 \leq 1$ if and only if $E_0 \leq 1$ for both models (5.3) and (5.12), besides, $|R_0 - 1| \geq |E_0 - 1|$ for Model (5.3), and $|\sqrt{R_0} - 1| \geq |E_0 - 1|$ for Model (5.12) without assumption (5.10).

The first part, $R_0 \leq 1$ if and only if $E_0 \leq 1$ was proven by Allen and van den Driessche under the assumption (16) in [5], i.e., $(F - V)^T = W(M - I)$, where F and V are Jacobian matrices defined in (4.1), M is a mean matrix of offspring distribution defined in Section 5.1, I is the identity matrix, and W is a positive diagonal matrix with each entry w_i representing the rate parameter at which lifespan of group i are exponentially distributed for $i = 1, \cdots n$ [92]. This assumption does not hold for models in (5.3) and (5.12).

Consistent trends in the extinction array w^* while changing one parameter through numerical simulations is helpful in deducing trends of extinction probability and possible interventions for vector-borne diseases. According to Equation (5.2), the probability of disease extinction is monotonically increasing (decreasing) with the increase (decrease) of the extinction array when the initial number of infection is fixed. The following biological interpretations of disease extinction or persistence are in terms of fixed initial number of infections. If contact rates from vectors to hosts (α, σ), or contact rates from hosts to vectors (β, ω) increase, then the probability for the disease to persist is higher. If death rates of hosts (d) increase, then the number of vectors is relatively dominant. Consequently, the disease is more likely to persist. Similarly, growing vector recruitment rates (η) increase probability for disease persistence. Higher incubation rates in vectors (φ) or hosts (ϵ) lead to faster vector or host infections, such that the disease tends to persist. On the contrary, increasing death rates of vectors (μ) may reduce rates of host infection, and, ultimately, may increase the likelihood of disease extinction. Increasing recovery rates of hosts (γ) may reduce the number of infections, such that probability of disease extinction increases. Increasing recruitment rate of hosts (ψ) may reduce vector infection rates and increase probability of disease extinction.

In summary, the resulting mathematical derivations and numerical simulations facilitate understanding thresholds for the spread of vector-borne diseases, as well as provide novel

insights into disease prevention, mitigation and control strategies.

Chapter 6

Conclusions and Future Work

6.1 Conclusions

Emerging and reemerging diseases continue to be major threats to an individual's heath and economy, although many factors such as improved sanitation and living conditions, development of antibiotics and vaccines, health care, and surveillance systems have contributed greatly to the reduction and effective control of mortality and morbidity from infectious diseases [50]. Uncertainties as to the underlying mechanisms and interactions still exist, impeding complete control or eradication of infectious diseases [50]. Most regions in the world have not reached a level of modernization as that of the industrialized world [50] and infectious diseases are mostly under control in these regions. Vector-borne diseases pose unique changes to public health because the epidemiology is closely linked with environmental factors such as climate, population migration, landscape, and complicated transmission mechanism of vector-transmitted pathogens. Global warning of vector-borne diseases has occurred due to increasing fear concerning this danger [112]. Many vector-borne diseases, including RVF, are re-invading many regions in Africa [112], and evidence has proven vector-borne diseases have emerged in new locations or reemerged as a significant problem to health of humans and animals after being under control in many regions of the world in the 1950s and 1960s [122]. To address the impacts of population migration and heterogeneity of environments on spatial and temporal evolution of RVF, a network

approach was applied.

The reproduction number, R_0, is an important concept in mathematical biology and epidemiology to determine whether a disease may invade a system or not. If $R_0 > 1$, then epidemic will spread, otherwise, the epidemic will die out. The reproduction number is also commonly used to quantify an epidemic by estimating the average number of secondary cases in a completely susceptible population.

In literature, most models ignored important vectors, important hosts, or spatial heterogeneity. In Chapter 2, a metapopulation model taking into account *Aedes* mosquito, *Culex* mosquito, livestock, and human populations was proposed. The spatial and temporal of RVF dynamics was studied through movement networks of mosquitoes, livestock, and humans. The model was applied to 2010 RVF outbreak in three provinces of South Africa. This model reproduced not only the trend of the occurrence, but also different starting times in different provinces by taking into account climate conditions in each province, which can not be realized in a homogeneous setting.

To facilitate comparing outputs of the model [131] with incidence data if available and implement simulations for thousands of nodes, Chapter 3 presented a discrete-time difference equation model. Stochastic parameters following PERT distributions can accommodate various species of mosquitoes. The movement of mosquitoes and livestock were modeled on different networks. The role of starting location has been shown to be important in the final size of rinderpest epidemic [79]. To investigate the role of starting location, and the size of initial infection in RVF virus spread, the roles of initial conditions wad studied through numerical simulations for hypothetical scenarios for ranching areas in Texas from 2005 to 2010. A surprising trend is that fewer initial infectious organisms result in a longer delay before a larger and more prolonged outbreak. The delay is likely caused by a lack of herd immunity while infections expand geographically before becoming an epidemic involving many dispersed farms and animals nearly simultaneously.

Very little work derived network-level reproduction number taking into account the cru-

cial biological mechanism, vertical transmission. The expression of R_0 is the sum of R_0 for vertical transmission and R_0 for horizontal transmission for the special model with only one ODE for infection due to vertical transmission and one ODE for infection due to horizontal transmission [73]. The reproduction number for homogeneous populations incorporating vertical transmission is approximated as the sum of R_0 for vertical transmission and R_0 for horizontal transmission [46], which is shown to be the upper bound of R_0 by rigorous derivation [131]. In Chapter 4, a network level reproduction number for diseases both vertically and horizontally transmitted among multiple species was derived. The complexity of computation was reduced by computing the spectral radius of a matrix reduced in size compared with the original next generation matrix. The formula was applied to an RVF metapopulation model on heterogeneous networks to derive the reproduction and its bounds. The roles of disease parameters and movement rates found through extensive numerical simulations provided insights into development of mitigation strategies.

The very little work on relationships between the reproduction number and extinction threshold for network-based vector-hosts models included deriving the relationships for an SIS multi-patch model and for a general model with an assumption on structures of matrices [5], which does not hold for both models in Chapter 5. Chapter 5 analytically derived novel relationships between network-level reproduction number and extinction threshold under certain assumptions. Numerical simulations showed the relationships exist without assumptions. Consistent trends of extinction arrays observed by varying one parameter at a time showed that extinction probability of vector-borne diseases may increase by properly controlling vector and host population size, and promptly detecting and applying treatment for hosts. Analytical and numerical results shed light on deriving relationships between R_0 and E_0, as well as connections between parameters and extinction probabilities for many other vector-borne diseases transmitted on heterogeneous works.

6.2 Future Work

The research presented in this dissertation raised more interesting questions to be answered. Several lines arising from this research are worth pursuing.

In this dissertation, the movement of mosquitoes is simplified by considering a fraction of mosquitoes migrating at each time step. Future work in follow-up mathematical models includes improvement of mosquito movement model by considering diffusion equations, which are partial differential equations with both time and space variables. Impacts of climate changes on the birth rates and development rates of mosquitoes were taken into account. However, carrying capacity, biting rate, birth rate, death rate, and many other characteristics of mosquitoes are also linked with weather variables. Hence, carrying capacities of mosquitoes dependent on climate factors, density dependent biting rates, weather dependent birth rate, death rate, incubation rate, and recovery rate will make the model more realistic. More climate factors, soil type, elevation, and other factors are to be considered in the future models.

When computing the reproduction number in Chapter 4, existences of unique DFE were proved. When $R_0 < 1$ and multiple stable equilibria coexist, backward bifurcation may occur. The existence, uniqueness, and stability of endemic equilibrium, as well as global stability of DFE when $R_0 < 1$ for vector-borne diseases involving vertical transmission are to be explored. Calibrating and validating models presented in this dissertation using real data will be intriguing. The reproduction number for the discrete-time model presented in Chapter 3 is to be derived. To determine key parameters and rank the significance of model parameters in predicting uncertainty of epidemic threshold, Partial Rank Correlation Coefficients with respect to R_0 for an RVF metapopulation model is to be computed in future work.

Following the deterministic model in Chapter 2 and deterministic model with stochastic parameters in Chapter 3, developing a stochastic model to take into account chances in disease transmission and deriving its extinction thresholds taking into account vertical

transmission can then be proposed. Future work may include studying how parameters in the model affect the probability, size and duration time of an outbreak and the confidence intervals of these characteristics to better understand dynamics of diseases.

Early detection of infected cattle is essential. After local and regional authorities are warned and response planning initiated, cattle movement restrictions, culling, insecticide treatments, quarantines, and other mitigation strategies to limit transmission may be effective. Impacts of livestock movement ban will be explored in future models.

Parameterizing the model using realistic mosquito field data from 1980 to 2011 in Kansas, and climate data for a separate mosquito population model may determine parameters on specific RVF competent vectors more accurately. Mosquito control strategies can then be tested using the parameters. Applying realistic cattle movement data and climate data to RVF metapopulation models will help to predict dynamics of Rift Valley fever. Maps generated by Geographic Information System will improve visualization.

Different age groups may have heterogeneous susceptibility, death rate, incubation rate, and behaviors in disease transmission. Incorporating age-structure into models in Chapters 2 and 3 may improve accuracy of modeling and provide more insights into disease intervention, control, and eradication. Robustness of different network structures, such as bipartite network, tripartite network, scale-free network, Erdős-Rényi and others to RVF invasion is to be studied. All these are left for the future work.

Bibliography

[1] European Food Safety Authority (EFSA). Opinion of the scientific panel on animal health and welfare (AHAW) on a request from the commission related to the risk of a Rift Valley fever incursion and its persistence within the community, 2005.

[2] S. Abdo-Salem, A. Waret-Szkuta, F. Roger, M. M. Olive, K. Saeed, and V. Chevalier. Risk assessment of the introduction of Rift Valley fever from the horn of Africa to Yemen via legal trade of small ruminants. *Tropical Animal Health and Production*, 43(2):471–480, 2011.

[3] F. R. Adler. The effects of averaging on the basic reproduction ratio. *Mathematical Biosciences*, 111(1):89–98, 1992.

[4] L. J. Allen and G. E. Lahodny Jr. Extinction thresholds in deterministic and stochastic epidemic models. *Journal of Biological Dynamics*, 6(2):590–611, 2012.

[5] L. J. Allen and P. van den Driessche. Relations between deterministic and stochastic thresholds for disease extinction in continuous- and discrete-time infectious disease models. *Mathematical Biolosciences*, 243(1):99–108, 2013.

[6] R. M. Anderson and R. M. May. The population-dynamics of micro-parasites and their invertebrate hosts. *Philosophical Transactions of the Royal Society of London Series B-Biological Sciences*, 291(1054):451–524, 1981.

[7] A. Anyamba, J. P. Chretien, J. Small, C. J. Tucker, P. B. Formenty, J. H. Richardson, S. C. Britch, D. C. Schnabel, R. L. Erickson, and K. J. Linthicum. Prediction of a Rift Valley fever outbreak. *Proceedings of the National Academy of Sciences*, 106(3):955–959, 2009.

[8] A. Anyamba, K. J. Linthicum, and C. J. Tucker. Climate-disease connections: Rift Valley fever in Kenya. *Cadernos de Saúde Pública*, 17 Suppl:133–140, 2001.

[9] J. Arino. Diseases in metapopulations. In Z. Ma, Y. Zhou, and J. Wu, editors, *Modeling and Dynamics of Infectious Diseases*, volume 11 of *Series in Contemporary Applied Mathematics*, pages 65–123. World Scientific, 2009.

[10] J. Arino, J. R. Davis, D. Hartley, R. Jordan, J. M. Miller, and P. van den Driessche. A multi-species epidemic model with spatial dynamics. *Mathematical Medicine and Biology*, 22(2):129–142, 2005.

[11] J. Arino, R. Jordan, and P. van den Driessche. Quarantine in a multi-species epidemic model with spatial dynamics. *Mathematical Biosciences*, 206(1):46–60, 2007.

[12] J. Arino and P. van den Driessche. The basic reproduction number in a multi-city compartmental epidemic model. *Lecture Notes in Control and Information Sciences*, 294:135–142, 2003.

[13] P. Bajardi, A. Barrat, F. Natale, L. Savini, and V. Colizza. Dynamical patterns of cattle trade movements. *PloS ONE*, 6(5):e19869, 2011.

[14] D. Balcan, V. Colizza, B. Goncalves, H. Hu, J. J. Ramasco, and A. Vespignani. Multiscale mobility networks and the spatial spreading of infectious diseases. *Proceedings of the National Academy of Sciences of the United States of America*, 106(51):21484–21489, 2009.

[15] M. Bates. *The natural history of mosquitoes*. MacMillan, New York, 1949.

[16] D. Bisanzio, L. Bertolotti, L. Tomassone, G. Amore, C. Ragagli, A. Mannelli, M. Giacobini, and P. Provero. Modeling the spread of vector-borne diseases on bipartite networks. *PloS ONE*, 5(11):e13796, 2010.

[17] F. Brauer, Z. Feng, and C. Castillo-Chavez. Discrete epidemic models. *Mathematical Biosciences and Engineering*, 7(1):1–15, 2010.

[18] T. Britton and D. Lindenstrand. Epidemic modelling: Aspects where stochasticity matters. *Mathematical Biosciences*, 222:109–116, 2009.

[19] S. Busenberg and K. L. Cooke. Models of vertically transmitted diseases with sequential- continuous dynamics. In V. Lakshmicantham, editor, *Nonlinear Phenomena in Mathematical Sciences*, pages 179–187. Academic Press, New York, 1982.

[20] S. Busenberg and K. L. Cooke. The population-dynamics of two vertically transmitted infections. *Theoretical Population Biology*, 33(2):181–198, 1988.

[21] S. Busenberg and K. L. Cooke. *Vertically transmitted diseases: models and dynamics*. Springer-Verlag, Berlin, 1993.

[22] D. V. Canyon, J. L. K. Hii, and R. Muller. The frequency of host biting and its effect on oviposition and survival in Aedes aegypti (Diptera: Culicidae). *Bulletin of Entomological Research*, 89(1):35–39, 1999.

[23] G. H. Cheng, X. Y. Cheng, T. Z. Huang, and T. Y. Tam. Some bounds for the spectral radius of the Hadamard product of matrices. *Applied Mathematics E-Notes*, 5:202–209, 2005.

[24] V. Chevalier, R. Lancelot, Y. Thiongane, B. Sall, A. Diaite, and B. Mondet. Rift Valley fever in small ruminants, Senegal, 2003. *Emerging Iinfectious Diseases*, 11(11):1693–1700, 2005.

[25] V. Chevalier, M. Pépin, L. Plée, and R. Lancelot. Rift Valley fever–a threat for Europe? *Eurosurveillance*, 15(10):19506–19517, 2010.

[26] N. Chitnis, J. M. Hyman, and J. M. Cushing. Determining important parameters

in the spread of malaria through the sensitivity analysis of a mathematical model. *Bulletin of Mathematical Biology*, 70(5):1272–1296, 2008.

[27] N. Chitnis, J. M. Hyman, and C. A. Manore. Modelling vertical transmission in vector-borne diseases with applications to Rift Valley fever. *Journal of Biological Dynamics*, 7(1):11–40, 2013.

[28] S. R. Chowdhury, C. Scoglio, and W. Hsu. Simulative modeling to control the foot and mouth disease epidemic. *Procedia Computer Science*, 1(1):2261–2270, 2010.

[29] CIESIN. Changes in the incidence of vector-borne diseases attributable to climate change. http://www.ciesin.columbia.edu/TG/HH/veclev2.html, 2007. (Center for International Earth Science Information Network). Accessed June 20, 2013.

[30] A. Cintrn-Arias, C. Castillo-Chvezl, L. M. Bettencourt, and H. T. Banks A. L. Lloyd. The estimation of the effective reproductive number from disease outbreak data. *Mathematical Biosciences and Engineering*, 255:261–282, 2009.

[31] A. C. Clements, D. U. Pfeiffer, V. Martin, C. Pittliglio, N. Best, and Y. Thiongane. Spatial risk assessment of Rift Valley fever in Senegal. *Vector Borne and Zoonotic Diseases*, 7(2):203–216, 2007.

[32] J. E. Cohen. Random evolutions and the spectral radius of a non-negative matrix. *Mathematical Proceedings of the Cambridge Philosophical Society*, 86(345):345–350, 1979.

[33] F. G. Davies. Risk of a Rift Valley fever epidemic at the haj in Mecca, Saudi Arabia. *Revue Scientifique et Technique*, 25(1):137–147, 2006.

[34] Department for Environment Food and Rural Affairs. Rift Valley fever. http://www.defra.gov.uk/foodfarm/farmanimal/diseases/atoz/riftvalleyfever/index.htm, 2010. Accessed Nov 10, 2010.

[35] Department of Agriculture Forestry and Fisheries of Republic of South Africa. Livestock number 96 to date. http://www.nda.agric.za/docs/statsinfo/LivestokNo96toDate.xls, 2010. Accessed Sep 26, 2010.

[36] O. Diekmann and J. A. P. Heesterbeek. *Mathematical Epidemiology of Infectious Diseases*. Wiley, Chichester, 2000.

[37] O. Diekmann, J. A. P. Heesterbeek, and J. A. J. Metz. On the definition and the computation of the basic reproduction ratio R0 in models for infectious diseases in heterogeneous populations. *Journal of Mathematical Biology*, 28(4):365–382, 1990.

[38] O. Diekmann, J. A. P. Heesterbeek, and M. G. Roberts. The construction of next-generation matrices for compartmental epidemic models. *Journal of the Royal Society Interface*, 7(47):873–885, 2010.

[39] Disease BioPortal. http://fmdbioportal.ucdavis.edu, 2010. Accessed Nov 23, 2010.

[40] B. J. Dominguez. Characterization of livestock herds in extensive agricultural settings in southwest Texas. Master's thesis, Texas A&M University, U.S.A, 2007.

[41] M. El-Doma. Analysis of an age-dependent SIS epidemic model with vertical transmission and proportionate mixing assumption. *Mathematical and Computer Modelling*, 29(7):31–43, 1999.

[42] B. J. Erasmus and J. A. W. Coetzer. The symptomatology and pathology of Rift Valley fever in domestic animals. *Contributions to Epidemiology and Biostatistics*, 3:77–82, 1981.

[43] C. Favier, K. Chalvet-Monfray, P. Sabatier, R. Lancelot, D. Fontenille, and M. A. Dubois. Rift Valley fever in West Africa: the role of space in endemicity. *Tropical Medicine & International Health*, 11(12):1878–1888, 2006.

[44] Florida Department of Health. Rift Valley fever. http://www.doh.state.fl.us/environment/medicine/arboviral/RiftValleyFever.html. Accessed Nov 30, 2010.

[45] J. E. Freier and L. Rosen. Vertical transmission of dengue viruses by mosquitoes of the Aedes scutellaris group. *The American Journal of Tropical Medicine and Hygiene*, 37(3):640–647, 1987.

[46] H. D. Gaff, D. M. Hartley, and N. P. Leahy. An epidemiological model of Rift Valley fever. *Electronic Journal of Differential Equations*, 2007(115):1–12, 2007.

[47] D. Gao, C. Cosner, R. S. Cantrell, J. C. Beier, and S. Ruan. Modeling the spatial spread of Rift Valley fever in Egypt. *Bulletin of Mathematical Biology*, 75(3):523–542, 2013.

[48] D. Gao and S. Ruan. An SIS patch model with variable transmission coefficients. *Mathematical Biosciences*, 232(2):110–115, 2011.

[49] D. Gao and S. Ruan. A multipatch malaria model with logistic growth populations. *SIAM Journal on Applied Mathematics*, 72(3):819–841, 2012.

[50] J. Giesecke. *Modern Infectious Disease Epidemiology*. CRC Press, 2001.

[51] B. Gomero. Latin Hypercube Sampling and Partial Rank Correlation Coefficient analysis applied to an optimal control problem. Master's thesis, the University of Tennessee, the United States, 2012.

[52] H. Gong, A. T. Degaetano, and L. C. Harrington. Climate-based models for West Nile Culex mosquito vectors in the Northeastern US. *International Journal of Biometeorology*, 55(3):435–446, 2010.

[53] N. J. Gotelli and C. M. Taylor. Testing metapopulation models with stream-fish assemblages. *Evolutionary Ecology Research*, 1(7):835–845, 1999.

[54] N. G. Gratz. Emerging and resurging vector-borne diseases. *Annual Review of Entomology*, 44:51–75, 1999.

[55] D. J. Gubler. The global emergence/resurgence of arboviral diseases as public health problems. *Archives of Medical Research*, 33(4):330–342, 2002.

[56] R. O. Hayes, C. H. Tempelis, A. D. Hess, and W. C. Reeves. Mosquito host preference studies in Hale county, Texas. *American Journal of Tropical Medicine and Hygiene*, 22:270–277, 1973.

[57] J. M. Heffernan, R. J. Smith?, and L.M. Wahl. Perspectives on the basic reproductive ratio. *Journal of the Royal Society Interface*, 2(4):281–293, 2005.

[58] Y. H. Hsieh, P. van den Driessche, and L. Wang. Impact of travel between patches for spatial spread of disease. *Bulletin of Mathematical Biology*, 69(4):1355–1375, 2007.

[59] C. J. Jones and J. E. Lloyd. Mosquitos feeding on sheep in southeastern Wyoming. *Journal of the American Mosquito Control Association*, 1(4):530–532, 1985.

[60] A. Jouan, B. Le Guenno, J. P. Digoutte, B. Philippe, O. Riou, and F. Adam. An RVF epidemic in southern Mauritania. *Annales de l'Institut Pasteur. Virology*, 139(3):307–308, 1988.

[61] R. R. Kao. Networks and models with heterogeneous population structure in epidemiology. *Network Science*, pages 51–84, 2010.

[62] T. R. Kasari, D. A. Carr, T. V. Lynn, and J. T. Weaver. Evaluation of pathways for release of Rift Valley fever virus into domestic ruminant livestock, ruminant wildlife, and human populations in the continental United States. *Journal of the American Veterinary Medical Association*, 232(4):514–529, 2008.

[63] M. J. Keeling and P. Rohani. *Modeling infectious diseases in humans and animals*. Princeton University Press, 2008.

[64] M. J. Keeling, M. E. J. Woolhouse, D. J. Shaw, L. Matthews, M. Chase-Topping, D. T. Haydon, S. J. Cornell, J. Kappey, J. Wilesmith, and B. T. Grenfell. Dynamics of the 2001 UK foot and mouth epidemic: Stochastic dispersal in a heterogeneous landscape. *Science*, 294(5543):813–817, 2001.

[65] S. K. Konrad, S. N. Miller, and W. K. Reeves. A spatially explicit degree-day model of Rift Valley fever transmission risk in the continental United States. *GeoJournal*, 2010.

[66] G. E. Lahodny Jr and L. J. Allen. Probability of a disease outbreak in stochastic multipatch epidemic models. *Bulletin of Mathematical Biology*, 75(7):1157–1180, 2013.

[67] J. Li, D. Blakeley, and R. J. Smith? The failure of R0. *Computational and Mathematical Methods in Medicine*, 2011, 2011.

[68] M. Y. Li, H. L. Smith, and L. C. Wang. Global dynamics of an SEIR epidemic model with vertical transmission. *SIAM Journal on Applied Mathematics*, 62(1):58–69, 2001.

[69] E. T. Linacre. A simple formula for estimating evaporation rates in various climates, using temperature data alone. *Agricultural Meteorology*, 18(6):409–424, 1977.

[70] K. J. Linthicum, A. Anyamba, S. C. Britch, J. P. Chretien, R. L. Erickson, J. Small, C. J. Tucker, K. E. Bennett, R. T. Mayer, E. T. Schmidtmann, T. G. Andreadis, J. F. Anderson, W. C. Wilson, J. E. Freier, A. M. James, R. S. Miller, B. S. Drolet, S. N. Miller, C. A. Tedrow, C. L. Bailey, D. A. Strickman, D. R. Barnard, G. G. Clark, and L. Zou. A Rift Valley fever risk surveillance system for Africa using remotely sensed data: potential for use on other continents. *Veterinaria Italiana*, 43(3):663–674, Jul-Sep 2007.

[71] K. J. Linthicum, A. Anyamba, C. J. Tucker, P. W. Kelley, M. F. Myers, and C. J. Peters. Climate and satellite indicators to forecast Rift Valley fever epidemics in Kenya. *Science*, 285(5426):397–400, 1999.

[72] K. J. Linthicum, F. G. Davies, A. Kairo, and C. L. Bailey. Rift Valley fever virus (family Bunyaviridae, genus Phlebovirus). isolations from Diptera collected during an inter-epizootic period in Kenya. *The Journal of Hygiene*, 95(1):197–209, 1985.

[73] M. Lipsitch, M. A. Nowak, D. Ebert, and R. M. May. The population dynamics of vertically and horizontally transmitted parasites. *Proceedings of the Royal Society B: Biological Sciences*, 260(1359):321–327, 1995.

[74] A. L. Lloyd, J. Zhang, and A. M. Root. Stochasticity and heterogeneity in host-vector models. *Journal of the Royal Society Interface*, 4(16):851–863, 2007.

[75] I. M. Longini. The generalized discrete-time epidemic model with immunity: a synthesis. *Mathematical Biosciences*, 82(1):19–41, 1986.

[76] P. M. Luz, C. J. Struchiner, and A. P. Galvani. Modeling transmission dynamics and control of vector-borne neglected tropical diseases. *PLoS Neglected Tropical Diseases*, 4(10):e761, 2010.

[77] S. Ma and Y. Xia. *Mathematical understanding of infectious disease dynamics*. World Scientific, 2009.

[78] L. A. Magnarelli. Host feeding patterns of Connecticut mosquitos (Diptera-Culicidae). *American Journal of Tropical Medicine and Hygiene*, 26(3):547–552, 1977.

[79] C. A. Manore, B. McMahon, J. Fair, J. M. Hyman, M. Brown, and M. LaBute. Disease properties, geography, and mitigation strategies in a simulation spread of rinderpest across the united states. *Veterinary Research*, 42:55, 2011.

[80] S. Marino, I. B. Hogueand, C. J. Ray, and D. E. Kirschner. A methodology for performing global uncertainty and sensitivity analysis in systems biology. *Journal of Theoretical Bbiology*, 254:178–196, 2008.

[81] V. Martin, V. Chevalier, P. Ceccato, A. Anyamba, L. De Simone, J. Lubroth, S. de La Rocque, and J. Domenech. The impact of climate change on the epidemiology and control of Rift Valley fever. *Revue Scientifique et Technique (International Office of Epizootics)*, 27(2):413–426, 2008.

[82] R. Métras, L. M. Collins, R. G. White, S. Alonso, V. Chevalier, C. Thuranira-McKeever, and D. U. Pfeiffer. Rift Valley fever epidemiology, surveillance, and control: what have models contributed? *Vector Borne and Zoonotic Diseases*, 11(6):761–771, 2011.

[83] C. G. Moore, R. G. McLean, C. J. Mitchell, R. S. Nasci, T. F. Tsai, C. H. Caslisher, A. A. Marfin, P. S. Moorse, and D. J. Gubler. *Guidelines for arbovirus surveillance programs in the United States*. Center for Disease Control and Prevention, 1993.

[84] Saul C. Mpeshe, Heikki Haario, and Jean M. Tchuenche. A mathematical model of Rift Valley fever with human host. *Acta Biotheoretica*, 59(3-4):231–250, 2011.

[85] F. Natale, A. Giovannini, L. Savini, D. Palma, L. Possenti, G. Fiore, and P. Calistri. Network analysis of Italian cattle trade patterns and evaluation of risks for potential disease spread. *Preventive Veterinary Medicine*, 92(4):341–350, 2009.

[86] National Climatic Center. NOAA Satellite and Information Service. Accessed April 18, 2012.

[87] National Institute for Communicable Diseases. Interim report on the Rift Valley fever (RVF) outbreak in South Africa. http://www.nicd.ac.za/?page=rift_valley_fever_outbreak&id=94, 2012. Accessed May 23, 2012.

[88] E. A. Newton and P. Reiter. A model of the transmission of dengue fever with an evaluation of the impact of ultra-low volume (ULV) insecticide applications on dengue epidemics. *The American Journal of Tropical Medicine and Hygiene*, 47(6):709–720, 1992.

[89] T. Niu, H. D. Gaff, Y. E. Papelis, and D. M. Hartley. An epidemiological model of Rift Valley fever with spatial dynamics. *Computational and Mathematical Methods in Medicine*, 2012.

[90] G. C. Olivier. An analysis of the South African beef supply chain: from farm to folk. Master's thesis, University of Johannesburg, South Africa, 2004.

[91] M. Otero and H. G. Solari. Stochastic eco-epidemiological model of dengue disease transmission by Aedes aegypti mosquito. *Mathematical Biosciences*, 223(1):32–46, 2010.

[92] S. Pénisson. *Conditional limit theorems for multitype branching processes and illustration in epidemiological risk analysis.* PhD thesis, Institut für Mathematik der Unversität Potsdam, Germany, 2010.

[93] C. J. Peters and K. J. Linthicum. Rift Valley fever. In G.B. Beran, editor, *Handbook of Zoonoses*, Section B: Viral, pages 125–138. CRC Press, Inc., Boca Raton, Fl, second edition, 1994.

[94] L. R. Petersen and J. T. Roehrig. West Nile virus: A reemerging global pathogen. *Emerging Infectious Diseases*, 7(4):611–614, 2001.

[95] R. J. Plemmons. M-matrix characterizations 1: Nonsingular M-matrices. *Linear Algebra and its Applications*, 18(2):175–188, 1977.

[96] H. D. Pratt and C. G. Moore. *Vector-borne disease control: mosquitoes of public health importance and their control.* U.S. Department of Health and Human Services, Atlanta, GA, 1993.

[97] O. M. Radostits. *Herd healthy: food animal production medicine.* Saunders, 2001.

[98] required. The legacy of Kermack and McKendrick. In D. Mollison, editor, *Epidemic*

Models: Their Structure and Relation to Data, pages 95–115. Cambridge University Press, Cambridge, UK, 1995.

[99] S. Riley. Coping without farm location data during a foot-and-mouth outbreak. *Proceedings of the National Academy of Sciences of the United States of America*, 107(3):957–958, 2010.

[100] P. Rohani, D. J. Earn, and B. T. Grenfell. Opposite patterns of synchrony in sympatric disease metapopulations. *Science*, 286(5441):968–971, 1999.

[101] R. Ross. Some quantitative studies in epidemiology. *Nature*, 4:466–467, 1911.

[102] R. Ross. An application of the theory of probabilities to the study of a priori pathometry. Part I. *Proceedings of the Royal Society of London. Series A*, 92(638):204–230, 1916.

[103] L. M. Rueda, K. J. Patel, R. C. Axtell, and R. E. Stinner. Temperature-dependent development and survival rates of Culex-quinquefasciatus and Aedes-aegypti (Diptera: Culicidae). *Journal of medical entomology*, 27(5):892–898, 1990.

[104] M. Salmani and P. van den Driessche. A model for disease transmission in a patchy environment. *Discrete and Continuous Dynamical Systems-Series B*, 6(1):185–202, 2006.

[105] R. F. Sellers, D. E. Pedgley, and M. R. Tucker. Rift Valley fever, Egypt 1977: disease spread by windborne insect vectors? *The Veterinary Record*, 110(4):73–77, 1982.

[106] Statistics South Africa. Agricultural Census (Census of Commercial Agriculture), 2007. http://www.statssa.gov.za/publications/statsdownload.asp?PPN=P1102&SCH=4534, 2009. Accessed Nov 22, 2010.

[107] Statistics South Africa. Domestic tourism survey 2009. http://www.statsonline.

gov.za/publications/statsdownload.asp?PPN=P0352.1&SCH=4702, 2010. Accessed Nov 23, 2010.

[108] Statistics South Africa. Mid-year population estimates. http://www.statsonline.gov.za/publications/P0302/P03022010.pdf, 2010. Accessed Nov 21, 2010.

[109] R. B. Stothers. Climatic and demographic consequences of the massive volcanic eruption of 1258. *Climatic Change*, 45(2):361–374, 2000.

[110] J. C. Swanson and J. Morrow-Tesch. Cattle transport: Historical, research, and future perspectives. *Journal of Animal Science*, 79:E102–E109, 2001.

[111] C. M. Taylor and R. J. Hall. Metapopulation models for seasonally migratory animals. *Biology Letters*, 8(3):477–480, 2012.

[112] R. S. J. Tol and H. Dowlatabadi. Vector-borne diseases, development & climate change. *Integrated Assessment*, 2:173–181, 2001.

[113] M. J. Turell and C. L. Bailey. Transmission studies in mosquitoes (Diptera: Culicidae) with disseminated Rift Valley fever virus infections. *Journal of Medical Entomology*, 24(1):11–18, 1987.

[114] M. J. Turell, C. L. Bailey, and J. R. Beaman. Vector competence of a Houston, Texas strain of Aedes Albopictus for Rift Valley fever virus. *Journal of the American Mosquito Control Association*, 4(1):94–96, 1988.

[115] M. J. Turell, M. E. Faran, M. Cornet, and C. L. Bailey. Vector competence of senegalese Aedes fowleri (Diptera: Culicidae) for Rift Valley fever virus. *Journal of Medical Entomology*, 25(4):262–266, 1988.

[116] M. J. Turell, W. C. Wilson, and K. E. Bennett. Potential for North American mosquitoes (Diptera: Culicidae) to transmit Rift Valley fever virus. *Journal of medical entomology*, 47(5):884–889, 2010.

[117] United States Department of Agriculture. 2007 census publications. http://www.agcensus.usda.gov/Publications/2007/Full_Report/Census_by_State/Texas/index.asp, 2007. Accessed April 15, 2012.

[118] P. van den Driessche and J. Watmough. Reproduction numbers and sub-threshold endemic equilibria for compartmental models of disease transmission. *Mathematical Biosciences*, 180(12):29–48, 2002.

[119] M. C. Vernon and M. J. Keeling. Representing the uk's cattle herd as static and dynamic networks. *Proceedings of the Royal Society B: Biological Sciences*, 276(1656):469–476, 2009.

[120] W. Wang and X. Q. Zhao. An epidemic model in a patchy environment. *Mathematical Biosciences*, 190(1):97–112, 2004.

[121] Weather Underground. http://www.wunderground.com, 2010. Accessed Nov 20, 2010.

[122] H. Wei, X. Li, and M. Martcheva. An epidemic model of a vector-borne disease with direct transmission and time delay. *Journal of Mathematical Analysis and Applications*, 342(2):895–908, 2008.

[123] J. W. Wekesa, B. Yuval, and R. K. Washino. Multiple blood feeding by Anopheles freeborni and Culex tarsalis (Diptera: Culicidae): Spatial and temporal variation. *Journal of Medical Entomology*, 34(2):219–225, 1997.

[124] M. J. Wonham, M. A. Lewis, J. Renclawowicz, and P. van den Driessche. Transmission assumptions generate conflicting predictions in host-vector disease models: a case study in West Nile virus. *Ecology Letters*, 9(6):706–725, 2006.

[125] C. W. Woods, A. M. Karpati, T. Grein, N. McCarthy, P. Gaturuku, E. Muchiri, L. Dunster, A. Henderson, A. S. Khan, R. Swanepoel, I. Bonmarin, L. Martin,

P. Mann, B. L. Smoak, M. Ryan, T. G. Ksiazek, R. R. Arthur, A. Ndikuyeze, N. N. Agata, C. J. Peters, and World Health Organization Hemorrhagic Fever Task Force. An outbreak of Rift Valley fever in Northeastern Kenya, 1997-98. *Emerging Infectious Diseases*, 8(2):138–144, 2002.

[126] World Animal Health Information Database. Summary of immediate notifications and follow-ups - 2010. http://www.oie.int/wahis/public.php?page=disease_immediate_summary, 2010. Accessed Oct 14, 2010.

[127] World Health Organization. Rift Valley fever. http://www.who.int/mediacentre/factsheets/fs207/en/, 2010. Accessed Nov 22, 2010.

[128] World Health Organization Multicentre Collaborative Network for Severe and Acute Respiratory Syndrome Diagnosis. A multicentre collaboration to investigate the cause of severe acute respiratory syndrome. *Lancet*, 361(9370):1730–1733, 2003.

[129] L. Xue, L. W. Cohnstaedt, H. M. Scott, and C. Scoglio. A hierarchical network approach for modeling Rift Valley fever epidemics with applications in North America. *PLos ONE*, 8(5):e62049., 2013.

[130] L. Xue and C. Scoglio. The network level reproduction number for infectious diseases with both vertical and horizontal transmission. *Mathematical Biosciences*, 243(1):67–80, 2013.

[131] L. Xue, H. M. Scott, L. W. Cohnstaedt, and C. Scoglio. A network-based meta-population approach to model Rift Valley fever epidemics. *Journal of Theoretical Biology*, 306(5):129–144, 2012.

[132] H. G. Zeller, D. Fontenille, M. Traore-Lamizana, Y. Thiongane, and J. P. Digoutte. Enzootic activity of Rift Valley fever virus in Senega. *American Journal of Tropical Medicine and Hygiene*, 56(3):265–272, 1997.

Appendix A

Appendix to Chapter 4

Theorem 7. *If both A and B are non-negative square matrices, then $\rho(A) \leq \rho(A+B)$.*

Proof. Recall that the Gelfand's formula is that

$$\rho(A) = \lim_{k\to\infty} \|A^k\|^{\frac{1}{k}}$$

for any matrix norm $\|\cdot\|$. If A, B are both non-negative, then $A \leq A+B$. Hence, $0 \leq A^k \leq (A+B)^k$ for any $k \in \mathbb{N}$. By the property of matrix norm, $0 \leq \|A^k\| \leq \|(A+B)^k\|$. Thus,

$$0 \leq \lim_{k\to\infty} \|A^k\|^{\frac{1}{k}} \leq \lim_{k\to\infty} \|(A+B)^k\|^{\frac{1}{k}}.$$

The theorem follows the Gelfand's formula. □

Theorem 8. *Let A_k $(k = 1, \cdots, m)$ be an $n \times n$ diagonal dominant matrix with $A_k^{-1} \geq 0$. Denote the (i,j) entry of A_k by a_{kij}. Let $a_k^L = \min_j(\sum_i a_{kij}) > 0$, $a_k^H = \max_j(\sum_i a_{kij})$, where $j = 1, \cdots, n$, then*

$$\prod_{k=1}^{m} \frac{1}{a_k^H} \leqslant \rho(\prod_{k=1}^{m} A_k^{-1}) \leqslant \prod_{k=1}^{m} \frac{1}{a_k^L}.$$

Proof. Clearly, $0 \leq a_k^L \mathcal{C} \leqslant \mathcal{C} A_k \leqslant a_k^H \mathcal{C}$, where $\mathcal{C} = [1\ 1 \cdots\ 1]_{1\times n}$. Since $A_k^{-1} \geqslant 0$, we obtain

$$0 \leq \frac{\mathcal{C}}{a_k^H} \leq \mathcal{C} A_k^{-1} \leq \frac{\mathcal{C}}{a_k^L}.$$

Similarly,

$$0 \leq \frac{\mathcal{C}}{a_k^H a_{k-1}^H} \leq \frac{\mathcal{C} A_{k-1}^{-1}}{a_k^H} \leq \mathcal{C} A_k^{-1} A_{k-1}^{-1} \leq \frac{\mathcal{C} A_{k-1}^{-1}}{a_k^L} \leq \frac{\mathcal{C}}{a_k^L a_{k-1}^L}.$$

Following the same argument,

$$\prod_{k=1}^{m}\frac{1}{a_k^H}\mathcal{C}\leqslant\mathcal{C}\prod_{k=1}^{m}A_k^{-1}\leqslant\prod_{k=1}^{m}\frac{1}{a_k^L}\mathcal{C}.$$

By Corollary 1 in [32], any $n\times n$ nonnegative matrix A satisfies:

$$\min_j(\sum_{i=1}^{n}a_{ij})\leqslant\rho(A)\leqslant\max_j(\sum_{i=1}^{n}a_{ij}). \tag{A.1}$$

Because the entries of $\mathcal{C}\prod_{k=1}^{m}A_k^{-1}$ is the sum of each column of matrix $\prod_{k=1}^{m}A_k^{-1}$, by Inequality (A.1),

$$\prod_{k=1}^{m}\frac{1}{a_k^H}\leqslant\rho(\prod_{k=1}^{m}A_k^{-1})\leqslant\prod_{k=1}^{m}\frac{1}{a_k^L}.$$

□

Theorem 9. *Matrices M_k and X_k in (4.14) are invertible, and M_k and X_k are nonnegative. Moreover, Matrices M_k^{-1} and X_k^{-1} are nonnegative matrices.*

Proof. Note that M_k is a diagonal dominant matrix of its column entries. By Theorem 1 in page 654 of [23], M_k and X_k are invertible. Next, matrix M_k^{-1} is proven to be nonnegative. Matrix M_k can be rewritten as follows.

$$M_k=\begin{bmatrix}\zeta_{k1}&-\omega_{k21}&\cdots&-\omega_{kn1}\\-\omega_{k12}&\zeta_{k2}&\cdots&-\omega_{kn2}\\\cdots&\cdots&\cdots&\cdots\\-\omega_{k1n}&-\omega_{k2n}&\cdots&\zeta_{kn}\end{bmatrix}=\oplus_{i=1}^{n}\zeta_{ki}-\begin{bmatrix}0&\omega_{k21}&\cdots&\omega_{kn1}\\\omega_{k12}&0&\cdots&\omega_{kn2}\\\cdots&\cdots&\cdots&\cdots\\\omega_{k1n}&\omega_{k2n}&\cdots&0\end{bmatrix}=:G-H.$$

Consequently,

$$G^{-1}=\oplus_{i=1}^{n}\zeta_{ki}^{-1}\quad\text{and}\quad G^{-1}H=\begin{bmatrix}0&\omega_{k21}\zeta_{k1}^{-1}&\cdots&\omega_{kn1}\zeta_{k1}^{-1}\\\omega_{k12}\zeta_{k2}^{-1}&0&\cdots&\omega_{kn2}\zeta_{k2}^{-1}\\\cdots&\cdots&\cdots&\cdots\\\omega_{k1n}\zeta_{kn}^{-1}&\omega_{k2n}\zeta_{kn}^{-1}&\cdots&0\end{bmatrix}.$$

Moreover, $0<\sum_{j=1}^{n}(G^{-1}H)_{ij}<1$, for all i. Hence, $\rho(G^{-1}H)<1$, i.e., $G^{-1}H$ is convergent (see [95]). Note that $G^{-1}\geqslant 0$, and $G^{-1}H\geqslant 0$. By Theorem 1 in [95], M_k is an M-matrix and $M_k^{-1}\geqslant 0$. By the same argument, X_k is an M-matrix and $X_k^{-1}\geqslant 0$. This finishes the proof. □